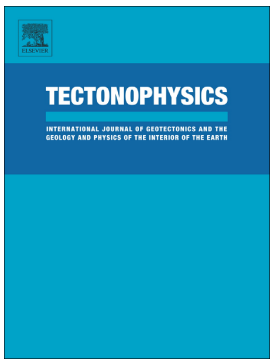

Along-strike segmentation in the northern Caribbean plate boundary zone (Hispaniola sector): Tectonic implications

A. Rodríguez-Zurrunero, J.L. Granja-Bruña, A. Muñoz-Martín, S. Leroy, U. ten Brink, J.M. Gorosabel-Araus, L. Gómez de la Peña, M. Druet, A. Carbó-Gorosabel

PII: S0040-1951(20)30005-6

DOI: https://doi.org/10.1016/j.tecto.2020.228322

Reference: TECTO 228322

To appear in: *Tectonophysics*

Received date: 12 November 2019

Revised date: 7 January 2020

Accepted date: 10 January 2020

Please cite this article as: A. Rodríguez-Zurrunero, J.L. Granja-Bruña, A. Muñoz-Martín, et al., Along-strike segmentation in the northern Caribbean plate boundary zone (Hispaniola sector): Tectonic implications, *Tectonophysics*(2018), https://doi.org/10.1016/j.tecto.2020.228322

To be submitted to Tectonophysics

Along-strike segmentation in the northern Caribbean plate boundary zone (Hispaniola sector): tectonic implications

A. Rodríguez-Zurrunero, (1*), J.L. Granja-Bruña, (1), A. Muñoz-Martín (1,2), S. Leroy (3), U. ten Brink (4), J.M. Gorosabel-Araus (1), L. Gómez de la Peña (5), M. Druet (6), A. Carbó-Gorosabel (1).

*Corresponding author: arzurrunero@ucm.es

(1) Applied Tectonophysics Group. Department of Geodynamics, Stratigraphy and Paleontology. Universidad Complutense, Madrid, Spain

(2) Instituto de Geociencias (UCM, CSIC), Madrid, Spain

(3) Sorbonne Université, INSU, CNRS, ISTeP, Paris, France

(4) U. S. Geological Survey Woods Hole. MA. USA.

(5) GEOMAR Helmholtz Centre of Ocean Research, Kiel, Germany.

(6) Instituto Geológico y Minero de España, Tres Cantos, Madrid. Spain.

Abstract

The North American (NOAM) plate converges with the Caribbean (CARIB) plate at a rate of 20.0 ± 0.4 mm/yr. towards 254 ± 1º. Plate convergence is highly oblique (20-10º), resulting in a complex crustal boundary with along-strike segmentation, strain partitioning and microplate tectonics. We study the oblique convergence of the NOAM and CARIB plates between southeastern Cuba to northern Puerto Rico using new swath multibeam bathymetry data and 2D multi-channel seismic profiles. The combined interpretation of marine geophysical data with the seismicity and geodetic data from public databases allow us to perform a regional scale analysis of the shallower structure, the seismotectonics and the slab geometry along the plate boundary. Due to differential rollback between the NOAM oceanic crust north of Puerto Rico and the relative thicker Bahamas Carbonate Province crust north of Hispaniola a slab tear is created at 68.5ºW. The northern margin of Puerto Rico records the oblique high-dip subduction and rollback of the NOAM plate below the island arc. Those processes have resulted in a forearc transpressive

tectonics (without strain partitioning), controlled by the Septentrional-Oriente Fault Zone (SOFZ) and the Bunce Fault Zone (BFZ). Meanwhile, in the northern margin of Hispaniola, the collision of the Bahamas Carbonate Province results in high plate coupling with strain partitioning: SOFZ and Northern Hispaniola Deformed Belt (NHDB). In the northern Haitian margin, compression is still relevant since seismicity are mostly associated with the deformation front, whereas strike slip earthquakes are hardly anecdotal. Although in Hispaniola intermediate-depth seismicity should disappear, diffuse intermediate-depth hypocenter remains evidencing the presence of remnant NOAM subducted slab below central and western Hispaniola. Results of this study improve our understanding of the active tectonics in the NE Caribbean that it is the base for future assessment studies on seismic and tsunamigenic hazard.

Highlights: Caribbean Plate, Hispaniola, subduction, collision, segmentation, strain partitioning.

1 Introduction

The highly oblique convergence between Caribbean (CARIB) and North American (NOAM) plates, as well as the along-strike contrasting structure and thickness of the NOAM incoming lithosphere are thought to be the main driving mechanisms for a complex geodynamics in the northeastern Caribbean with the development of block tectonics and plate boundary segmentation (Fig. 1; e.g., Byrne et al., 1985; Mann et al., 1995, 2002; Jansma et al., 2000; Calais et al., 2002; 2016). This segmentation of the plate boundary leads to a great variability in the tectonic structure along strike, identifying from E to W three well-differentiated tectonic regimes: high oblique subduction without the development of strain partitioning in Puerto Rico (ten Brink and Lin, 2004; Laurencin et al., 2019); oblique collision/underthrusting with the development of strain partitioning in Hispaniola (Mann et al., 1995, 2002; Dolan et al., 1998); and left-lateral strike slip in the Windward Passage and south of Cuba (Calais et al., 1991; Calais and Mercier de Lepinay, 1995). The majority of these studies carried out in the NE Caribbean region were mostly focused

on a single tectonic domain. Regional tectonic studies carried out in the region in the 80s and 90s of the 20th century were mostly based on GLORIA large-range side-scan sonar, initial multibeam echo-sounder systems and widely-spaced and low-resolution seismic reflection profiles (Calais et al., 1991; Dillon et al., 1992, 1996; Dolan et al., 1998). As a result, first order tectonic structures were identified but not all well characterized because of data limitations and coverage. Two questions are still open, such as how the transition between the different tectonic domains takes place and what is the relationship of the along-strike tectonic segmentation observed in the plate boundary and the geometry of the downgoing NOAM slab.

The aim of this study is to investigate and characterize and improve previous interpretations on the first and second order tectonic structures along and across the plate boundary, and their relationship to the slab geometry between western Puerto Rico and eastern Cuba. This subject is addressed by means of the combined interpretation of mostly new marine geophysical data and seismicity and geodetic data from public databases. For this study the compilation of several multibeam datasets has permitted by first time to build a continuous and high-resolution digital elevation model along the plate boundary. The integration of bathymetry data with seismic reflection profiles (mostly from new acquisition), as well as the analysis of the 3D seismicity distribution, focal mechanisms and GPS-derived velocities have allowed us to perform a regional scale analysis of the shallower structure, the seismotectonics and the NAOM slab geometry along the plate boundary. Results of this study would improve our understanding of the tectonics in the NE Caribbean, that it is the base to better asses the seismic and tsunamigenic hazard.

2 Tectonic Setting

The CARIB plate is a small lithospheric plate between the North American and South American plates that moves eastward (70º) at a rate of 18-20 ± 3 mm/yr. (Fig. 1; DeMets et al., 2000; Mann et al., 2002; Calais et al., 2016). The motion of the CARIB plate relative to NOAM plate in the NE Caribbean involves oblique convergence and frontal subduction of the Atlantic oceanic lithosphere under the Lesser Antilles, transitioning to oblique subduction without strain partitioning in Puerto Rico and oblique collision with strain partitioning in Hispaniola, and to

pure strike-slip motion along the southern margin of Cuba (e.g. Calais et al., 2016). The direction of convergence between NOAM and CARIB plates is highly oblique at the plate boundary (≥10º), resulting in the development of a complex tectonic with strain partitioning along the island arc (e.g., Mann et al., 1995, 2002; Calais et al., 2002; ten Brink and Lin, 2004; Jansma and Mattioli, 2005; ten Brink and López-Venegas et al., 2012). Seismological studies and geological observations indicate the existence of microplates and tectonic blocks (e.g., Gonave microplate, Hispaniola block, Septentrional block and Puerto Rico-Virgin Islands (PRVI) block; Fig. 1; Byrne et al., 1985; Reid et al., 1991; Mann et al., 1995; Jansma et al., 2000).

The transition from the Puerto Rico Trench to the Hispaniola Trench is marked by a significant decrease in water depth of the trenches and the change in orientation from E-W to ENE-WSW (Fig. 1). This change is located where the buoyant Bahamas Carbonate Province (BCP) (22-27 km-thick; Dolan et al., 1998) collides with the Hispaniola island arc along a 350-km-long segment (Dolan et al., 1998; Mann et al., 2002; Calais et al., 2002; Pérez-Estaún et al., 2007; Calais et al., 2016). The collision process began in the Eocene and has conditioned every structural, seismological, and sedimentological feature in the northern margin of the CARIB plate (Pindell and Barrett, 1990; Dolan et al., 1998; Mann et al., 2002). This collision produces a slowdown of the subduction process, because the morphology of the banks increases the frictional resistance on the subduction interface, resulting in a collisional margin (Dolan et al., 1998; Pérez-Estaún et al., 2007). Geodetic data show that Hispaniola's motion toward the E with respect to the CARIB plate, is slowed by the collision of the BCP with the NE of the island (Jansma et al., 2000; Calais et al., 2002; DeMets et al., 2010). From N to S there is an increase in the rate of motion and in the eastward component (Calais et al., 2016). This variation indicates that in Hispaniola the accommodation of strain is highly distributed, and the strain is accommodated by the coexistence of sub-parallel structures to the collision margin. The Northern Hispaniola Deformed Belt (NHDB) accommodates the movement normal to the margin and the left-lateral strike slip faults accommodates the displacement parallel to the margin (Septentrional - Oriente Fault Zone (SOFZ) and Enriquillo - Plantain Garden Fault Zone (EPGFZ); Mann et al., 1995;

Dolan et al., 1998). Model slip rates based on GPS-derived velocities in Hispaniola indicates that these faults are all locked (Jansma et al., 2000; Calais et al., 2002). The NHDB are currently accommodating elastic strain at a rate of 1–3mm/yr^{-1} (Deformation front), 10–12mm/yr^{-1} (SOFZ) and 5–7mm/yr^{-1}, respectively (EPGFZ; Calais et al. 2002; Manaker et al. 2008; Calais et al. 2010; Benford et al. 2012; Symithe et al., 2015).

In the NE of the Caribbean, major destructive historical earthquakes (Mw=7.3 at Mona Passage, Mw=7.3 in the Virgin Islands; Reid and Taber, 1919) and with instrumental record (Ms=7.6 at Mona Passage in 1943, Ms=8.1 on the NE coast of Hispaniola in 1946; Dolan and Wald, 1998) have been reported (Fig. 1). Seismicity is clustered near the plate boundary without almost CARIB intraplate events (Engdahl and Villaseñor, 2002). The maximum focal depths exceed 250 km in the subduction zone of the Lesser Antilles, but deep events also occur northern Puerto Rico (150 km) and northeastern of Hispaniola. The majority of the focal depths do not exceed 70 km-deep and most are associated with the large structures developed along the collision margin (NHDB, SOFZ and EPGFZ), highlighting the May 7th, 1842 event with Mw=8.0 (McCann, 2006; Mw=7.8 by Russo and Villaseñor, 1995: Mw=7.6 by ten Brink et al. 2011), the seismic crisis of 1943-1953 with five events of Mw>7.0 and the seismic crisis of 2003 with a main shock of Mw=6.3 and a large aftershock of Mw=5.3 (Dolan and Bowman, 2004) (Fig. 1).

3 Data Collection and Analysis

The study was based on a combined analysis and interpretation of high-resolution multibeam bathymetry data, 2D multi-channel seismic reflection data, seismicity and focal mechanisms and GPS data. Data collected during the NORCARIBE marine geophysical cruise (R/V Sarmiento de Gamboa, 2013) include continuous and high-resolution multibeam coverage of the northern margin of the Dominican Republic area, covering an area of approximately 15,000 km^2, between water depths of -500 and -4,300 m (Fig. 2; Rodríguez-Zurrunero et al., 2019). The processed data was interpolated yielding a regular grid of 30 m-interval. Multibeam bathymetry data of Haiti and eastern Cuba are from HAITI-SIS 1&2 cruises (2012 and 2013) on board the R/V L'Atalante

(Leroy et al., 2015), providing a 25 m-gridded bathymetric map. The eastern region was completed with a 50 m-gridded multibeam data from a compilation of several USGS/NOAA cruises (Andrews et al., 2013). The multibeam bathymetry coverage has been completed with the GEBCO Digital Atlas with a 30 arc-second of resolution (Weatherall et al., 2015), and onshore data is from the SRTM mission with a 30 m of resolution (Far and Kobrick, 2000; http://edc.usgs.gov/). All datasets were merged to build for the first time a continuous and high-resolution digital elevation model along the plate boundary.

For this study we have mostly used new 2D multi-channel seismic reflection data recorded during NORCARIBE and HAITI-SIS 1&2 cruises and old seismic data in western Puerto Rico Trench from IG1503 cruise, provided by the Academic Seismic Portal managed by University of Texas-Institute for Geophysics (Christeson et al., 2017). In NE Hispaniola we used single-channel profiles from the MW8908 cruise (Dolan et al., 1998), but in this study most of them are just referenced since they were already interpreted in Rodriguez-Zurrunero et al. (2019). In this study we show a re-interpreted seismic profile of the most representative line from the MW8908 cruise (Fig. 3). The multi-channel seismic profiles of NORCARIBE were acquired with ten GGUN-II® guns with a total volume of 1750 c.i. submerged at 5 m, firing at 37.5 m shooting interval. The recording system consisted of a 3000 m-long digital streamer, with 240 channels regularly spaced at 12.5 m. Processing of NORCARIBE seismic data includes swell noise filtering, linear noise deconvolution, detailed velocity analysis, Surface-related multiple elimination (SRME) and Dip-moveout (DMO) demultiple stack, prestack time migration and stacking. The multi-channel seismic profiles of HAITI-SIS 1&2 cruises were acquired with a source comprising two GI air guns (2.46 L, 150 c.i.) and with a streamer with a 600 m-long streamer with 24 traces operated at an approximate speed of 9.7 knots (Leroy et al., 2015). Processing of HAITI-SIS 1&2 seismic data included CDP gathering (6-fold), binning at 25 m, detailed velocity analysis, stack and post-stack time migration. The multi-channel seismic data of the IG1503 cruise (1975) were acquired using 3 Bolt 4200 air-gun array with a total volume of 73,74L and 24 channels (Ladd et al.,

1977). Processing of IG1503 seismic data included demultiple, CDP sorting, band-pass filtering (corner frequencies 12 and 45 Hz), and AGC scaling with a 500-ms window (Ladd et al., 1981).

Earthquake epicenters were sourced from the Bulletin of the International Seismological Centre (ISC Bulletin; http://www.isc.ac.uk/iscbulletin/), filtered by magnitude > 3.5 and dates between 1900 and 2018. The historical earthquakes in the study area come from the Reviewed ISC Bulletin, which is manually checked by ISC analysts and relocated. CMT focal mechanism solutions correspond to the Harvard Global CMT catalogue (www.globalcmt.org) between 1976 and 2019. Long term GPS velocity field solutions from UNAVCO (https://www.unavco.org) given in the North American referenced frame (NAM08). Solutions are from the most recent "snapshot" velocity solution, generated approximately monthly (May, 2019).

4 Domains characterization

Tectonic setting in northern Caribbean is complex because of the oblique convergence between NOAM and CARIB plates and the significant along-strike changes in crustal thickness of the NOAM incoming plate. We have divided the study region into five tectonic domains from E to W (Fig. 3): a) Oblique Subduction Domain (OSD), northwest Puerto Rico; b) Oblique Collision Domain (OCD), north-east Hispaniola; c) Oblique Underthrusting Domain (OUD), north-central Hispaniola; d) Left-Lateral Strike-Slip Domain (SSD) north Haiti and; e) Northern Cuba Collision Domain (NCD).

The data analysis and interpretation of each domain is primarily based on new high-resolution bathymetric and multichannel data (i.e., shallow crustal structure) and then integrated with the spatial analysis of seismicity, CMT focal solutions and GPS-derived velocities (i.e., seismotectonics and kinematics).

4.1 Oblique Subduction Domain (OSD)

The OSD is located at the eastern part of the study area, between longitudes 68.5ºW-67.2ºW (Fig. 3). The singular characteristic of this tectonic domain related to the other studied domains is that the thicker (continental or transitional?) crust of the Bahamas Carbonate Province (BCP) is not

involved at the present in the oblique convergence between the NOAM and CARIB plates (Fig. 3, Fig. 4). Mann et al. (2002), and Mondziel et al. (2010) suggested that the BCP continues SE into the forearc (e.g. the Mona Block), which they defined it as an asperity that cannot be subducted (Fig. 3). Thus in the OSD, flat-bottom Nares Abyssal Plain (NOAM oceanic crust) is being subducted beneath the island arc very obliquely (250º; McCann et al., 1982; Sykes et al., 1982; McCann & Haberman, 1989; DeMets et al., 2000; Calais et al., 2016). The combination of the high-resolution bathymetry and multichannel seismic data together with seismicity and GPS data allow the detailed analysis of the three main tectonic regions of this domain: the Outer-trench wall, the Puerto Rico Trench and the northeastern Hispaniola forearc (Fig. 3).

4.1.1 Shallow structure of the OSD

4.1.1.1 Outer-trench wall

Along the entire outer-trench wall of the western end of Puerto Rico Trench, bathymetry data shows collapsed blocks of Navidad Bank and a rough seafloor evidencing widespread areas of mass-wasting processes associated to intense faulting (frequent structural seafloor escarpments) (Fig. 4 and Zoom 4 in Fig. 5; App B). These features were firstly noticed by ten Brink et al. (2004) from multibeam seafloor mapping and were interpreted as main sediment sources for the elongated basin developed along the axial zone of Puerto Rico Trench. The outer-trench wall deepens towards the south from 5300 m-deep in the outer rise to 8300 m-deep of the axis of the Puerto Rico Trench (Figs. 4 and 5). Based on submersible dive samples, Le Pichon et al. (1985) estimated a subsidence rate of 1cm/yr. in this area (6000 m of subsidence in 600k years). Bathymetric escarpments are mainly NE-SW trending, are 5-12 km-spaced and have vertical steps of 150-300 m that becomes smaller to the east (Fig. 4; App. A). These structural escarpments are the result of recent south-dipping normal fault activity that locally allow to outcrop the oceanic basement of the NOAM plate (Zoom 4 in Fig. 5).

4.1.1.2 Puerto Rico Trench

The axial region of the western Puerto Rico Trench is sub-parallel to average NOAM-CARIB plate convergence vector (Fig. 3) and consists of an almost featureless, flat-bottomed and

elongated bathymetric depression of 10-15 km-wide, with depths averaging 8300 m (Figs. 2 and 4; App B). To the west this elongated bathymetric depression becomes progressively narrower and abruptly disappears where the seafloor-depth sharply decreases connecting with the eastern end of the Hispaniola Trench (8300 m-deep at Puerto Rico Trench to 5600 m-deep at eastern Navidad Basin; see the axial bathymetric profile in Fig. 3 and Fig. 4).

Seismic data shows that the sedimentary fill of the Puerto Rico Trench consists of sub-horizontal levels characterized by continuous, tightly spaced and high-amplitude reflectors, reaching 0.7 sTWT of turbidite sedimentary thickness (Zoom 3 in Fig. 5). The turbidite filling is onlapping to the north over the NOAM faulted and tilted oceanic blocks. Below the turbidite infill of the Puerto Rico Trench, the south dipping basement reflectors of the top of the oceanic blocks of NOAM plate, can be inferred (Fig. 5). Near the compressive deformation front, the sedimentary filling is being progressively deformed by imbricate blind thrust faults, forming narrow and smooth E-W trending anticlines ridges on the seafloor, suggesting active accretion driven by subduction (Zoom 3 in Fig. 5).

4.1.1.3 Northeastern Hispaniola forearc

The OSD forearc comprises the transition from Hispaniola forearc to Puerto Rico forearc (Fig. 3) along the northern slope of the Mona Passage. The offshore OSD forearc includes the Insular Shelf and the Insular Slope which are separated by a concave break slope (Figs. 3 and 4). In turn, based on sedimentological, structural and morphological (slope) criteria, we have subdivided the Insular Shelf and the Insular Slope. The Insular Shelf have been divided into a proximal and distal zones also limited by a break slope (Fig. 4 and Zoom 1 in Fig. 5; App B). Due to the structural complexity of the Insular Slope, we subdivided it into three zones for better analysis: the upper slope, the middle slope and the lower slope (Fig. 4). The boundary between the upper-middle and middle-lower slopes are marked by two major structural features: the SOFZ and the BFZ (Fig. 4). Furthermore, the Insular Slope has two singular morphostructural features (the Mona Rift and the Mona Block; Fig. 4) which confer distinctive tectonic characteristics to this part of the forearc

and are different from the forearc north of Puerto Rico. The distinctive tectonic of this area will be discussed in the discussion section.

The Hispaniola Insular Shelf covers a large area, reaching 85 km. It consists of a Late Miocene-Present carbonate platform (de Zoeten and Mann, 1999, and references therein). The proximal shelf is characterized by a fairly flat carbonate shelf, up to 100-120 m water-deep. Seismic data shows a featureless fill of 0.2 sTWT-thick, composed of continuous, parallel, closely spaced, high-amplitude reflectors that become transparent with depth (Fig. 5). The distal shelf is characterized by an uniform tilting (~2-3º) towards the N-NW with water depths up to 800 m. In this zone, the seismic profile shows a sedimentary infill of 0.4-0.6 sTWT-thick and is mainly composed of continuous, more irregular and spaced, high-amplitude reflectors that goes deeper to a chaotic succession of discontinuous and low-amplitude reflectors (Zoom 1 in Fig. 5A). The processes of tilting and collapse observed in the distant shelf seems to be similar to the observed the Oligo-Pliocene carbonate platform north of Puerto Rico (i.e., east of Mona Rift) since Middle Pliocene (Moussa et al., 1987; ten Brink, 2005; Grindlay et al., 2005a, b). The driven mechanism for such tilting and collapse was attributed to several processes: collision of the NOAM and CARIB slabs in depth (e.g., van Gestel et al. 1998), to the BCP sweeping sideways under the forearc (Mann et al., 2002; Grindlay et al., 2005a, b; Mondziel et al., 2010) and only to the collapse or retreat of the undergoing NOAM slab in this area (ten Brink, 2005).

The Upper Slope of the Forearc extends from the Insular Shelf edge to the E-W main trace of the SOFZ to the north (slope break, ~3500 m-deep; Fig. 2, Fig. 4). It consists of a series of N-tilted blocks, divided by E-W trending north-dipping normal faults (Fig. 4, Fig. 5). The seismic profile (Fig. 5) shows a seismic continuity and lateral coherence with the reflectors of the distal Shelf, suggesting that the upper slope is the highly deformed and collapsed part of the shelf.

The Middle Slope consists of a wide area (~50 km) between 3500-7000 m water-deep limited to the south by the SOFZ and to the north by the BFZ (Fig. 5) .The SOFZ that can be followed from the west, along the south coast of the Samana Peninsula, to the east along the south wall of Mona Block (Fig. 4).The main trace of the SOFZ shapes an E-W trending structural depression with a

mean bathymetric scarp of 400 m (Figs. 2 and 4). South of the Mona Block the SOFZ conforms a highly incised submarine valley with a vertical bathymetric step of 1000 m (Figs. 2, 4 and 5). Bathymetry data as well as the reflection seismic profile show the horsetail play of the BFZ in its western termination, with several SW-NE trending oblique faults, giving an anastomosed morphology and forming an associated 30 km-width NE-SW trending transpressive belt composed by sequences of S-shaped ridges parallel to the faults (Figs. 4 and 5). Also elongated basins associated to branches of the BFZ have been identified (e.g., Maimon Basin in Fig. 4). Ten Brink and Lin, (2004) previously interpreted these structures as deformation due to the feathered termination of BFZ. The fault branches generally do not seem to disturb the main SOFZ trace that appears to be continuing undisturbed farther to the east, until Mona Block .All these features evidence the left-lateral strike-slip component of the BFZ and the associated structures (Figs. 4 and 5).

The Lower Slope covers a narrow area (20 km-width) between 7000-8300 m water-deep and is bounded to the north by the Puerto Rico Trench and to the south by the BFZ (Figs. 2 and 4). This area has a smooth relief and a gentle average slope (~5º; App. A), except in the BFZ, where it forms a strip of E-W trending anticline ridges in its northern block. These ridges seems to be the surface expression of an associated transpressive belt (Figs. 4 and 5), but limited resolution of the seismic data precludes to observe the internal structure of the ridges.

We have also analyzed the two singular morphostructural features (the Mona Rift and the Mona Block.

a) The Mona Block is a 42 km x 60 km high standing carbonate structure that rises up to 6.5 km above the surrounding seafloor (relative to the Mona Rift seafloor), reaching a minimum water depth of 966 m (Figs. 2 and 4) giving a lenticular map-view shape (Fig. 4). Inside this feature, two areas can be distinguished: The Upper Mona Block and the Collapsed Mona Block.

- The Upper Mona Block, a shallower area, located to the south, which forms a narrow and elongated E-W trending ridge of 13 km-width that extends off and deepens towards

the E, intersecting the Mona Rift (Fig. 4). The Upper Mona Block was interpreted by Mondziel et al. (2010) as a region of post- Pliocene uplift because of the observed back- tilting of seismic reflectors and onlapping of sedimentary cover. Seismic profiles (e.g., Figure 12 in Mondziel et al., 2010) and dredges (Fox and Heezen, 1975; Perfit et al., 1980) show that this shallow part of the Mona Block consists of a carbonate platform that overlays an uplifted Cretaceous Blue Schist terrain composed of banded black marbles, siltstone and micaceous marble. Fox and Heezen, (1975) and Perfit et al. (1980) on the basis of core samples taken in Upper Mona Block and in the Middle Slope (Fig. 4), suggested that the Mona Block is a piece of a continuous strip of uplifted blue schist terrains with black marbles related to the obduction of carbonate materials in the forearc derived from the BCP during the Cretaceous subduction. In contrast, Mann et al. (2002), and Mondziel et al. (2010) suggested that the Mona Block is the southeastern end of the BCP trying to subduct.

- The Collapsed Mona Block (Fig. 4), a 30 km-width deeper area, located to the north, formed by down-dropped carbonate blocks limited by E-W trending oblique normal faults (Fig. 4; Figure 12 in Mondziel et al., 2010). These faults laterally displace the blocks forming Z-shaped ridges (Inset in App B). The Collapsed Mona Block seems to be the result of the rapid subsidence of the Mona Reentrant and the Trench, where the carbonate layers have been tilted and slumped down.

b) The Mona Rift is a roughly north-south trending depression of approximately 40 km-long, an average of 15 km-wide and 2-3.5 km-deep relative to the surrounding seafloor (Fig. 4). The Mona Rift separates Hispaniola and Puerto Rico forearcs (Fig. 3) and probably accommodates minor E-W extension between Hispaniola and Puerto Rico (ten Brink et al., 2004). Based on observations made by Lopez-Venegas et al. (2008) and ten Brink et al. (2004), the Mona Rift NW of Puerto Rico consists of three en-echelon depressions (5000, 7800, and 8150 m of water depth; Mona Rift and Mona Reentrants 1&2; Fig. 4) that extend almost to the BFZ. Extension rate across the predominantly north–south rift has been estimated to be up to 5±4 mm/yr. (Jansma et al., 2000). Chaytor and ten Brink, (2010)

suggest diagonal opening at N55°E which is backed by GPS-derived velocities. Previous studies show that the Mona Rift is the surface expression of a half-graben structure (Mondziel et al., 2010) in which the eastern wall has a steeper slope that the western wall. However, bathymetry and slope data show that the upper part of the western wall is steeper than on the east (App. A). The apparent gently slope seen by Mondziel et al. (2010) in the western wall may be dominated by a series of landslide debris.

4.1.2 Seismicity and kinematics of OSD

In the study area (western end of Puerto Rico Trench), the dip of the NOAM subducting slab is greater than towards the east (ten Brink et al., 2005), dipping 30º to a depth of 100 km (Fig. 7a). Intermediate-depth seismicity below the Puerto Rico Trench (Fig. 7a) indicates that high normal faulting and widespread mass-wasting processes and collapsed blocks along the entire outer-trench wall were suggested to be a consequence of the high dipping angle of the NOAM subducting slab in this area (ten Brink, 2005). The high dipping angle causes a high curvature in a thin oceanic crust resulting in bend-faulting and associated mass-wasting processes in the subducting slab closer to the trench (e.g., Jones et al., 1978). This process is similar to that observed in other high angle subduction areas (Chile: Contreras-Reyes and Osses, 2010; Mariana Trench: Emry et al., 2014; Nicaragua: Ivandic et al., 2008; Japan: Kobayashi et al., 1998). The high dip angle of the relative thin of the downgoing NOAM oceanic slab (Fig 7a) results in low plate coupling in this area. The low plate coupling means that there is no strain partitioning in this area which, together with the high obliquity of the convergence in this area (Fig.3) leads to a wide region of transpressive tectonics.

Interplate hypocenters recorded in the OSD forearc shows the NOAM slab geometry, with shallow earthquakes with depths <35 km near the trench that progressively deepens towards the south, reaching 200 km depth (Fig. 6 and Fig. 7a, b) and evidencing the active subduction of the NOAM oceanic crust beneath the island arc (Masson and Scanlon, 1991; McCaffrey, 2002; Calais et al., 2016; Meighan et al., 2013). Focal mechanisms from interplate earthquakes show almost pure reverse component with NW-SE nodal planes (Figs. 6 and 7b). Majority of shallow

earthquakes in the forearc (<35 km) are overriding events which are clustered in the SOFZ trace near the Mona Block and less frequently in the BFZ (Fig. 6). These suggest that the accommodation of the deformation in the overriding plate occur mainly in the SOFZ and secondarily in the BFZ by oblique thrust faults associated to the transpressive belt. Also there is a N-S linear cluster of shallow earthquakes in the Mona Rift with an associated focal mechanism with pure normal component showing NW-SE extension (Fig. 6). The average velocity derived from GPS of Mona Passage relative to NOAM (Fig. 3) is 10-13 mm/yr. in direction 64º. This trending is oblique to the plate boundary and agrees with the occurrence of thrust faults interplate earthquakes with nodal planes perpendicular to the convergence direction and with little strike-slip component.

In the western end of Puerto Rico Trench (between 67.5ºW-69.0ºW; Fig. 6) there is cluster of intermediate-depth earthquakes (>70 km; Fig- 7b). Localized mid-depth seismicity as well as the abrupt change in depth of the trench toward the W could indicate that between the subduction and collision domains would be an active vertical slab tear. Intermediate-depth seismicity clusters associated with a slab tear are found in other locations with similar tectonic processes: in the northeast Caribbean (ten Brink et al., 2005; Meighan et al. 2013), Alboran Sea (Buforn et al., 2004), the southern end of the Lesser Antilles (Clark et al., 2008), in the northern Andean Margin (Gutscher et al., 1999) and the northern end of the Tonga trench (Millen and Hamburger, 1998). Also, the slab tear marks the change in crustal thickness of the NOAM plate, from the thin oceanic NOAM crust at Nares Plain to a thicker NOAM crust in the BCP. Tear faulting at along-strike changes in the subducting slab, from oceanic crust to thickened transitional/continental crust was observed in the North Andean Margin where the Carnegie Ridge has been colliding with the margin since at least 2 Ma (Gutscher et al., 1999). In Fig. 7b is shown the interference between the two geometries of the subducting slab both sides of the tear fault, showing that to the west the slab shallows, where it dips 10º. The geometry of the interpreted subducted slabs (dashed black lines) matches with that modeled by Hayes et al. (2018) (dotted red lines in Fig. 7b).

However, earthquake locations in this area are very poor, especially before the early 2000s making the Benioff zone geometry unreliable.

A slab edge at similar location was previously suggested by van Benthem et al. (2013 and 2014) based on regional tomography data and mechanical modelling. Harris et al. (2018), based on tomographic P-wave model of the upper mantle, proposed a slab tear in the Mona Passage down to a depth of ~300 km and with 100 km wide. They related the slab tearing with the presence of microplates at the northern boundary of the CARIB plate. They suggest that the presence of microplates facilitate differential trench retreat/rollback, which results in slab segmentation tear.

4.2 Oblique Collision Domain (OCD)

The OCD is characterized by high-standing carbonate spurs which are obliquely indenting into the island arc at the seafloor surface (Fig. 3). That indicates that the thicker crust of the BCP cannot truly subducts beneath the CARIB plate (Dolan et al., 1998; Rodríguez-Zurrunero et al., 2019).

4.2.1 Shallow structure of the OCD

4.2.1.1 Eastern Bahamas Carbonate Province

The OCD is occupied by the eastern end of the BCP, mostly represented by Silver, Santisima Trinidad and Navidad banks (Fig. 4; App B and C). The carbonate banks are obliquely impinged into the island arc, forming an almost continuous 175 km-wide collision strip (Dolan et al., 1998). Due to the collision, the southern slope of the banks has suffered great erosion and dismantling, showing a terraced morphology as the result of a strong S-dipping normal bend-faulting (Rodriguez-Zurrunero et al., 2019). The fault trending changes counterclockwise, from E-W trending in the Silver Spur to an SW-NE trending in its eastern termination and connecting with the outer-trench wall structures of Puerto Rico Trench (Fig. 4, App B). This change in the orientation of the faults match with the slab tear and would be related to the varying of the subduction dip angle and crustal thickness between the NOAM oceanic and NOAM BCP. The amount of vertical fault throw is variable, from tens to hundreds of meters, showing greater

vertical throw farther from the plate boundary, locally allowing the outcrop of the carbonate basement (Figs. 9, 11 and 12 in Rodriguez-Zurrunero et al., 2019). The parallelism observed between the structures in the BCP and the plate boundary points out that these faulting is the result of the bending of the incoming plate (Rodriguez-Zurrunero et al., 2019), as we observed in the OSD and similar to those well-documented in many subduction settings (e.g., Jones et al., 1978; Hilde, 1983 and references therein; von Huene and Culotta, 1989). The bending-associated faulting is intersected by SSW-NNE trending morphological scarps (Fig. 4). These scarps laterally bound the banks and define the passages between them. The bank's bounding scarps and the channels have had structural control which are interpreted by Mullins et al. (1992) as ancient structures inherited from an Early Cretaceous rifting stage of the North Atlantic. This could be a first-order mechanism for the bank segmentation and basin physiography in the southeast BCP (Freeman-Lynde and Ryan, 1987). Currently, these inherited structures act as transverse fault of the incoming plate, which would play a significant role in accommodating the along-strike change in the plate coupling, the amount of shortening or the stress fields because of the transition between subduction in the Puerto Rico Trench to a collision/underthrusting towards the W (Fig. 4; Dolan et al., 1998; Rodriguez-Zurrunero et al., 2019).

4.2.1.2 Eastern Hispaniola Trench

In the OCD the Hispaniola Trench is composed by an alternation of bathymetric highs and lows deepening from W to E, from 4500 m-deep in the Santisima Trinidad Basin to 8350 m-deep in the Puerto Rico Trench (axial profile in Fig.3). The highs correspond to the Bahamas carbonate spurs that are impinged into the Forearc and the lows are occupied by isolated and E-W trending elongated basins with a turbiditic fill of 1.5-2.0 sTWT-thick, similar to those observed in the NOAM north of Puerto Rico (Fig. 4; Figs. 15 and 16 in Rodriguez-Zurrunero et al., 2019). The bathymetric steps (highs) to the E between trench basins match with the transverse tear faults on the Navidad and Santisima Trinidad flanks (Fig. 4, App B), both adjusting the huge difference in water depth between the Puerto Rico and the Hispaniola trenches (~4150 m difference, Fig. 2) and crustal thickness. Under the turbiditic fill of the trench basins, can be inferred a stepped

southward dipping basement from the Bahamas Banks (Figs. 11, 12 and 16 in Rodriguez-Zurrunero et al., 2019).

4.2.1.3 Northeastern Hispaniola Forearc

According to its morphostructural features, two areas are distinguished (Fig. 4):

a) The Middle-lower Forearc, located between the elongated basin (BFZ) and the deformation front (2600-4500 m water-depth), in which the Northern Hispaniola Deformed Belt (NHDB) is developed. Here, the NHDB does not have seafloor morphological expression, and is only inferred in the middle slope by a series of 3-4 NW-SE trending anticline ridges (Figs. 4 and 9). These ridges are very limited in width and length, reaching only 1-2 km-width and 8-10 km-length along-strike. Seismic profiles show that the NHDB is covered by a thick blanket of slope sediments that covers an inactive N-verging imbricate system (Fig. 9). The lower slope shows a gentle slope locally affected by widespread slumped area (Fig. 4; App. A). The imbricate system locally has incorporated carbonate material from the southern flank of the BCP evidencing the offscraping and accretion process (accreted carbonate block in Fig. 12 in Rodriguez-Zurrunero et al., 2019).

b) The Upper Forearc covers 35 km-width is located between an elongated E-W trending >1 sTWT-thick slope basin to the north and the SOFZ onshore which comprises an almost non-existent Insular Shelf, only represented in Bahia Escocesa (averaging 5 km-width). A submersible dive 55 km east of Samana Peninsula encountered white, gray and black marble extremely fractured by two vertical fracture sets (Heezen et al., 1985; Fig. 3), similar to those found E in the Mona Block (Fox and Heezen, 1980; Fig.3). The Camu Fault Zone (CFZ) was defined as a major left-lateral strike-slip fault that runs parallel to the SOFZ (Fig. 4; Pindell and Draper, 1991). It is not known if the CFZ has experienced Quaternary movement (Pindell and Draper, 1991), but Draper and Nagle (1991) suggested that the CFZ has accommodated at least 60 km of left-lateral strike-slip motion since Eocene time. The CFZ merges eastward with the NW trending oblique reverse faults southwest of the La Cabrera Promontory and may ends at the Nagua Lineament (Fig. 4). North of the CFZ is the Cabrera Promontory (Fig. 4), 11 levels of marine terraces which

have suffered continuous uplift and southward-tilting since the Lower Pleistocene (Diaz de Neira et al., 2017). The high uplifting of the Cabrera Promontory would be directly related with the indenting of the Silver Spur (Fig. 4). Between the Septentrional Cordillera and the Samana Peninsula there is a flat marshly lowland. It is limited to the east with the SW-NE Nagua Lineament, interpreted by Dolan et al. (1998) as a transtensional transfer fault. Dolan et al. (1998) speculated that the Nagua Lineament continue to the northeast and connects with a S-dipping reverse fault with significant reverse strike-slip component that bound the elongated slope basin. They suggested that this offshore structure could be the source of the August 4th, 1946 tsunami. However, Rodriguez-Zurrunero et al. (2019) precludes the offshore-onshore continuity of the Nagua Lineament.

4.2.2 Seismicity and kinematics of the OCD

Seismicity map shows higher occurrence of crustal earthquakes (<35 km) mainly concentrated along an NW-SE trending band between the compressive deformation front and the SOFZ (Fig. 6). There have been no records of focal mechanisms in OCD since 1976. The only known focal mechanisms from the 1946 and 1948 seismic crisis (Dolan and Wald, 1998) which corresponds with shallow (<15 km) E-W trending nodal planes sub-parallel to the plate boundary: a low angle nodal plane dipping to the south and a sub-vertical nodal plane. These mechanisms would be related to the accommodation of convergence at the collision-subduction interface (detachment) and/or to active thrust faults into the NHDB (Dolan et al., 1998). The absence of significant instrumental earthquakes may be related to a quiet period caused by stress relaxation after the high magnitude (max magnitude recorded: M = 8.1 in 1946 earthquake; Dolan et al., 1998) 1943-1953 seismic crisis. GPS-derived velocities north of SOFZ, in Samana Peninsula and Septentrional Cordillera, shows 2 to 4 mm/yr. motion toward 45º-60º relative to the North American plate (Fig. 3). This strike is almost perpendicular to the plate boundary and agrees with the occurrence of historic seismic crisis of 1946 with pure thrust fault focal mechanism in the Septentrional Block and the NHDB. This different GPS vectors (convergence rate and direction) form observed south of SOFZ was interpreted as a result of a very high plate coupling due to high

thickness and buoyancy of the BCP (Calais et al., 1991; Calais et al., 2002; Jansma et al., 2000; Mann et al. 2002; De Zoeten and Mann, 1999). However, south of the SOFZ, GPS-derived velocities show a 7-9 mm/yr. motion towards 070-080º relative to the NOAM plate. This orientation is similar to GPS vectors in the Mona Passage and parallel to the NOAM-CARIB plate convergence direction. Many authors indicated that this area is characterized by the active collision process of the BCP transitional crust with the Septentrional Block in a strain partitioning model (Dolan et al., 1998; Calais et al., 2002; Mann et al., 2002). In this model the Septentrional Block (NHDB, Samana Peninsula and Septentrional Cordillera) accommodates the vertical component perpendicular to the plate boundary due to the collision process whereas the SOFZ accommodates the movement to the E of the Hispaniola Block. This model is consistent with GPS data north the SOFZ and higher occurrence of crustal earthquakes (Figs. 3 and 7c), and also large magnitude historical earthquakes with pure thrust fault mechanism evidences high plate coupling due to the active indenting of the Silver Spur and Navidad Bank, and the subsequent uplift of the Cabrera Promontory and the Septentrional (Diaz de Neira et al., 2017; Mann et al., 199).

Gaps in intermediate-depth seismicity is common in locations where an oceanic plateau or other buoyant structural high collides with the trench (McCann et al., 1979). However, in the OCD there is a cluster of mid-deep seismicity (50-175 km) that disappears towards the W (Fig. 6, 7c, and 8g). The cluster of mid-depth seismicity in this area would be expression of the vertical slab tear (which comprises a rupture area) between NOAM oceanic and NOAM BCP (described in the previous section) or/and that the relative thinner crust of the southeastern edge of the NOAM BCP is still actively subducting beneath the CARIB plate but with a relative lower dip (15º; Fig. 7 b and c).

4.3 Oblique Underthrusting Domain (OUD)

The OUD is defined as the tectonic domain where there is a well-developed, thicker and continuous basin along the western Hispaniola Trench. The development of a relatively wide trench means that the high-standing spurs of the BCP are farther away from the deformation front

and are dipping beneath the turbiditic fill of the Hispaniola Trench and the Forearc (Fig. 3). Its eastern boundary is where the Silver Spur impinges into the IM in the vicinity of La Cabrera Promontory, and to the west in the azimuth change of the Deformation Front changes to an E-W trending at 72.3ºW (Fig. 10).

4.3.1 Shallow structure of the OUD

4.3.1.1 Central Bahamas Carbonate Province

The OUD is occupied by the Mouchoir Bank which consists of an irregular morphology formed by a succession of salients (or spurs) and bankward amphitheater morphologies (or scallops; Mullins and Hine, 1989; Rodriguez-Zurrunero et al., 2019) (Figs. 3 and 10, App C). Although high-resolution multibeam bathymetry data only covers the southern slope of Mouchoir Bank, it can be inferred from altimetry-derived satellite data (GEBCO) that the SW slope facing the Caicos Basin has the same morphology (Figs. 3 and 10). As in the OCD, structural escarpments parallel to the convergent margin are south-dipping recent normal faulting resulting from the bending of the incoming plate (Zoom 1 in Fig. 12). Erosive escarpments are very sinuous and longer, higher and more frequent in the middle and upper slope than the lower slope (Fig. 10, App. A). The seismic profile located to the west allows to observe that the NE-SW trending elongated spur continue below the Caicos Basin and probably below the Deformation Front (Fig. 11).

4.3.1.2 Western Hispaniola Trench

In the OUD, the Hispaniola Trench is represented by the Hispaniola Basin which opens to the west at longitude 71.8ºW to form the Caicos Basin (Fig. 3). The Hispaniola Basin consists of a NW-SE trending sinuous featureless, elongated, flat-bottomed depression with average water depth of 4200 m (Figs 2 and 3; Rodriguez-Zurrunero et al., 2019). The width of the Hispaniola Basin is variable and is conditioned by the irregular morphology of the Bahamas Banks. To the E, The Hispaniola Basin is interrupted by the Silver Spur where the water depth decreases to 2500 m and producing a bathymetric step of 300 m compared to the trench basins of the OCD (axial profile in Fig. 3). The sedimentary fill of Hispaniola and Caicos basins consists of horizontal to

sub-horizontal turbiditic infill with at least 2 sTWT-thickness defined by at least 2 seismic units (Figs. 11 and 12; Rodriguez-Zurrunero et al., 2019). In the southern part of the basins, turbidite layers are progressively tilted towards the N, folded and finally incorporated into the NHDB (Fig. 13).

4.3.1.3 Northern Hispaniola Forearc

The OUD is characterized by the variable development of the NHDB: a well-developed north-verging imbricate fold and trust system formed by a sequence of fold-propagation faults (Figs. 9, 12 and Zoom 2 in Fig. 13; Rodriguez-Zurrunero et al., 2019). But, the along-strike development of the imbricated system as well as the number of anticline ridges is very variable along the margin (Fig. 10, App C). The NHDB is formed by an along-strike succession of broad salients (up to 25 km-width) where there is a well-developed deformed belt (e.g. south of Caicos Basin) and narrow recesses where anticline ridges are difficult to observe (Fig. 10). The alternation of salients and recesses have been interpreted in many imbricate thrust belts as consequence of differential sediment accretion and/or the topography of the incoming plate (e.g., Scholl et al., 1980; Dominguez et al., 2000; Marshak, 2004; Granja-Bruña et al., 2009). Seismic profile of Fig. 13 show the most representative section of the offshore forearc in the OUD which allowed us, based on structural criteria, to distinguish three parts (Fig. 13): a) the lower forearc in which the frontal part of the accretionary prism of the NHDB is developed. It is composed of low-angle thrust faults and duplex (Zoom 2 in Fig. 13). Locally, back thrusts are developed shoreward of frontal ridge forming a triangular zone. b) In the middle forearc is developed the upper part of the NHDB, in which the imbricated system is rising vertically and becomes inactive. Thrust faults are covered by modern slope sediments and can only be inferred by overlying north-verging anticline ridges. c) The upper forearc where the NHDB disappears. It shows an irregular flat-topped seafloor intersected by the SOFZ and forming a transpressive belt (Zoom 1 in Fig. 13).

The upper slope, northeast and east of Tortue Island, shows a well-developed incised canyon whose headers are laterally displaced (5-18 km) and occasionally disconnected from the northern margin of Haiti by the action of the left-lateral strike-slip SOFZ (Fig. 10). This shift of canyon

networks near Tortue Island was previously observed by Leroy et al. (2015) which calculated an offset of 16.5 km.

In this area, east of Tortue Island, there is a change in the morphology of the seafloor and in the internal structures of the forearc. The lower slope is steeper (App. A), and has a more diffuse and narrower imbricated system (Figs. 10 and 11), although it still well-developed, unlike the SSD as will be seen in the next section. The greatest change is recorded in the upper slope, which presents a very irregular seafloor, giving a karst morphology (Figs. 10 and 11; Leroy et al., 2015). The internal structure shows a sedimentary filling of up to 0.8 sTWTs slightly deformed forming soft ripples. These rippled reflectors are intersected by small faults. Oliveira de Sa, (2019) relates the formation of this morphology called "honeycomb" with these fractures suggesting that the current sedimentary infill would be constituted by impermeable carbonate materials similar to that found onshore near Monte Cristi. Differential compaction would explain the rippled geometry of the sedimentary infill and would cause the upwards migration of fluids from the lower sequences through the fractures, causing the dissolution of the seafloor carbonate materials. It also suggests that the fractures could be the fault planes of a creeping process, which would result in the rippled morphology. Similar dissolution morphologies along with internal creeping of the sedimentary infill have been found in Carnegie Ridge (Michaud et al., 2018). Beneath the current sedimentary infill there are numerous reverse blind faults which one in the middle slope could act currently as transcurrent blind faults since the canyon networks show slightly laterally displacement (Figs. 10 and 11). The mapped transcurrent blind fault could be the inactive extension towards the W of the SOFZ Dominican segment and may play an important role in the strain partitioning in this area, thus accommodating some of the lateral component of oblique convergence.

4.3.2 Seismicity and kinematics of the OUD

In the OUD, intermediate-depth seismicity almost disappears and crustal seismicity (<35 km) is dominant, and is concentrated between the deformation front and the Cibao Valley (Fig. 6). Earthquake epicentral distribution shows a shallow subducted slab where it dips averaging 10º.

Together with the total absence of intermediate-depth seismicity suggesting the disappearance of the subduction of the NOAM by changing to an oblique collision/underthrusting process of the NOAM thickened Bahamas with the island arc (Fig. 8d). Focal mechanisms in this area corresponds to the 2003 seismic crisis north of Puerto Plata (Dolan and Bowman, 2004). This focal mechanisms are from interplate shallow earthquakes (15 km-depth) with pure reverse component and E-W trending nodal plane dipping to the south and are directly related to the underthrusting interface or the active mega-thrusts of the NHDB (Figs. 6 and 8d). GPS-derived velocities relative to NOAM north of SOFZ, shows 2 to 4 mm/yr. with a strike almost perpendicular to the plate boundary. This agrees with the 2003 historic seismic crisis with pure thrust fault focal mechanisms in Puerto Plata. These facts show that most of strain is accommodated by reverse faulting sub-parallel to the deformation front and related to the NHDB and the Septentrional Block in a strain partitioning model with high coupling. South of the SOFZ, GPS-derived data shows a motion rate of 7-9 mm/yr. sub-parallel to the trace of the SOFZ (70º-80º; Fig. 3). However, paleoseismological studies showed that the SOFZ has not caused any significant earthquakes in the last 900 years (Prentice et al., 2003). Highly relevant is the lack of shallow earthquakes with associated left-lateral CMT solutions in the vicinity of the SOFZ (Fig. 6). Only two focal mechanisms of transcurrent component are found, but at greater depths (30-50 km-depth; Fig. 8d and e). The near absence of focal mechanism of transcurrent component suggest that the accommodation of the E-W component of displacement would be aseismicaly. An alternative explanation was suggested by ten Brink et al. (2011, 2013). According to these papers the 1562 and 1842 historical earthquakes ruptured the SOFZ, and the recurrence interval is ~300 yr., therefore, strain has not been built up.

However there is a scattered cluster of intermediate-depth earthquakes below Central Cordillera which source could not be accurately determined. Corbeau et al. (2017, 2019) proposed that this diffuse intermediate-depth seismicity and also the deep focal mechanisms of transcurrent component in the SOFZ are related with a slab break-off of an older NOAM oceanic subducted slab.

4.4 Left-lateral Strike-slip Domain (SSD)

4.4.1 Shallow structure of the SSD

4.4.1.1 Bahamas Carbonate Province and Hispaniola Trench

Multibeam bathymetry data and seismic profiles south of Great Inagua Bank indicate that the bank have quite same morphological and structural characteristics to Mouchoir Bank (Figs. 14 and 15). However, seismic profile (Fig. 15) do not show any tilted block from the BCP below the Northern Haitian Basin, but a continuous high-amplitude south dipping reflector can be followed below the HT and the Forearc. Between the Caicos Basin and Great Inagua Bank there is a NE-SW trending scarp (Fig. 14) similar to the inherited transverse faults observed in the OCD, in the passages between banks.

In the SSD, the extensive Caicos basin is replaced by an E-W trending narrow trench (Northern Haitian Basin) that gradually shallows towards the W to 3000 m of water depth (Axial profile in Fig. 3). The seismic profile in this area shows a sediment thickness of the trench of up to 1.3 sTWT (Zoom 2 in Fig. 15). In addition, MTDs have been found at the southern boundary of the trench (Zoom 2 in Fig. 15). The modern sedimentary filling is being eroded by a highly incised axial submarine channel-levee system which captures the flows from the Windward Passage and BCP and channels them towards the Caicos Basin (Figs. 14 and 15). Gloria data from Dillon et al. (1992) shows that the channel-levee system continues to the E, along the southern edge of Caicos Basin, to the Hispaniola Basin (Figs. 10 and 14). Seismic profile show that the horizontal shape of modern reflectors precludes significant post-tilting (Zoom 2 in Fig. 15).

4.4.1.2 Forearc of the SSD

In the SSD the seafloor morphology and internal structure of the forearc changes drastically from eastern studied domains. The upper slope, north and east of Tortue Island, present a very irregular seafloor, suggesting a karst morphology (Leroy et al., 2015). Meanwhile, the western edge is occupied by the Windwards Passage Sill, a narrow east-west trending submarine ridge (25 km-wide and 125 km-long) between the Punta Caleta off Cuba and the northwestern peninsula of Haiti that rises up 1000 m above the Windward Passage Deep and the HT. (Figs. 3, 14, 15 and 16;

Calais and de Lépinay, 1995). The Tortue Island represents the emerged eastern end of the Windwards Sill. The upper part is bounded to the south by the SOFZ which forms the Tortue Channel, an E-W trending elongated deep depression with 700 m-deep relative to surrounding seafloor. Towards the W, the SOFZ forms a positive flower structure at depth (Zoom 1 in Fig. 15). New seismic profiles allow to differentiate three seismic sequences (B, A and A') already defined by Calais and de Lépinay (1995) (Fig. 15). A lower sequence (B) formed by almost transparent, chaotic and discontinuous reflectors. This sequence is folded forming wide synclines and anticlines in which these last ones have been decapitated. An intermediate sequence (A) settled in angular discordance that fills up the synclines of the lower sequence. It shows high-amplitude and continuous reflectors that locally present a divergent configuration. And an upper sequence (A') with high-amplitude parallel and continuous reflectors that become transparent in depth. This sequence overlies the lower and intermediate sequences by a marked erosive surface.

The middle and lower forearc show continuous step slope (20º) and a smooth seafloor (Fig. 14, App A). Canyon networks in the middle slope locally show slightly laterally displacement caused by minor transcurrent blind faults (Figs. 14 and 15) similar that those in the western end of the OUD. In the SSD there is not a well-developed imbricated system (Fig. 14 and Zoom 2 in Fig 15). Most deformation is located near the deformation front, forming 1-2 narrow buried frontal thrust sheets, and near the SOFZ. Between the deformation front and the SOFZ there is an 80 km-wide area with little recent deformation (Windward Passage Sill and its prolongation to E), just some MTDs close to the plate boundary and the older blind reverse faults that at the present act as transcurrent faults (dashed lines in Fig. 14) which accommodates some of the lateral component of the oblique convergence (Figs. 14, 15 and 16).

Seismic layers (reflectors B, A' and A; Calais and Mercier de Lepinay, 1995), structures and shallow morphology of the Windward Passage Sill, Tortue Island and the drowned platform with karstic morphology to the east, suggest that it has suffered strong uplifting followed by current subsidence with minor lateral displacement (Leroy et al., 2015). According to paleoreconstructions made by Calais and Mercier de Lepinay (1995) and Calais et al. (2016) the

collision of Hispaniola against the BCP in Late Pliocene (2 Ma) locked the strike-slip motion in the Hispaniola Trench and causing it to shift to a single fault (SOFZ) along the Tortue Channel (Leroy et al., 2015). The strike-slip fault along the Hispaniola Trench was then reactivated as a reverse fault (Dillon et al., 1992), constituting the current Deformation Front. At the same time, due to Hispaniola-BCP collision, the Septentrional Cordillera underwent great uplift. In contrast, the forearc in the SSD is suffering high subsidence. It is defined by a low-active imbricate system and a little deformed area conformed by the Windward Passage Sill with transcurrent blind faults that may accommodate some of the lateral component of oblique convergence. (Figs. 14, 15 and 16).

4.4.2 Seismicity and kinematics of the SSD

The SSD shows much less seismicity and poorly located (Fig. 6). It is clustered in a very narrow strip that comprises Turtle Island and the Trans-Haitian Belt and its extension offshore westwards into the Gulf of Gônave (NHTB; Figs. 6 and 8e). This cluster of earthquakes is very shallow (< 35 km) and epicenters are focused in the SOFZ and in the NHTB-Gulf of Gônave (Figs. 6 and 8e). Two focal mechanisms in north of Tortue Island are interplate earthquakes (nucleated at the detachment; 20-35km-depth) and show pure to slightly oblique thrust fault with nodal planes with E-W strike. This indicates that the convergence component associated with the collision process is still very relevant (Figs. 6 and 8e). A strike-slip focal mechanism is found in the Tortue Channel at a depth of 35 km and shows a focal solution of nearly pure left-lateral strike-slip fault (Figs. 6 and 8e). Also GPS vectors south of Tortue Island (Fig. 3) reflects still relevant oblique convergence component. Predicted slip rates (in mm/yr.) of active faults from the block show a strain partitioning model with a convergent slip component at the deformation front with a rate of 3.8 mm/yr. and a transcurrent component at the SOFZ with a slip rate of 14.4 mm/yr. (Fig. 5 in Benford et al., 2012). All suggest strain partitioning in this area with a highly localized deformation. The compression component is slightly less important than in the east but still relevant, forming a low-active compressive system (Fig. 15) and where the transcurrent strain is predominant, clustering in the SOFZ (Figs. 14, 15 and 16).

Although this area shows a little seismic record, recent studies carried out by Corbeau et al. (2017 and 2019) reveal that this area is subject to more seismicity than previously believed. Moreover, these studies show a dozen intermediate-depth earthquakes (>70 km) under Haiti, with a 260 km-depth event in the south of the island. Corbeau et al. (2019) propose that this intermediate seismicity is the result of deep deformation caused by a remnant lithospheric slab inherited from the southward subduction of the NOAM. In addition, authors propose that the scarcity of intermediate seismicity, compared to the east, below Central Cordillera, may be the effect of the lack of a dense seismic network or that they show the western boundary.

4.5 Northern Cuba Collision Domain (NCD)

The western part of the study area comprises the Northern Cuba Collision Domain. It extends from the Windward Passage to the east, extending to the W along the SOFZ south of Cuba to the Cayman Trough. The orientation of the Deformation Front to the northeast of Cuba shifts again into a NE-SW trending (Fig. 14). In the Windward Passage, the boundary between the NOAM and CARIB shifts to the south to the SOFZ, placing Cuba into the NOAM plate (Fig. 14).

4.5.1 Shallow structure of the NCD

4.5.1.1 Windward Passage and Southern Cuba

The Windward Passage is a 90 km-wide strait located between southeastern Cuba and the northwestern peninsula of Haiti (Fig. 14, App D). The Windward Passage consists of the Windward Passage Deep and the Windward Passage Sill.

The Windward Passage Deep is a rectangular depression of 50 km-length and 10 km-wide ranging 3500-3750 m-deep (Figs. 2 and 14). Calais et al. (1991) confirmed by geological information that the SOFZ in not connected, through the Windward Passage, with the deformation front in the SSD, which had previously assumed from seismological data (Molnar and Sykes, 1969; Kelleher et al., 1973; Sykes et al., 1982). Also, Calais et al. (1991) showed that the Windward Passage Deep could not be interpreted as an active pull-apart basin, as was previously assumed. They interpreted the tectonic regime in the Windward Passage area as a pure

left-lateral strike slip. Fig. 16 shows a sedimentary fill of 0.7 sTWT-thick composed of high-amplitude, continuous and parallel reflectors. In the south wall of the Windward Passage Deep, below the erosive surfaces there is a sequence of older sediments (B sequence) tilted to the south and affected by north-verging reverse faulting (Fig. 16). At the northern boundary of the Windward Passage Deep, the sediments are uplifted by folding and reverse faulting, forming a broad antiform of 5 km-wide with slight vergence to the south (Zoom 1 in Fig. 16). This anticline is the morphological expression of a positive flower structure associated to the SOFZ.

Figure 16 shows the Windward Passage Sill with the same sedimentary sequences already observed and defined further east in the Fig. 15. At the northern boundary of the Windward Passage Sill, there is a narrow N-verging imbricate system (Fig. 16). The sediments of the relatively shallow (3200 m water depth) Hispaniola Trench are tilted to the north and incorporated in the active imbricated fold-and-thrust system (Fig. 16). The Windward Passage Sill also registered current transpressional deformation as indicates the positive flower structure in its middle part (Zoom 2 in Fig. 16). This structure could be the westward continuation of the blind transcurrent faults in the middle slope of the OUD and the SSD.

The southern margin of Cuba is occupied by the Santiago Deformed Belt (Fig. 14). Calais et al. (1991) defined the Santiago Deformed Belt and the SOFZ as an active compressive area extending along the southern margin of Cuba. They related this E-W trending deformed belt to a regional transpressional tectonic due to oblique movement along the SOFZ. Calais and Mercier de Lepinay (1995) showed no significant transpression across the Windward Passage, compressive deformation is restricted to the relay zones of the SOFZ. Furthermore, they indicated that smooth folding observed at Windward Passage can be explained in the frame of pure strike slip, as shown before by analog models (Odonne and Vialon, 1983; Sylvester, 1989). However, Leroy et al. (1996), and later Corbeau et al. (2016) defined a compressive area from south of Windward Passage to north of Jamaica in agreement with GPS data, thus extending the transpressive regime southeastwards to include the Gulf of Gônave.

4.5.1.2 Northeastern Cuba

Due to the low cover of high-resolution bathymetry data, the northeastern Cuba margin can only be characterized by the seismic reflection profile. The seismic profile shows a forearc with a low and continuous slope composed by a deep platform composed by a 2 sTWT-thick sedimentary fill (Fig. 17). Towards the north there are three series of anticline ridges forming a narrow fold-and-thrust imbricate system (Zoom 1 in Fig. 17). The Cuba Basin has an average water-deep of 3000 m and is composed of high-thick sedimentary fill of at least 2.2 sTWT-thick in which isolated carbonate spurs from the BCP are found (Figs. 3 and 14). At the southern boundary of the Cuba Basin, the sediments are folded and incorporated into the imbricate system (Zoom 1 in Fig. 17).

4.5.2 Seismicity of the NCD

Shallow seismicity is clustered in Cuba´s southern margin, in the SDB and the SOFZ trace, although there is some dispersed seismicity in its northern margin (Fig. 6). Focal mechanisms show strike-slip and oblique thrust faulting which are related with the SOFZ and the SDB respectively.

The northern Cuba margin shows a diffuse shallow seismicity with a focal mechanism that shows slightly oblique thrust fault with nodal plans with an E-W strike, indicating that there is still a convergence component associated with the collision process (Fig. 6 and 7f).

5 Discussion

Many tectonic studies were made in the northern CARIB plate, but many of them only were focused in one tectonic domain, and then suffer from a large scale and integrating approach to understand the along-strike plate boundary transition. From the analysis of continuous geophysical information (high-resolution bathymetry, seismic reflection, and seismological data) we have addressed the study of along-strike variations on crustal structure of the NOAM-CARIB plate boundary, and the relation with the geometry and thickness of the downgoing slab from Puerto Rico to Cuba. Our results allow us to propose conceptual models to summarize the structure and main tectonic features for each tectonic domain along the NOAM-CARIB plate boundary, as well as how the transition between such domains is taking place.

Oblique Subduction Domain

The high oblique convergence of the thin NOAM oceanic crust in the OSD leads to the increase of the slab angle, and in turn, to a rollback process with the formation of two slab tears at 65ºW (Meighan et al., 2013, ten Brink and Lopez-Venegas (2012) and 68.5ºW (this study). Meighan et al. (2013) and ten Brink and Lopez-Venegas, (2012) proposed that the slab tear at 65ºW might have caused by increasing of trench curvature due to counterclockwise rotation of the PRVI block and the subduction of a large seamount. Furthermore, we have observed a cluster of intermediate-depth earthquakes (Fig. 8g) suggesting the existence of a slab tear at 68.5º W, between the thin oceanic NOAM subducting slab and the relative thicker and buoyant colliding BCP transitional crust (Fig. 19). This slab tear is analogous to that observed in the North Andean Margin, where the relative thicker Carnegie Ridge has been colliding with the margin since at least 2 Ma (c.f. Gutscher et al., 1999). Previous studies (Harris et al., 2018) also proposed a slab tear in the Mona Passage down to a depth of ~300 km and 50 km-width. This slab tear of 50 km-width proposed by Harris et al. (2018) nearly matches in location and depth with the slab tear proposed in this study at 68.5ºW (Fig. 18). Moreover, GPS data reflects the along-strike variation in crustal thickness of the subducting slab. They show, from E to W, the diachronic evolution of the slow-down and stop of subduction process and the beginning of the collision of the thickened BCP crust with the island arc (Calais et al., 2016). In Mona Passage and Puerto Rico, GPS vectors show average convergence rates of 10-13 mm/yr. relative to NOAM plate reference (Fig. 3) with almost parallel trending to the direction of plate convergence. It contrasts with GPS measurements to the west, in the Cabrera Promontory and Sosua Peninsula, showing much lower convergence rate relative to NOAM (2-4 mm/yr.; Fig. 3) with a trend normal to the plate boundary.

In addition, the oblique convergence in the OSD gives rise to the formation of strike-slip fault systems sub-parallel to the trench: the SOFZ and the BFZ. However, unlike eastwards of the Mona Rift, where the rollback results in an overall subsidence of the whole region, in this area a broad zone with transpressive tectonics in the forearc is formed, highly controlled by the SOFZ

and the BFZ, which coexist for at least 170 km. The rollback of the downgoing NOAM oceanic slab and the consequent high dip angle of the slab (Fig. 19) are the responsible of the transpressive tectonics without strain partitioning in the OSD, characterized by a starved trench (Section A in Fig. 18).

In contrast with the other tectonic domains further to the W, the BFZ is very close to the trench, highly limiting the width of the accretionary prism. Ten Brink and Lin (2004) proposed that the change in the distance of the strike-slip fault to the trench between Puerto Rico and Hispaniola is caused by variations in the Coulomb stresses in the forearc region by the shift in the slip direction due to the change in the direction of the margin to an E-W trending. Laurencin et al. (2019), based on data taken in the northern Lesser Antilles, showed that the 850- km- long Bunce Fault is a structural boundary separating the very narrow, sediment- starved trench. They proposed, in a long-term margin erosion, an alternative scenario of a strike- slip system that initiated at greater distance from the trench, at the rear of an initially larger and progressively eroded accretionary domain. However, they pointed out that the Bunce Fault proximity to the trench might be primarily controlled by the major mechanical weakness at the toe of the prism backstop. The hypothesis proposed by Laurencin et al. (2019) is only applicable to the east of the Mona Rift since there is only one transcurrent structure, the BFZ. However, in the OSD there are two parallel transcurrent fault systems (SOFZ and BFZ) coexisting along 170 km, which accommodate oblique convergence in this area forming broad transpressive belts. Nonetheless, in our region, the BFZ cuts through the accretionary prism in this part of the PRT, and is not along a backstop. West of Mona Rift, the BFZ starts feathering out to several strands as is typical at the end of strike-slip faults, and therefore it definitely cannot be running along a backstop. Further exhaustive studies would be necessary to quantify how much strain is accommodated in each structure (SOFZ or BFZ, with their associated transpressive belt).

Oblique Collision Domain

In the OCD, active collision of the transitional crust of the BCP with the island arc occurs (Dolan et al., 1998). Due to the collision with BCP (high thickness and buoyancy) the OCD forearc

shows high plate coupling with strain partitioning (Calais et al., 1991; 2002; Jansma et al., 2000; Mann et al., 2002; De Zoeten and Mann, 1999) having: a) a deformation front with E-W strike where little deformation is accumulated, with accretion of materials derived from the BCP (Rodriguez Zurrunero et al., 2019); b) a wide "welded" accretion prism that it is mostly buried (inactive). Here, the entrance of thick crust blocks the subduction, and currently prevents the growth of a the imbricated system (that is buried); c) the high uplift suffered by the 11 level terraces of Cabrera Promontory due to the indentation of the Silver Spur.

Compared to northern Puerto Rico and in the context of strain partitioning, the BFZ disappears, shifting all the transcurrent component towards the south, to the SOFZ (Section B in Fig. 18). This shifting seems to take place through a relay zone in the eastern offshore of Samana Peninsula. Nevertheless, the relay between SOFZ and BFZ takes place where the BCP is colliding with the island arc. The collision process might result in the welding of the accretionary prism, where the BFZ developed, producing the feather termination and its relay towards the weakness zone of the SOFZ farther to the south.

Despite there is an active collision in the shallower crust, intense intermediate-depth seismicity remains (i.e., subduction-related seismicity; Fig. 8g). This fact might suggest that the thinner crust of the southeastern edge of the BCP is still actively subducting beneath the CARIB plate with a lower dip (Fig. 19). The subduction in this part may be due to a thinner BCP crust at its eastern end or to larger plate pull forces exerted by the mantle on this part of the plate or both. A study from ten Brink et al. (2013), based on seismicity and tomography, proposed a continuous slab of 450 km-long covering the OUD, the OCD and the OSD which extends from the surface to a depth of 500 km in the northern Caribbean. This area matches with the rupture area of the 1943-1953 seismic crisis. However, this hypothesis does neither agree with the slab tear found at 68.5ºW nor with the variations in the earthquake distribution described in this study. Calais et al. (1992) and more studies on Haiti conducted by Corbeau et al. (2017 and 2019) suggested the existence of intermediate-depth seismicity associated to a slab break-off of an inherited NOAM subducted slab (see next subsection). The low seismicity below Hispaniola could be due to the lack of a

dense seismic network in this area. Therefore, with the results obtained in this study and supported by studies from ten Brink et al. (2013) and Corbeau et al. (2017 and 2019), we propose an alternative geometry to undergoing slab (Fig. 19), with and continuous NOAM subducted slab below Hispaniola that would explain the intermediate seismicity.

An alternative hypothesis was proposed by van Benthem et al. (2014), suggesting that the intermediate-depth seismicity in the OCD and in the OUD, below Central Cordillera, may be the lateral push by the edge of the NOAM subducted slab onto the CARIB plate. However, there is not structural and geodetic observations at surface or deep seismicity and focal mechanism data that could support this hypothesis. Also, as Calais et al. (2016) pointed out, the existence of a continuous slab in this region has been challenged, its geometry through time is poorly constrained, and it is unclear against what the slab edge would be pushing to.

Oblique Underthrusting Domain

The oblique underthrusting of thick crust has been widely studied by numerous authors (Scholl et al., 1980; Mullins et al., 1991; Dolan et al., 1998; Dominguez et al., 2000; Marshak, 2004; Granja-Bruña et al., 2009; 2014; Rodriguez-Zurrunero et al., 2019). Our data confirm that the OUD follows a strain partitioning tectonic model consisting of a NW-SE trending accretionary prism that accommodates the convergence (vertical) component and the SOFZ and CFZ fault system that accommodate the strike-slip (horizontal) component (Section C in Fig. 18). On the western end of the OUD, there is a jog between two branches of the SOFZ (Haitian and Dominican Republic segments). This southward shift of the SOFZ in the Haiti area may be due to the along-strike interaction of the Septentrional Block with Windward Passage Sill, which prevents the progression towards the W of the Dominican segment of the SOFZ, or at least being much less active (Section C and D in Fig. 18).

However, there is a lack of shallow earthquakes with associated left-lateral CMT solutions in the vicinity of the SOFZ and CFZ (Fig. 6 and 7g). The majority of focal mechanisms are shallow (~ 15 km) and with a pure reverse component. These focal mechanisms were associated to the

NHDB and the Deformation Front (Dolan and Bowman, 2004). The lack of seismicity associated with the SOFZ may suggest that the accommodation of the horizontal component of displacement would be aseismic. An alternative explanation was given by ten Brink et al. (2011 and 2013), were large earthquakes in 1562 and 1842, as well as ~900 years ago are related to the SOFZ, with a recurrence interval of ~ 300 years. At present the SOFZ are in the middle of the inter-seismic cycle and therefore there is little seismic activity.

Diffuse intermediate-depth hypocenters recorded below Central Cordillera (Fig. 8 d and g) in Hispaniola might be seismically associated to a slab break-off of an inherited NOAM subducted slab (Calais et al., 1992; Corbeau et al., 2017). New data from Corbeau et al. (2019) reveals that below Haiti there are still intermediate-depth earthquakes, suggesting that the remnant NOAM subducted slab could continue towards the west, comprising central and western Hispaniola. Also Nuñez et al. (2019) using 2-D P wave velocity models, show at southern Hispaniola an anomalous zone of lateral velocity variation in the mantle that might be associated with a possible detached oceanic slab from NOAM. The buoyant BCP transitional lithosphere that is currently in the collision process was previously connected to the NOAM subducted slab (Fig. 19). This leads to tensile stresses between the two lithospheres driving into the detachment of the NOAM subducted slab from the currently colliding BCP lithosphere at the surface (e.g., Davies and von Blanckenburg, 1995; Wortel and Spakman, 1992). An alternative explanation for the intermediate-depth seismicity may be the lateral push by the edge of the NOAM subducted slab onto the CARIB plate proposed by van Benthem et al., 2014 as we indicated before. Nevertheless, there is not structural observations at surface nor deep focal mechanisms corresponding to the E-W compression.

Left-lateral Strike-slip Domain

In the SSD there is another change in the margin orientation, turning into an E-W trending. Here, the orientation of the margin influences the tectonics in the overriding plate. The shift to an E-W trending leads into the almost parallelism between the NOAM-CARIB convergence vector and

the margin. This fact, within a strain partitioning model, results in the predominance of the strike-slip component over the orthogonal convergence component. This leads to the transpressive uplift of Tortue Island, associated with the SOFZ, and the low-active or inactive imbricated system at the front as a consequence of the lower weight of the orthogonal component (Section E in Fig. 18). The currently inactive imbricated system could be inherited from the epoch when the Hispaniola was in the south of Cuba (Calais and Mercier de Lepinay, 1995; Calais et al., 2016). Between the currently inactive imbricate system and the SOFZ, there is an 80 km-width area almost without current deformation (Windward Passage Sill and its prolongation to the E).

We agree with Calais and Mercier de Lepinay (1995) suggestion in which they do not observe transpression in the SOFZ. Focal mechanisms (Fig. 8g) show strain partitioning with reverse faulting and are associated with the deformed belt, not with SOFZ. There is only one focal mechanism associated with the SOFZ, showing a nearly pure left-lateral strike-slip solution. The large uplift that the Tortue Island suffered is consistent with the paleoconstructions made by Calais and Mercier de Lepinay (1995) and Calais et al. (2016), which show that in Late Pliocene (2 Ma) the Septentrional Cordillera and the Tortue Island undergo great uplift.

However, to the west, the margin orientation shifts again to a NE-SW trending and the convergence component becomes more relevant with the development of compressive structures in the Windward Passage Sill and the NE margin of Cuba. Also, Corbeau et al. (2019) show an almost pure reverse focal mechanism located in the Windward Passage, evidencing the relevant convergence component in this area. Thus, we can determine that along the entire margin of Hispaniola, the orientation of the margin also influence the structural framework in the overriding plate. When the margin has a more oblique orientation relative to the NOAM-CARIB convergence vector (OSD and SSD), the strike-slip component is more relevant. This causes the imbricated system associated with the convergence component to be less active. On the other hand, when the margin has a more orthogonal direction relative to the NOAM-CARIB convergence vector (NW-SE trending), the convergence component predominates, which leads to a good development of the imbricated system.

6 Summary and conclusions

The NE Caribbean shows a clear example of an along-strike segmented plate boundary. Here, from E to W, is taking place the transition from a frontal subduction in the Lesser Antilles, to an oblique subduction without strain partitioning north of Puerto Rico, to a collision/underthrusting along Hispaniola and to strike-slip south of Cuba. The transition from an oblique subduction without strain partitioning and low coupling to an oblique collision with strain partitioning and high coupling is marked by the entering into the trench of the thickened crust of the BCP. Towards the W, the boundary from oblique collision to a transcurrent regime is diffuse. Although the Windward Passage and southern Cuba has been considered as a plate boundary of pure left-lateral strike-slip, numerous compressive structures are still observed in this area. Thus, from E to W we conclude that:

a) A vertical slab tear is found at 68.5ºW due to along-strike changes in crustal thickness of the incoming plate. The slab tear separates subducting oceanic crust north of Puerto Rico with thickened BCP crust which is obliquely colliding with Hispaniola. This slab tear marks the boundary between oblique subduction and collision, although seismicity shows that the eastern end of the BCP, between the Silver Spur and the slab tear, is still actively subducting beneath CARIB. An alternative model is the existence of an inherited continuous subducted NOAM slab which below Hispaniola. The changes in the geometry of the downgoing NOAM slab greatly influence structural features on the overriding plate. There is a transition from a transpressive regime without strain partitioning to NW of Puerto Rico, to a collision regime with strain partitioning N of Hispaniola.

b) Northern Hispaniola margin is characterized by the oblique collision of the BCP with the island arc. There is high coupling with strain partitioning. A relative wide accretionary wedge accommodates the convergence component normal to the margin, and landward, the conjugate left-lateral strike slip system, composed of the SOFZ and the CFZ, accommodates the transcurrent component. The SOFZ and the CFZ show transpression since Late Pliocene (2 Ma) which have uplifted and shaped the Septentrional Cordillera.

In the collision margin, the intermediate-depth seismicity should disappear. However, beneath Central Cordillera and Haiti, diffuse intermediate-depth hypocenter still remains. These hypocenters might indicate the presence of a detached remnant NOAM subducted slab below central and western Hispaniola.

c) The Haitian N margin is characterized by much less seismicity than to the E and highly localized in the Tortue Island and the Trans-Haitian Belt. Seismicity and GPS data show a strain partitioning model with focal mechanisms of pure reverse nodal planes associated with the detachment and strike-slip focal mechanisms associated with SOFZ. Bathymetry data and seismic reflection profiles reveals two distinct areas:

- An eastern area, around Tortue Island, which shows a low-active imbricated system and show a zone of 80 km-width without recent deformation. All suggest high localized deformation, in a strain partitioning model with the prevalence of the SOFZ strike-slip displacement with respect to the convergence at the Deformation Front.
- A western area that in which the collision process still remains, with the development of compressive structures in the Windward Passage Sill (positive flower structure) and the NE margin of Cuba (imbricate fold-and-thrust system).

The documented along-strike boundary segmentation of the plate boundary is essential for the assessment of seismic hazard in the region. This segmentation, and hence variations in the plate coupling (non-coupled, partially-coupled and highly-coupled) determine the maximum earthquake size and structural features of the overriding plate.

Acknowledgements

This work was supported by the Spanish Ministry of Innovation and Science projects (Projects: REN2003-08520; CTM2006-13666 and CGL2010- 17715), by Institut des Sciences de la Terre de Paris (ISTeP) projects (HAITI-SIS 1&2; DOI:10.17600/12010070 and 10.17600/13010080), and by the U.S. Geological Survey Coastal and Marine Geology Program (Caribbean earthquake and tsunami hazards project).We are indebted to the crew and technicians of the R/V Sarmiento

de Gamboa, L'Atalante and Ron Brown for their professional help at sea. We would like to thank Jordane Corbeau and an anonymous reviewer for the valuable revision and suggestions to improve the quality of the paper. A. Rodriguez-Zurrunero was supported by a PhD. grant from Universidad Complutense de Madrid (CT45/15 - CT46/15). This work was also funded by CARESOIL (S2013/MAE-2739), I+D CARESOIL (S2018/EMT-4317) and MARIBNO projects (PGC2018-095999-B-I00).

References

Andrews, B. D., Ten Brink, U. S., Danforth, W. W., Chaytor, J. D., Granja Bruña, J. L., Llanes Estrada, P., et al. (2013). Bathymetric Terrain Model of the Puerto Rico Trench and the Northeastern Caribbean Region for Marine Geological Investigations. Retrieved from https://pubs.usgs.gov/of/2013/1125/

Benford, B., Demets, C., & Calais, E. (2012). GPS estimates of microplate motions, northern Caribbean: Evidence for a Hispaniola microplate and implications for earthquake hazard. *Geophysical Journal International*, *191*(2), 481–490. https://doi.org/10.1111/j.1365-246X.2012.05662.x

Buforn, E., Bezzeghoud, M., Udías, A., & Pro, C. (2004). Seismic sources on the Iberia-African plate boundary and their tectonic implications. *Pure and Applied Geophysics*. https://doi.org/10.1007/s00024-003-2466-1

Bunce, E. T. (1966). The Puerto Rico Trench. In W.H. Poole (Ed.), *Geol. Surv. Can.* (66th–15th ed., pp. 165–175).

Byrne, D. B., Suarez, G., & McCann, W. R. (1985). Muertos Trough subduction—microplate tectonics in the northern Caribbean? *Nature*, *317*(6036), 420–421. https://doi.org/10.1038/317420a0

Reid H. F., and Taber S., (1920). The Porto Rico Earthquake of 1918. Report of the Earthquake Investigation Commission. *Geological Magazine*. https://doi.org/10.1017/s0016756800106491

Calais, E., & de Lepinay, B. M. (1991). From transtension to transpression along the northern Caribbean plate boundary off Cuba: implications for the Recent motion of the Caribbean plate. *Tectonophysics*. https://doi.org/10.1016/0040-1951(91)90367-2

Calais, E., Béthoux, N., & de Lépinay, B. M. (1992). From transcurrent faulting to frontal subduction: A seismotectonic study of the Northern Caribbean Plate Boundary from Cuba to Puerto Rico. Tectonics. https://doi.org/10.1029/91TC02364

Calais, E., & De Lépinay, B. M. (1995). Strike-slip tectonic processes in the northern Caribbean between Cuba and Hispaniola (Windward Passage). *Marine Geophysical Researches*. https://doi.org/10.1007/BF01268051

Calais, E., Mazabraud, Y., Mercier de Lépinay, B., Mann, P., Mattioli, G., & Jansma, P. (2002). Strain partitioning and fault slip rates in the northeastern Caribbean from GPS measurements. *Geophysical Research Letters*, *29*(18), 3-1-3–4. https://doi.org/10.1029/2002GL015397

Calais, E., Freed, A., Mattioli, G., Amelung, F., Jónsson, S., Jansma, P., et al. (2010). Transpressional rupture of an unmapped fault during the 2010 Haiti earthquake. *Nature Geoscience*, *3*(11), 794–799. https://doi.org/10.1038/ngeo992

Calais, É., Symithe, S., Mercier de Lépinay, B., & Prépetit, C. (2016). Plate boundary segmentation in the northeastern Caribbean from geodetic measurements and Neogene geological observations. *Comptes Rendus - Geoscience*. https://doi.org/10.1016/j.crte.2015.10.007

Chaytor, J. D., & ten Brink, U. S. (2010). Extension in Mona Passage, Northeast Caribbean. Tectonophysics. https://doi.org/10.1016/j.tecto.2010.07.002

Christeson, G., Shipley, T., Gahagan, L., Johnson, K., and Davis, M. (2017). Academic Seismic Portal (ASP) at UTIG.

Clark, S. A., Sobiesiak, M., Zelt, C. A., Magnani, M. B., Miller, M. S., Bezada, M. J., & Levander, A. (2008). Identification and tectonic implications of a tear in the South American plate at the southern end of the Lesser Antilles. *Geochemistry, Geophysics, Geosystems*. https://doi.org/10.1029/2008GC002084

Conolly, J. R., & Ewing, M. (1967). Sedimentation in the Puerto Rico Trench. *Journal of Sedimentary Research*. https://doi.org/10.1306/74D7164A-2B21-11D7-8648000102C1865D

Contreras-Reyes, E., & Osses, A. (2010). Lithospheric flexure modelling seaward of the Chile trench: Implications for oceanic plate weakening in the Trench Outer Rise region. Geophysical Journal International. https://doi.org/10.1111/j.1365-246X.2010.04629.x

Corbeau, J., Gonzalez, O. L., Clouard, V., Rolandone, F., Leroy, S., Keir, D., Prépetit, C. (2019). Is the local seismicity in western Hispaniola (Haiti) capable of imaging northern Caribbean subduction? Geosphere. https://doi.org/10.1130/GES02083.1

Corbeau, J., Rolandone, F., Leroy, S., Guerrier, K., Keir, D., Stuart, G., Meyer, B. (2017). Crustal structure of western Hispaniola (Haiti) from a teleseismic receiver function study. Tectonophysics. https://doi.org/10.1016/j.tecto.2017.04.029

Corbeau, J., Rolandone, F., Leroy, S., Meyer, B., Mercier De Lépinay, B., Ellouz-Zimmermann, N., & Momplaisir, R. (2016). How transpressive is the northern Caribbean plate boundary? Tectonics. https://doi.org/10.1002/2015TC003996

DeMets, C., Jansma, P. E., Mattioli, G. S., Dixon, T. H., Farina, F., Bilham, R., et al. (2000). GPS geodetic constraints on Caribbean-North America plate motion. *Geophysical Research Letters*, *27*(3), 437–440. https://doi.org/10.1097/00003226-200101000-00021

Díaz De Neira, J. A., & Escuer Solé, J. (2007). Geomorphic evolution of the Dominican Cordillera Oriental. Boletin Geologico y Minero. 118.

Díaz de Neira, J. A., Braga, J. C., Pérez Cerdán, F., & Lopera, E. (2017). Marine terraces of the Promontorio de Cabrera (Pleistocene, northern Dominican Republic). *BOLETÍN GEOLÓGICO Y MINERO*. https://doi.org/10.21701/bolgeomin.128.3.007

Dillon, W. P., Austin, J. A., Scanlon, K. M., Terence Edgar, N., & Parson, L. M. (1992). Accretionary margin of north-western Hispaniola: morphology, structure and development of part of the northern Caribbean plate boundary. *Marine and Petroleum Geology*, *9*(1). https://doi.org/10.1016/0264-8172(92)90005-Y

Dillon, W. P., Edgar, N. T., Scanlon, K. M., & Coleman, D. F. (1996). A review of the tectonic problems of the strike-slip northern boundary of the Caribbean Plate and examination by GLORIA: Chapter 9. https://doi.org/10.1017/cbo9780511529481.013

Dolan, J. F., & Mann, P. (1998). Active strike-slip and collisional tectonics of the Northern Caribbean plate boundary zone. Geological Society of America.

Dolan, J. F., & Bowman, D. D. (2004). Tectonic and Seismologic Setting of the 22 September 2003, Puerto Plata, Dominican Republic Earthquake: Implications for Earthquake Hazard in Northern Hispaniola. *Seismological Research Letters*, *75*(5), 587–597. Retrieved from http://dx.doi.org/10.1785/gssrl.75.5.587

Dolan, J. F., Mullins, H. T., & Wald, D. J. (1998). Active tectonics of the north-central Caribbean; oblique collision, strain partitioning, and opposing subducted slabs. Active strike-slip and collisional tectonics of the northern Caribbean Plate boundary zone. (Vol. 326). https://doi.org/-

Dolan, J. F., & Wald, D. J. (1998). The 1943-1953 north-central Caribbean earthquakes: Active tectonic setting, seismic hazards, and implications for Caribbean-North America plate motions. *Geological Society of America Special Paper*, *326*, 143–169.

Dominguez, S., Malavieille, J., & Lallemand, S. E. (2000). Deformation of accretionary wedges in response to seamount subduction: Insights from sandbox experiments. *Tectonics*, *19*(1), 182–196. https://doi.org/10.1029/1999TC900055

Edgar, N. T. (1991). Structure and geologic development of the Cibao Valley, northern Hispaniola. https://doi.org/10.1130/spe262-p281

Emry, E. L., Wiens, D. A., & Garcia-Castellanos, D. (2014). Faulting within the Pacific plate at the Mariana Trench: Implications for plate interface coupling and subduction of hydrous minerals. Journal of Geophysical Research: Solid Earth. https://doi.org/10.1002/2013JB010718

Engdahl, E. R., & Villaseñor, A. (2002). 41 Global seismicity: 1900-1999. In *International Geophysics*. https://doi.org/10.1016/S0074-6142(02)80244-3

Escuder-Viruete, J., & Pérez-Estaún, A. (2006). Subduction-related P-T path for eclogites and garnet glaucophanites from the Samaná Peninsula basement complex, northern Hispaniola. *International Journal of Earth Sciences*. https://doi.org/10.1007/s00531-006-0079-5

Escuder-Viruete, J., Pérez-Estaún, A., Gabites, J., & Suárez-Rodríguez, Á. (2011). Structural development of a high-pressure collisional accretionary wedge: The Samaná complex, Northern Hispaniola. Journal of Structural Geology. https://doi.org/10.1016/j.jsg.2011.02.006

Ewing, M., & Heezen, B. C. (1955). Puerto Rico Trench Topographic and Geophysical Data. https://doi.org/10.1130/spe62-p255

Farr, T. G., & Kobrick, M. (2000). Shuttle radar topography mission produces a wealth of data. *Eos*. https://doi.org/10.1029/EO081i048p00583

Fox, P. J., & Heezen, B. C. (1975). Geology of the Caribbean Crust. In *The Gulf of Mexico and the Caribbean*. https://doi.org/10.1007/978-1-4684-8535-6_10

Freeman-Lynde, R. P., & Ryan, W. B. F. (1987). Subsidence history of the Bahama Escarpment and the nature of the crust underlying the Bahamas. *Earth and Planetary Science Letters*, *84*(4), 457–470. https://doi.org/10.1016/0012-821X(87)90010-0

Goreau, P. D. E. (1983). *The tectonic evolution of the North Central Caribbean plate margin*. Woods Hole, MA: Massachusetts Institute of Technology and Woods Hole Oceanographic Institution. https://doi.org/10.1575/1912/2417

Granja Bruña, J. L., Carbó-Gorosabel, A., Llanes Estrada, P., Muñoz-Martín, A., ten Brink, U. S., Gómez Ballesteros, M., et al. (2014). Morphostructure at the junction between the Beata ridge and the Greater Antilles island arc (offshore Hispaniola southern slope). *Tectonophysics*, *618*, 138–163. https://doi.org/10.1016/j.tecto.2014.02.001

Granja Bruña, J. L., Muñoz-Martín, A., ten Brink, U. S., Carbó-Gorosabel, A., Llanes Estrada, P., Martín-Dávila, J., et al. (2010). Gravity modeling of the Muertos Trough and tectonic implications (north-eastern Caribbean). *Marine Geophysical Research*. https://doi.org/10.1007/s11001-010-9107-8

Granja Bruña, J. L., ten Brink, U. S., Carbó-Gorosabel, A., Muñoz-Martín, A., & Gómez Ballesteros, M. (2009). Morphotectonics of the central Muertos thrust belt and Muertos Trough (northeastern Caribbean). *Marine Geology*, *263*(1–4), 7–33. https://doi.org/10.1016/j.margeo.2009.03.010

Grindlay, N. R., Abrams, L. J., Del Greco, L., & Mann, P. (2005). Toward an integrated understanding of Holocene fault activity in western Puerto Rico: Constraints from high-resolution seismic and

sidescan sonar data. In *Special Paper 385: Active Tectonics and Seismic Hazards of Puerto Rico, the Virgin Islands, and Offshore Areas*. https://doi.org/10.1130/0-8137-2385-x.139

Grindlay, N. R., Mann, P., Dolan, J. F., & van Gestel, J.-P. (2005). Neotectonics and subsidence of the northern Puerto Rico–Virgin Islands margin in response to the oblique subduction of high-standing ridges. In *Special Paper 385: Active Tectonics and Seismic Hazards of Puerto Rico, the Virgin Islands, and Offshore Areas*. https://doi.org/10.1130/0-8137-2385-x.31

Gutscher, M. A., Malavieille, J., Lallemand, S., & Collot, J. Y. (1999). Tectonic segmentation of the North Andean margin: Impact of the Carnegie Ridge collision. *Earth and Planetary Science Letters*. https://doi.org/10.1016/S0012-821X(99)00060-6

Harris, C. W., Miller, M. S., & Porritt, R. W. (2018). Tomographic Imaging of Slab Segmentation and Deformation in the Greater Antilles. *Geochemistry, Geophysics, Geosystems*. https://doi.org/10.1029/2018GC007603

Hayes, G. P., Moore, G. L., Portner, D. E., Hearne, M., Flamme, H., Furtney, M., & Smoczyk, G. M. (2018). Slab2, a comprehensive subduction zone geometry model. *Science*. https://doi.org/10.1126/science.aat4723

Hernaiz Huerta, P. P., Pérez-Valera, F., Abad, M., Monthel, J., & Diaz de Neira, A. (2012). Mélanges and olistostromes in the Puerto Plata area (northern Dominican Republic) as a record of subduction and collisional processes between the Caribbean and North-American plates. Tectonophysics. https://doi.org/10.1016/j.tecto.2011.10.020

Hilde, T. W. C. (1983). Sediment subduction versus accretion around the pacific. *Tectonophysics*, *99*(2–4), 381–397. https://doi.org/10.1016/0040-1951(83)90114-2

Huw Davies, J., & von Blanckenburg, F. (1995). Slab breakoff: A model of lithosphere detachment and its test in the magmatism and deformation of collisional orogens. *Earth and Planetary Science Letters*. https://doi.org/10.1016/0012-821X(94)00237-S

Isacks, B., Sykes, L. R., & Oliver, J. (1969). Focal mechanisms of deep and shallow earthquakes in the Tonga-Kermadec region and the tectonics of Island arcs. *Bulletin of the Geological Society of America*. https://doi.org/10.1130/0016-7606(1969)80[1443:FMODAS]2.0.CO;2

Ivandic, M., Grevemeyer, I., Berhorst, A., Flueh, E. R., & McIntosh, K. (2008). Impact of bending related faulting on the seismic properties of the incoming oceanic plate offshore of Nicaragua. Journal of Geophysical Research: Solid Earth. https://doi.org/10.1029/2007JB005291

Jansma, P. E., & Mattioli, G. S. (2005). GPS results from Puerto Rico and the Virgin Islands: Constraints on tectonic setting and rates of active faulting. In *Special Paper 385: Active Tectonics and Seismic Hazards of Puerto Rico, the Virgin Islands, and Offshore Areas* (pp. 13–30). https://doi.org/10.1130/0-8137-2385-X.13

Jansma, P. E., Mattioli, G. S., Lopez, A., DeMets, C., Dixon, T. H., Mann, P., & Calais, E. (2000). Neotectonics of Puerto Rico and the Virgin Islands, northeastern Caribbean, from GPS geodesy. *Tectonics*. https://doi.org/10.1029/1999TC001170

Jones, G., Hilde, T. W., Sharman, G., & Agnew, D. (1978). *Fault Patterns in Outer Trench Walls and their Tectonic Significance*. *Journal of Physics of the Earth* (Vol. 26). https://doi.org/10.4294/jpe1952.26.Supplement_S85

Joyce, J. (1991). Blueschist metamorphism and deformation on the samana peninsula; A record of subduction and collision in the Greater Antilles. Special Paper of the Geological Society of America. https://doi.org/10.1130/SPE262-p47

Kelleher, J., Sykes, L., & Oliver, J. (1973). Possible criteria for predicting earthquake locations and their application to major plate boundaries of the Pacific and the Caribbean. *Journal of Geophysical Research*. https://doi.org/10.1029/jb078i014p02547

Kobayashi, K., Nakanishi, M., Tamaki, K., & Ogawa, Y. (1998). Outer slope faulting associated with the western Kuril and Japan trenches. Geophysical Journal International. https://doi.org/10.1046/j.1365-246X.1998.00569.x

Ladd, J. W., Tai-Chang Shih, & Tsai, C. J. (1981). Cenozoic tectonics of central Hispaniola and adjacent Caribbean Sea. *American Association of Petroleum Geologists Bulletin*.

Ladd, J. W., Worzel, J. L., & Watkins, J. S. (1977). Multifold seismic reflection records from the northern Venezuela Basin and the north slope of the Muertos Trench. https://doi.org/10.1029/me001p0041

Laurencin, M., Marcaillou, B., Graindorge, D., Lebrun, J. - F., Klingelhoefer, F., Boucard, M., Schenini, L. (2019). The Bunce Fault and Strain Partitioning in the Northern Lesser Antilles. Geophysical Research Letters. https://doi.org/10.1029/2019gl083490

Le Pichon, X., Iiyama, J., Bourgois, J., Mercier de Le´ pinay, B., Tournon, J., & Muller, C., Butterlin, J., G. (1985). First results of the test dives of the French submersible NAUTILE in the Puerto Rico trench (Greater Antilles). *C.R. Acad. Sci. Paris, Ser IIB, 10,* 743–749.

Leroy, S., Mauffret, A., Patriat, P., & Mercier De Lépinay, B. (2000). An alternative interpretation of the Cayman trough evolution from a reidentification of magnetic anomalies. Geophysical Journal International. https://doi.org/10.1046/j.1365-246X.2000.00059.x

Leroy, S., Mercier De Lépinay, B., Mauffret, A., & Pubellier, M. (1996). Structural and tectonic evolution of the eastern Cayman Trough (Caribbean Sea) from seismic reflection data. AAPG Bulletin.

Leroy, S., Ellouz-Zimmermann, N., Corbeau, J., Rolandone, F., de Lépinay, B. M., Meyer, B., et al. (2015). Segmentation and kinematics of the North America-Caribbean plate boundary offshore Hispaniola. *Terra Nova*. https://doi.org/10.1111/ter.12181

López-Venegas, A., ten Brink, U., Geist, E. (2008). Submarine landslide as the source for the October 11, 1918 Mona Passage tsunami: Observations and modeling. Marine Geology. https://doi.org/10.1016/j.margeo.2008.05.001

Manaker, D. M., Calais, E., Freed, A. M., Ali, S. T., Przybylski, P., Mattioli, G., et al. (2008). Interseismic plate coupling and strain partitioning in the Northeastern Caribbean. *Geophysical Journal International*, *174*(3), 889–903. https://doi.org/10.1111/j.1365-246X.2008.03819.x

Mann, P., Calais, E., Ruegg, J. C., DeMets, C., Jansma, P. E., & Mattioli, G. S. (2002). Oblique collision in the northeastern Caribbean from GPS measurements and geological observations. *Tectonics*, *21*(6). https://doi.org/10.1029/2001TC001304

Mann, P., Draper, G., & Lewis, J. F. (1991). An overview of the geologic and tectonic development of Hispaniola. Special Paper of the Geological Society of America. https://doi.org/10.1130/SPE262-p1

Mann, Paul; Grindlay, N.; Dolan, J. F. (1999). Penrose conference report:subduction to strike-slip transition on plate boundaries.

Mann, P., Hempton, M. R., Bradley, D. C., & Burke, K. (1983). Development of Pull-Apart Basins. *The Journal of Geology*. https://doi.org/10.1086/628803

Mann, P., Taylor, F. W., Edwards, R. L., & Ku, T. L. (1995). Actively evolving microplate formation by oblique collision and sideways motion along strike-slip faults: An example from the northeastern Caribbean plate margin. *Tectonophysics*, *246*(1–3), 1–69. https://doi.org/10.1016/0040-1951(94)00268-E

Marshak, S. (2004). Salients, Recesses, Arcs, Oroclines, and Syntaxes — A Review of Ideas Concerning the Formation of Map-view Curves in Fold-thrust Belts. *Thrust Tectonics and Hydrocarbon Systems: AAPG Memoir 82*, *82*(1893), 131–156.

Masson, D. G., & Scanlon, K. M. (1991). The neotectonic setting of Puerto Rico. *Geological Society of America Bulletin*. https://doi.org/10.1130/0016-7606(1991)103<0144:TNSOPR>2.3.CO;2

Mccaffrey, R. (2002). Crustal Block Rotations and Plate Coupling. https://doi.org/10.1029/gd030p0101

McCann, W. R., Nishenko, S. P., Sykes, L. R., & Krause, J. (1979). Seismic gaps and plate tectonics: Seismic potential for major boundaries. *Pure and Applied Geophysics PAGEOPH*. https://doi.org/10.1007/BF00876211

McCann, W. R., Dewey, J. W., Murphy, A. J., & Harding, S. T. (1982). A large normal-fault earthquake in the overriding wedge of the Lesser Antilles subduction zone: the earthquake of 8 October 1974. Bulletin of the Seismological Society of America.

McCann, W. R., & Habermann, R. E. (1989). Morphologic and geologic effects of the subduction of bathymetric highs. Pure and Applied Geophysics PAGEOPH. https://doi.org/10.1007/BF00874624

McCann, W. R. (2006). Estimating the threat of tsunamigenic earthquakes and earthquake induced-landslide tsunamis in the Caribbean. In *Caribbean tsunami hazard* (pp. 43–65).

Meighan, H. E., Pulliam, J., Ten Brink, U., & Lõpez-Venegas, A. M. (2013). Seismic evidence for a slab tear at the Puerto Rico Trench. *Journal of Geophysical Research: Solid Earth*. https://doi.org/10.1002/jgrb.50227

Michaud, F., Collot, J. Y., Ratzov, G., Proust, J. N., Dano, A., Lebrun, J. F., De Min, L. (2018). A honeycomb seafloor morphology in carbonate sediment of the Carnegie Ridge (offshore Ecuador): Formation and potential geodynamic significance. Geology. https://doi.org/10.1130/G45285.1

Millen, D. W., & Hamburger, M. W. (1998). Seismological evidence for tearing of the Pacific plate at the northern termination of the Tonga subduction zone. *Geology*. https://doi.org/10.1130/0091-7613(1998)026<0659:SEFTOT>2.3.CO;2

Molnar, P., & Sykes, L. R. (1969). Tectonics of the caribbean and middle america regions from focal mechanisms and seismicity. *Bulletin of the Geological Society of America*. https://doi.org/10.1130/0016-7606(1969)80[1639:TOTCAM]2.0.CO;2

Mondziel, S., Grindlay, N., Mann, P., Escalona, A., & Abrams, L. (2010). Morphology, structure, and tectonic evolution of the Mona canyon (northern Mona passage) from multibeam bathymetry, side-scan sonar, and seismic reflection profiles. *Tectonics*. https://doi.org/10.1029/2008TC002441

Moussa, M. T., Seiglie, G. A., Meyerhoff, A. A., & Taner, I. (1987). The Quebradillas Limestone (Miocene- Pliocene), northern Puerto Rico, and tectonics of the northeastern Caribbean margin. *Geological Society of America Bulletin*. https://doi.org/10.1130/0016-7606(1987)99<427:TQLMNP>2.0.CO;2

Mullins, H. T., & Hine, A. C. (1989). Scalloped bank margins: beginning of the end for carbonate platforms? *Geology*, *17*(1), 30–33. https://doi.org/10.1130/0091-7613(1989)017<0030:SBMBOT>2.3.CO;2

Mullins, H. T., Breen, N., Dolan, J., Wellner, R. W., Petruccione, J. L., Gaylord, M., et al. (1992). Carbonate platforms along the southeast Bahamas-Hispaniola collision zone. *Marine Geology*, *105*(1–4), 169–209. https://doi.org/10.1016/0025-3227(92)90188-N

Nuñez, D., Córdoba, D., Kissling, E. (2019). Seismic structure of the crust in the western Dominican Republic. *Tectonophysics*. https://doi.org/10.1016/j.tecto.2019.228224

Odonne, F., & Vialon, P. (1983). Analogue models of folds above a wrench fault. *Tectonophysics*. https://doi.org/10.1016/0040-1951(83)90168-3

Oliveira de Sa, A. (2019). Relations entre systèmes tectoniques et sédimentaires sur la bordure nord de la plaque Caraïbe: la faille Oriente-Septentrionale de Cuba à Hispaniola. Master's thesis, ISTEP, UPMC, Paris, France.

Pérez-Estaún, A., Hernaiz Huerta, P. P., Lopera, E., Joubert, M., Escuder Viruete, J., Díaz de Neira, A., et al. (2007). Geología de la República Dominicana: De la construcción de arco-isla a la colisión arco-continente. *Boletin Geologico y Minero*, *118*(2), 157–174.

Perfit, M. R., Heezen, B. C., Rawson, M., & Donnelly, T. W. (1980). Chemistry, origin and tectonic significance of metamorphic rocks from the Puerto Rico Trench. *Marine Geology*. https://doi.org/10.1016/0025-3227(80)90069-9

Pindell, J. L., & Barrett, S. F. (1990). Geological evolution of the Caribbean region; A Plate tectonic perspective. *The Geology of North America*. https://doi.org/n/a

Pindell, J. L., & Draper, G. (1991). Stratigraphy and geological history of the Puerto Plata area, northern Dominican Republic. Special Paper of the Geological Society of America. https://doi.org/10.1130/SPE262-p97

Prentice, C. S., Mann, P., Peña, L. R., & Burr, G. (2003). Slip rate and earthquake recurrence along the central Septentrional fault, North American-Caribbean plate boundary, Dominican Republic. *Journal of Geophysical Research: Solid Earth*, *108*(B3). https://doi.org/10.1029/2001JB000442

Reid, J. A., Plumley, P. W., & Schellekens, J. H. (1991). Paleomagnetic evidence for Late Miocene counterclockwise rotation of North Coast carbonate Sequence, Puerto Rico. *Geophysical Research Letters*. https://doi.org/10.1029/91GL00401

Rodríguez-Zurrunero, A., Granja-Bruña, J. L., Carbó-Gorosabel, A., Muñoz-Martín, A., Gorosabel-Araus, J. M., Gómez de la Peña, L., et al. (2019). Submarine morpho-structure and active processes along the North American-Caribbean plate boundary (Dominican Republic sector). *Marine Geology*. https://doi.org/10.1016/j.margeo.2018.10.010

Russo, R. M., & Villasenor, A. (1995). The 1946 Hispaniola earthquakes and the tectonics of the North America-Caribbean plate boundary zone, northeastern Hispaniola. *Journal of Geophysical Research*, *100*(B4), 6265–6280. https://doi.org/10.1029/94JB02599

Scholl, D. W., Von Huene, R., Vallier, T. L., & Howell, D. G. (1980). Sedimentary masses and concepts about tectonic processes at underthrust ocean margins (subduction). *Geology*, *8*(12), 564–568. https://doi.org/10.1130/0091-7613(1980)8<564:SMACAT>2.0.CO

Seiglie, G. A., Froelich, P. N., & Pilkey, O. H. (1976). Deep-sea sediments of Navidad Basin: correlation of sand layers. *Deep-Sea Research and Oceanographic Abstracts*, *23*(1), 89–101. https://doi.org/10.1016/0011-7471(76)90811-1

Sykes, L. R., McCann, W. R., & Kafka, A. L. (1982). Motion of Caribbean Plate during last 7 million years and implications for earlier Cenozoic movements. *Journal of Geophysical Research: Solid Earth*. https://doi.org/10.1029/jb087ib13p10656

Sylvester, A. G. (1989). Strike-slip faults. *Bulletin of the Geological Society of America*. https://doi.org/10.1130/0016-7606(1988)100<1666:SSF>2.3.CO;2

Symithe, S., Calais, E., De Chabalier, J. B., Robertson, R., & Higgins, M. (2015). Current block motions and strain accumulation on active faults in the Caribbean. Journal of Geophysical Research: Solid Earth. https://doi.org/10.1002/2014JB011779

Ten Brink, U., Lin, J. (2004). Stress interaction between subduction earthquakes and forearc strike-slip faults: modeling and application to the northern Caribbean plate boundary. J. Geophys. Res. 109, B12310. doi:1029/2004JB003031, 2004.

Ten Brink, U., Danforth, W., Polloni, C., Andrews, B., Llanes, P., Smith, S., Parker, E., Uozumi, T. (2004). New Seafloor Map of the Puerto Rico Trench Helps Assess Earthquake and Tsunami Hazards. Eos, Transactions American Geophysical Union. 85 (37), 349–354. 10.1029/2004EO370001.

Ten Brink, U. (2005). Vertical motions of the Puerto Rico Trench and Puerto Rico and their cause. *Journal of Geophysical Research: Solid Earth*. https://doi.org/10.1029/2004JB003459

Ten Brink, U. S., Bakun, W. H., & Flores, C. H. (2011). Historical perspective on seismic hazard to Hispaniola and the northeast Caribbean region. *Journal of Geophysical Research: Solid Earth*, *116*(12). https://doi.org/10.1029/2011JB008497

Ten Brink, U. S., Bakun, W. H., & Flores, C. H. (2013). Seismic hazard from the Hispaniola subduction zone: Correction to "Historical perspective on seismic hazard to Hispaniola and the northeast Caribbean region." Journal of Geophysical Research: Solid Earth, 118(10), 5597–5600. https://doi.org/10.1002/jgrb.50388

Ten Brink, U. S., Bakun, W. H., & Flores, C. H. (2013). Reply to a comment by Carol S. Prentice, Paul Mann, and Luis R. Peña on: Historical perspective on seismic hazard to Hispaniola and the northeast Caribbean region" by U. ten Brink et al. (2011). *Journal of Geophysical Research: Solid Earth*. https://doi.org/10.1002/jgrb.50147

Ten Brink, U. S., & López-Venegas, A. M. (2012). Plate interaction in the NE Caribbean subduction zone from continuous GPS observations. *Geophysical Research Letters*, *39*(10). https://doi.org/10.1029/2012GL051485

Van Benthem, S., Govers, R., Spakman, W., & Wortel, R. (2013). Tectonic evolution and mantle structure of the Caribbean. *Journal of Geophysical Research: Solid Earth*. https://doi.org/10.1002/jgrb.50235

Van Benthem, S., Govers, R., & Wortel, R. (2014). What drives microplate motion and deformation in the northeastern Caribbean plate boundary region? *Tectonics*, *33*(5), 850–873. https://doi.org/10.1002/2013TC003402

Von Huene, R., & Culotta, R. (1989). Tectonic erosion at the front of the Japan Trench convergent margin. *Tectonophysics*, *160*(1–4), 75–90. https://doi.org/10.1016/0040-1951(89)90385-5

Weatherall, P., Marks, K. M., Jakobsson, M., Schmitt, T., Tani, S., Arndt, J. E., et al. (2015). A new digital bathymetric model of the world's oceans. *Earth and Space Science*, *2*(8), 331–345. https://doi.org/10.1002/2015EA000107

Weber, J. C., Dixon, T. H., DeMets, C., Ambeh, W. B., Jansma, P., Mattioli, G., et al. (2001). GPS estimate of relative motion between the Caribbean and South American plates, and geologic implications for Trinidad and Venezuela. *Geology*. https://doi.org/10.1130/0091-7613(2001)029<0075:GEORMB>2.0.CO;2

Winslow, M. A., Guglielmo, G., Nadai, A. C., Vega, L. A., & McCann, W. R. (1991). Tectonic evolution of the San Francisco Ridge of the eastern Cibao basin, northeastern Hispaniola. https://doi.org/10.1130/spe262-p301

Wortel, M. J. R., & Spakman, W. (1992). Structure and dynamics of subducted lithosphere in the Mediterranean region. *Proc. Kon. Ned. Akad. v. Wetensch*.

Zoeten, R. De, & Mann, P. (1999). Chapter 11 Cenozoic el mamey group of northern hispaniola: a sedimentary record of subduction, collisional and strike-slip events within the north America-Caribbean plate boundary zone. *Sedimentary Basins of the World*. https://doi.org/10.1016/S1874-5997(99)80045-8

Figures captions

Fig. 1 Sketched tectonic setting of Caribbean Plate. The tectonic features marked with red lines show the plate boundary. Bold black lines denote major structures. Blue dashed box shows the study area. H: Haiti; DR: Dominican Republic; PR: Puerto Rico; J: Jamaica. SOFZ: Septentrional Oriente Fault Zone; NHDB: North Hispaniola Deformed Belt; BFZ: Bunce Fault Zone; EPGFZ: Enriquillo-Plantain-Garden Fault Zone.

Fig. 2 Digital Elevation Model (DEM) derived from the multibeam bathymetry data and completed with data from GEBCO and SRTM datasets (Weatherall et al., 2015; Far and Kobrick, 2000) and locations of the seismic profiles detailed in this paper. Black lines show multi-channel seismic data from the HAITI-SIS cruises, red lines show multi-channel seismic data from the NORCARIBE cruise (30 m resolution), orange line show single-channel seismic data from the MW8909 cruise and green line show multi-channel seismic data from the IG1503 cruise. Yellow marks the boundary of 50 m-gridded multibeam data from a compilation of USGS/NOAA cruises (Andrews et al., 2014). Blue line marks the boundary of 30 m-gridded multibeam data from HAITI-SIS cruises (Leroy et al., 2015). PR; Puerto Rico. Inset shows tracks from HAITI-SIS, NORCARIBE, MW8909 and IG1503 seismic cruises.

Fig. 3 A) Enlarged map of the study area showing the tectonic domains described in the text, and the morphostructural provinces. The dashed black lines mark the base of the southern slope of BCP, the Puerto Rico Trench outer wall and the island shelf edge. Dotted red line shows the bathymetric profile path of Fig. 3B. The black arrow indicates the averaged plate convergence direction of NOAM relative to CARIB. The red arrows indicate GPS derived velocity map expressed in the North American referenced frame (NAM08) with an ellipse error of 95% of confidence. PRT: Puerto Rico Trench; HT: Hispaniola Trench; ST Bank: Santisima Trinidad Bank; BFZ: Bunce Fault Zone; SOFZ: Septentrional Oriente Fault Zone; PRVI Block: Puerto Rico-Virgin Islands Block. Inset shows with dashed lined boxes the regions used to describe the respective tectonic domains in the study area. B) Bathymetric profile along the axial region of the Northern Cuba, Northern Haiti, Hispaniola and Puerto Rico Trenches.

Fig. 4 Morphostructural interpretation of the northwestern Puerto Rico region. See location in Fig. 3. Red dots show most representative core samples from Fox and Heezen (1975) and Perfit (1980), and submergible dive 55 from Heezen (1985).

Fig. 5 A) Post-stack migrated MCS profile. See location in Figs. 2 and 4. V.E. is 4x on the seafloor. B) Line drawing interpretation. Inset 1 shows a zoom of the Insular Shelf northeast of Hispaniola. Inset 2 shows a zoom of the transpressive belt associated with the SOFZ. Inset 3 shows a zoom of the Puerto Rico Trench. Inset 4 shows a zoom of the faulted blocks of the outer-trench wall.

Fig. 6 Seismicity map showing earthquakes recorded since 1900 with M>3.5 (NEIC catalogue: http://earthquake.usgs.gov/regional/neic/) and focal mechanisms since 1976 (Harvard CMT catalogue). Epicenters are represented as a function of depth on a color scale. Grey boxes indicate seismicity sections showed in Figs. 7 and 8. SOFZ: Septentrional-Oriente Fault Zone; BFZ: Bunce Fault Zone

Fig. 7 Seismicity sections (A-C) showing hypocenter distribution with M>3.5 (NEIC catalogue: http://earthquake.usgs.gov/regional/neic/). The focal mechanisms are in vertical projection (CMT catalogue: www.globalcmt.org). Dashed black lines shows the slab top proposed in this study and dotted red line shows the geometry of the slab proposed by Hayes (2018). Their location is indicated in Fig. 6

Fig. 8 Seismicity sections (D-G) showing hypocenter distribution with M>3.5 (NEIC catalogue: http://earthquake.usgs.gov/regional/neic/). The focal mechanisms are in vertical projection (CMT catalogue: www.globalcmt.org). Dashed black lines shows the slab top proposed in this study and dotted red line shows the geometry of the slab proposed by Hayes (2018). Their location is indicated in Fig. 6

Fig. 9 A) Stacked SCS profile modified from Rodriguez-Zurrunero et al. (2019). See location in Figs. 2 and 4. V.E. is 4x on the seafloor. B) Line drawing interpretation.

Fig. 10 Morphostructural interpretation of northern Hispaniola region. See location in Fig. 3. See Fig. 4 for legend.

Fig. 11 A) Post-stack migrated MCS profile. See location in Figs. 2 and 10. V.E. is 4x on the seafloor. B) Line drawing interpretation. See legend in Fig. 5. Inset 1 shows a zoom of structure in the northern wall

of the SOFZ trace. Inset 2 shows a zoom of the buried frontal anticline in the Caicos Basin. Inset 3 shows a zoom of buried faulted BCP blocks.

Fig. 12 A) Pre-stack migrated MCS profile. See location in Figs. 2 and 10. V.E. is 6x on the seafloor. B) Line drawing interpretation. See legend in Fig. 5. Inset 1 shows a zoom of the highly faulted BCP blocks.

Fig. 13 A) Pre-stack migrated MCS profile. See location in Figs. 2 and 10. V.E. is 6x on the seafloor. B) Line drawing interpretation. See legend in Fig. 5. Inset 1 shows a zoom of the structure between a jog of the SOFZ. Inset 2 shows a zoom of the imbricate fold-and-thrust system in the Lower Forearc.

Fig. 14 Morphostructural interpretation of northwestern Haiti and southeastern Cuba. See location in Fig. 3. See Fig. 4 for legend.

Fig. 15 A) Post-stack migrated MCS profile. See location in Figs. 2 and 14. V.E. is 4x on the seafloor. B) Line drawing interpretation. See legend in Fig. 5. Inset 1 shows a zoom of the SOFZ trace in the Tortue Channel. Inset 2 shows a zoom of the transpressive southern wall of the Northern Haitian Basin.

Fig. 16 A) Post-stack migrated MCS profile. See location in Figs. 2 and 14. V.E. is 4x on the seafloor. B) Line drawing interpretation. See legend in Fig. 5. Inset 1 shows a zoom of antiform associated with the SOFZ in the boundary between the Windward Passage Deep and the Windward Passage Sill. Inset 2 shows a zoom of the sequences of the Windward Passage Sill.

Fig. 17 A) Post-stack migrated MCS profile. See location in Figs. 2 and 14. V.E. is 4x on the seafloor. B) Line drawing interpretation. See legend in Fig. 5. Inset 1 shows a zoom of the imbricate fold-and-thrust system in the northeastern Cuba margin.

Fig. 18 Proposed conceptual models (A-C) for each tectonic domain. SOFZ: Septentrional Oriente Fault Zone; BFZ: Bunce Fault Zone; CFZ: Camu Fault Zone; BCP: Bahamas Carbonate Province.

Fig. 19 3-D view of the proposed geometry for the NOAM slab in the northeastern NOAM-CARIB plate boundary. PR: Puerto Rico

App. A. Gradient map (degrees) of the study area derived from all multibeam bathymetry datasets. See legend for color interpretation.

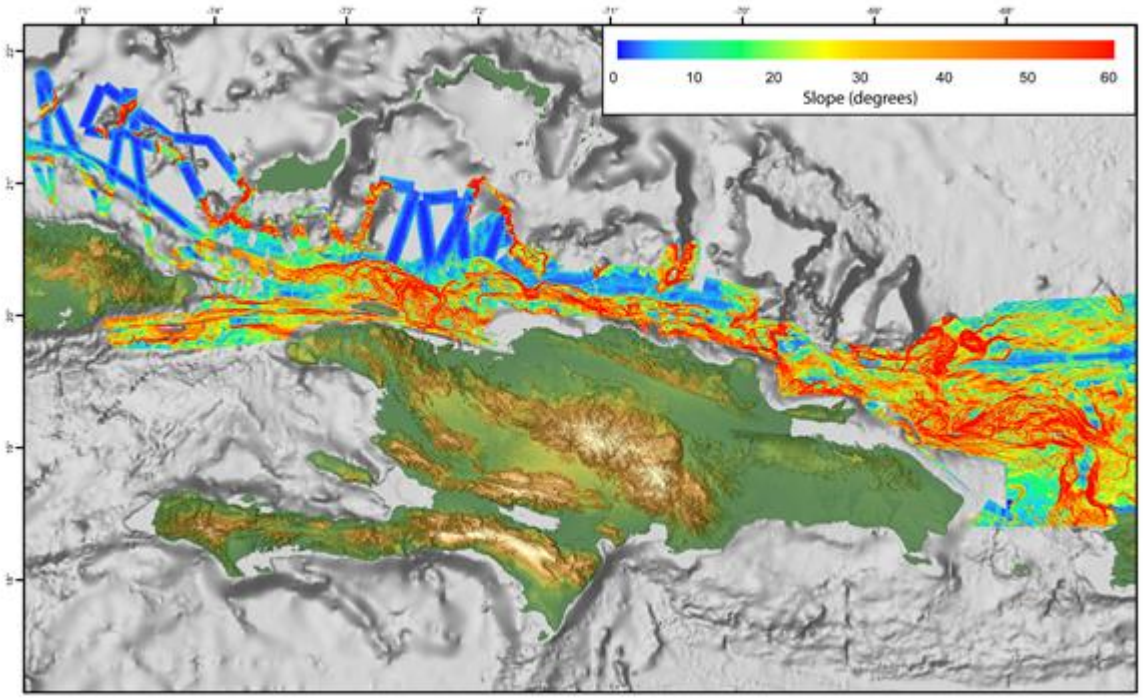

App. B. DEM of the OSD and the OCD derived from the multibeam bathymetry data and completed with data from GEBCO and SRTM datasets (Weatherall et al., 2015; Far and Kobrick, 2000). Same data extent as Fig. 4.

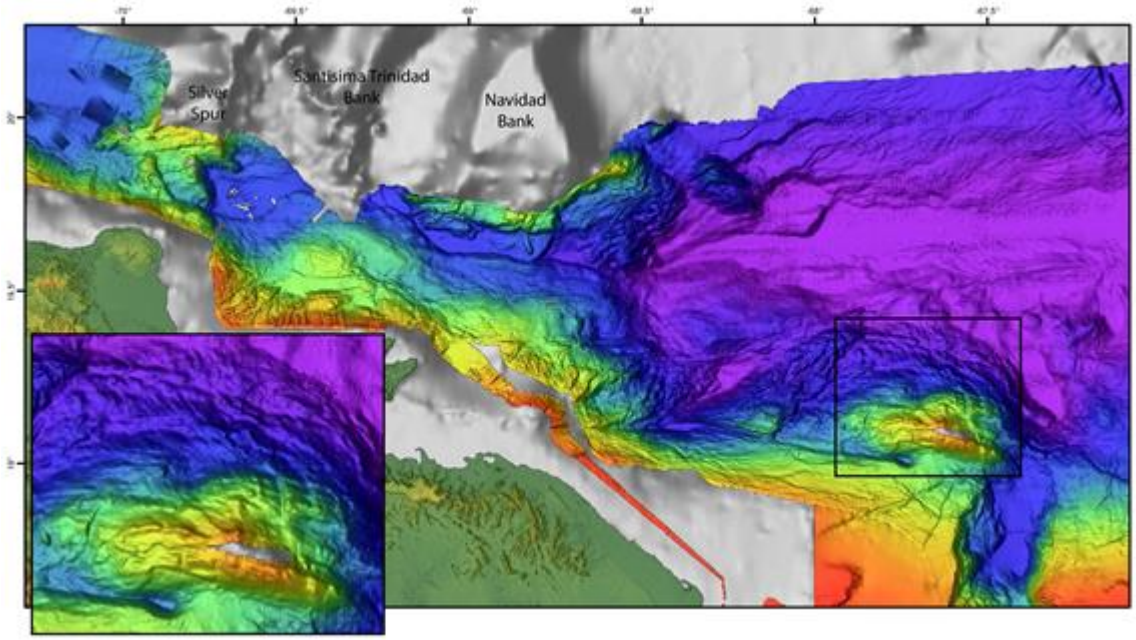

App. C. DEM of the OUD derived from the multibeam bathymetry data and completed with data from GEBCO and SRTM datasets (Weatherall et al., 2015; Far and Kobrick, 2000). Same data extent as Fig. 10.

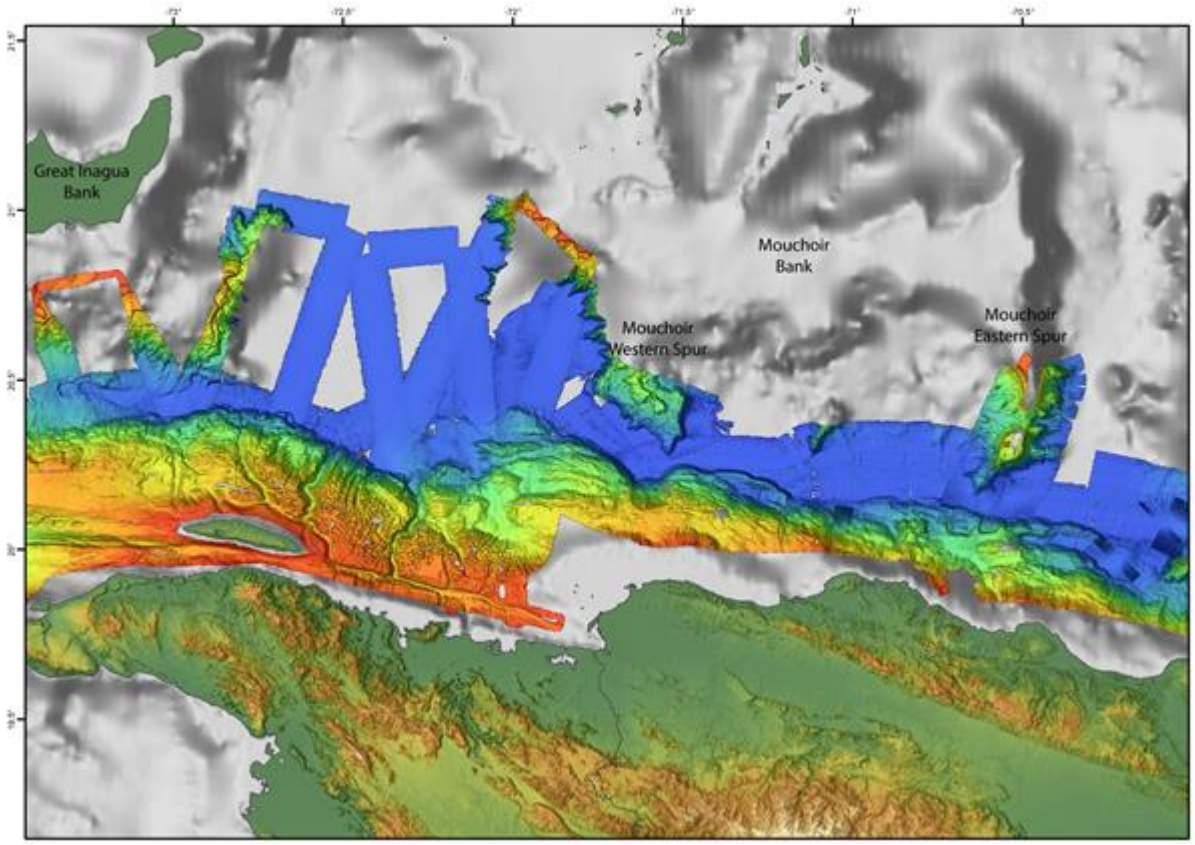

App. D. DEM of the SSD derived from the multibeam bathymetry data and completed with data from GEBCO and SRTM datasets (Weatherall et al., 2015; Far and Kobrick, 2000). Same data extent as Fig. 14.

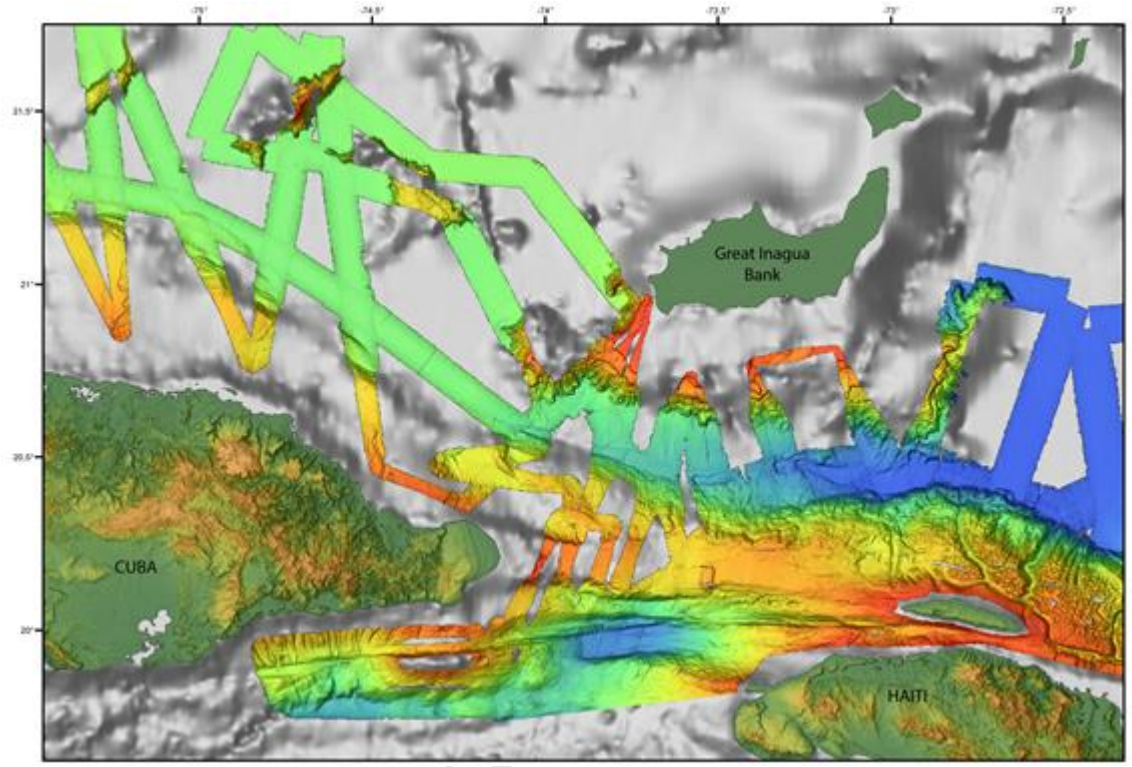

CRediT author

Alvaro Rodriguez-Zurrunero: Conceptualization, Writing - Original Draft, Writing - Review & Editing, Methodology, Formal analysis, Investigation, Visualization

Jose Luis Granja-Bruña: Conceptualization**,** Writing - Review & Editing, Supervision

Alfonso Muñoz-Martin: Conceptualization, Writing - Review & Editing, Supervision

Sylvie Leroy: Writing - Review & Editing

Uri ten Brink: Writing - Review & Editing

Jose Miguel Gorosabel-Araus: Conceptualization, Formal analysis

Laura Gomez de la Peña: Formal analysis

Maria Druet: Formal analysis

Andres Carbó-Gorosabel: Conceptualization, Resources

Declaration of interests

☒ The authors declare that they have no known competing financial interests or personal relationships that could have appeared to influence the work reported in this paper.

☐The authors declare the following financial interests/personal relationships which may be considered as potential competing interests:

Highlights:

Along-strike variations of tectonic framework in northeastern Caribbean margin are studied

Shallow plate boundary structure related to the slab geometry has been defined

First-order fault systems and its associated features have been mapped along the margin

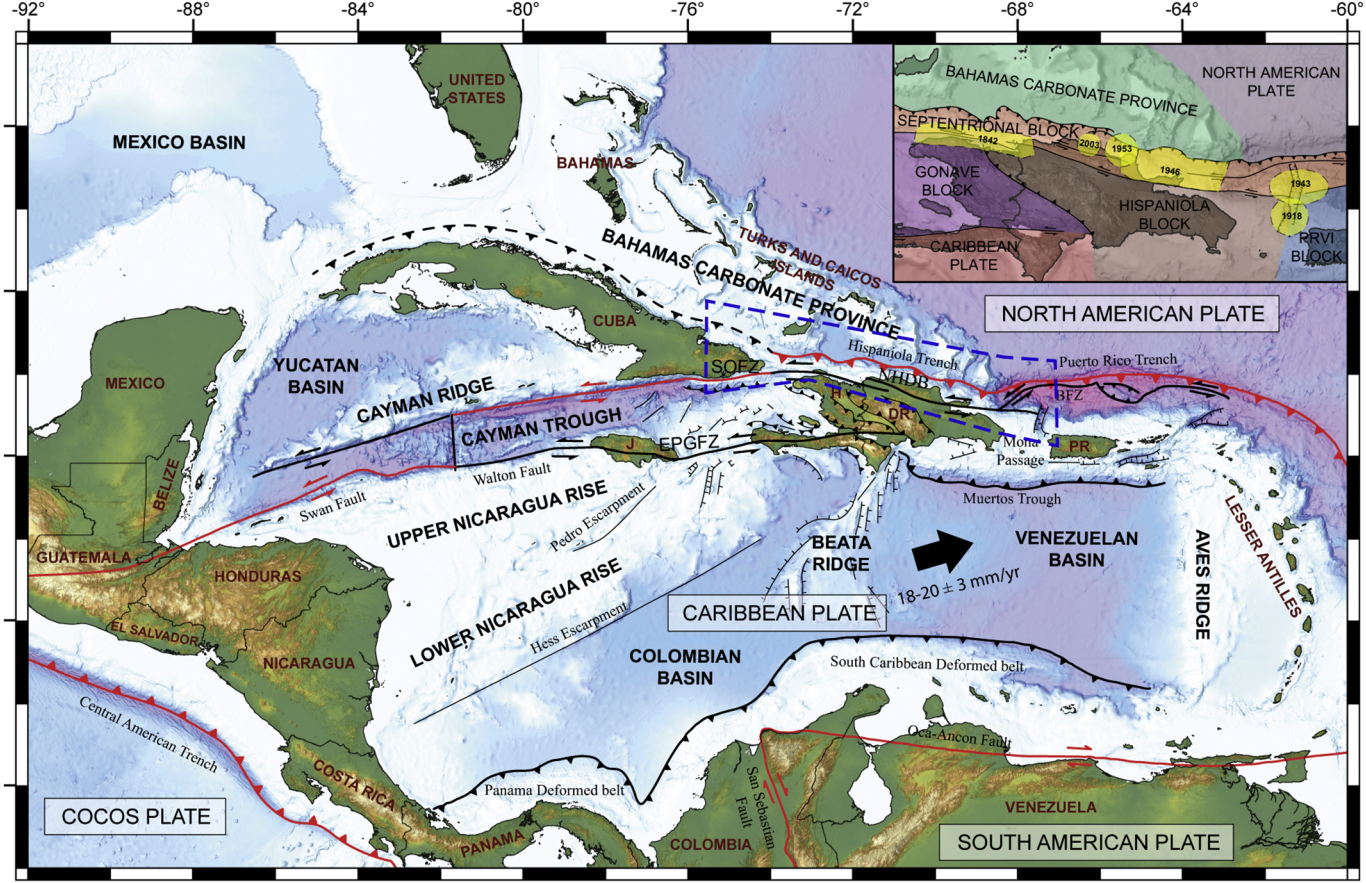
-92°
-88°
-84°
-80°
-76°
-72°
-68°
-64°
-60°
26°
22°
18°
14°
10°
UNITED STATES
MEXICO BASIN
BAHAMAS
TURKS AND CAICOS ISLANDS
BAHAMAS CARBONATE PROVINCE
CUBA
NORTH AMERICAN PLATE
MEXICO
YUCATAN BASIN
CAYMAN RIDGE
CAYMAN TROUGH
SOFZ
Hispaniola Trench
Puerto Rico Trench
NHDB
DR
BFZ
PR
Mona Passage
EPGFZ
Walton Fault
Swan Fault
Muertos Trough
BELIZE
GUATEMALA
HONDURAS
EL SALVADOR
NICARAGUA
UPPER NICARAGUA RISE
Pedro Escarpment
LOWER NICARAGUA RISE
Hess Escarpment
BEATA RIDGE
CARIBBEAN PLATE
18-20 ± 3 mm/yr
VENEZUELAN BASIN
AVES RIDGE
LESSER ANTILLES
COLOMBIAN BASIN
South Caribbean Deformed belt
Oca-Ancon Fault
Central American Trench
COSTA RICA
Panama Deformed belt
San Sebastian Fault
VENEZUELA
COCOS PLATE
PANAMA
COLOMBIA
SOUTH AMERICAN PLATE
BAHAMAS CARBONATE PROVINCE
NORTH AMERICAN PLATE
SEPTENTRIONAL BLOCK
1842
2003
1953
1946
1943
1918
GONAVE BLOCK
HISPANIOLA BLOCK
CARIBBEAN PLATE
PRVI BLOCK

Figure 1

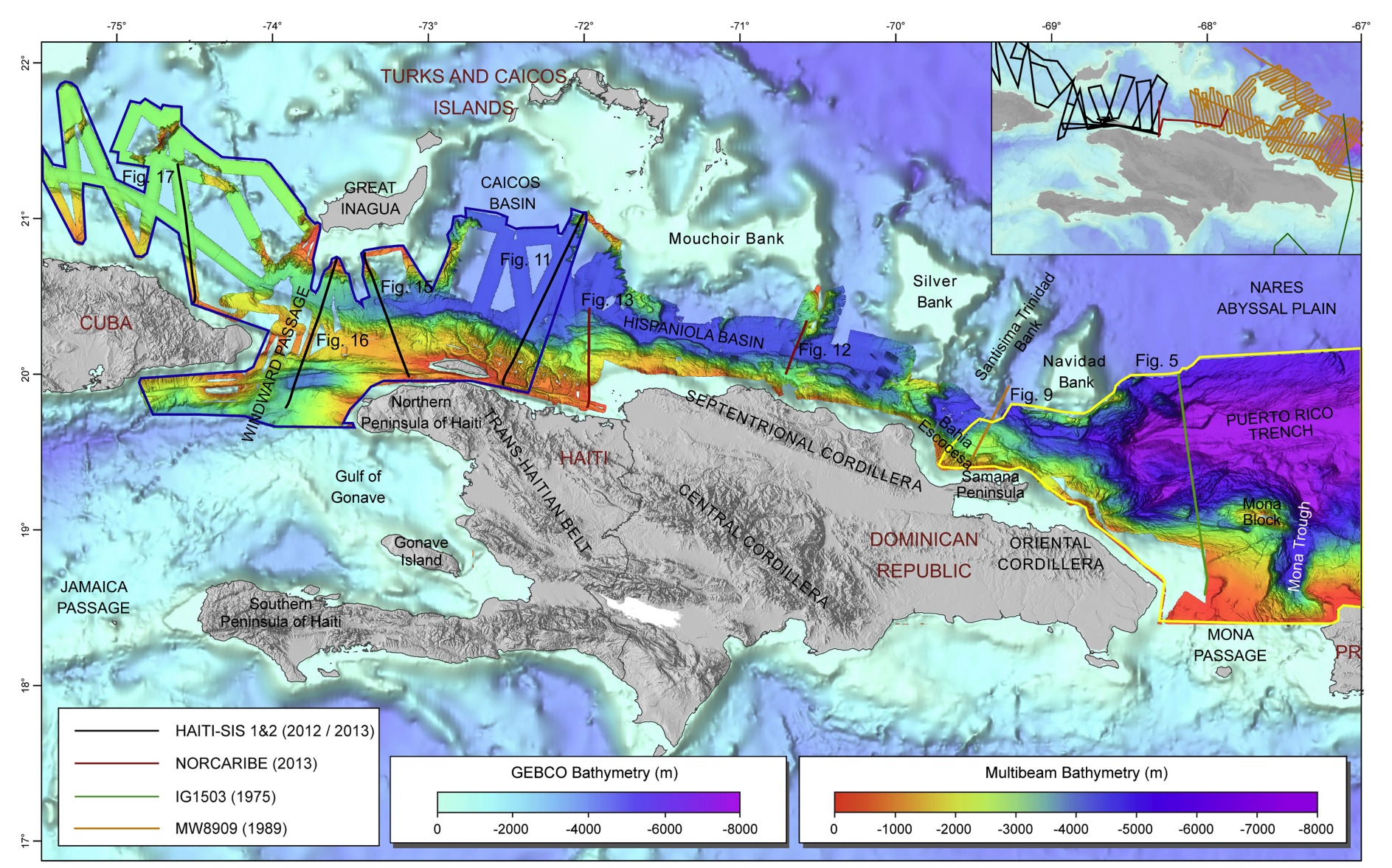
TURKS AND CAICOS ISLANDS
GREAT INAGUA
CAICOS BASIN
Mouchoir Bank
Silver Bank
Navidad Bank
Santisima Trinidad Bank
NARES ABYSSAL PLAIN
CUBA
WINDWARD PASSAGE
HISPANIOLA BASIN
Northern Peninsula of Haiti
TRANS-HAITIAN BELT
HAITI
SEPTENTRIONAL CORDILLERA
CENTRAL CORDILLERA
Gulf of Gonave
Gonave Island
Bahia Escocesa
Samana Peninsula
PUERTO RICO TRENCH
Mona Block
Mona Trough
DOMINICAN REPUBLIC
ORIENTAL CORDILLERA
JAMAICA PASSAGE
Southern Peninsula of Haiti
MONA PASSAGE
PR
Fig. 17
Fig. 16
Fig. 15
Fig. 11
Fig. 13
Fig. 12
Fig. 9
Fig. 5
-75°
-74°
-73°
-72°
-71°
-70°
-69°
-68°
-67°
22°
21°
20°
19°
18°
17°
HAITI-SIS 1&2 (2012 / 2013)
NORCARIBE (2013)
IG1503 (1975)
MW8909 (1989)
GEBCO Bathymetry (m)
0
-2000
-4000
-6000
-8000
Multibeam Bathymetry (m)
0
-1000
-2000
-3000
-4000
-5000
-6000
-7000
-8000

Figure 2

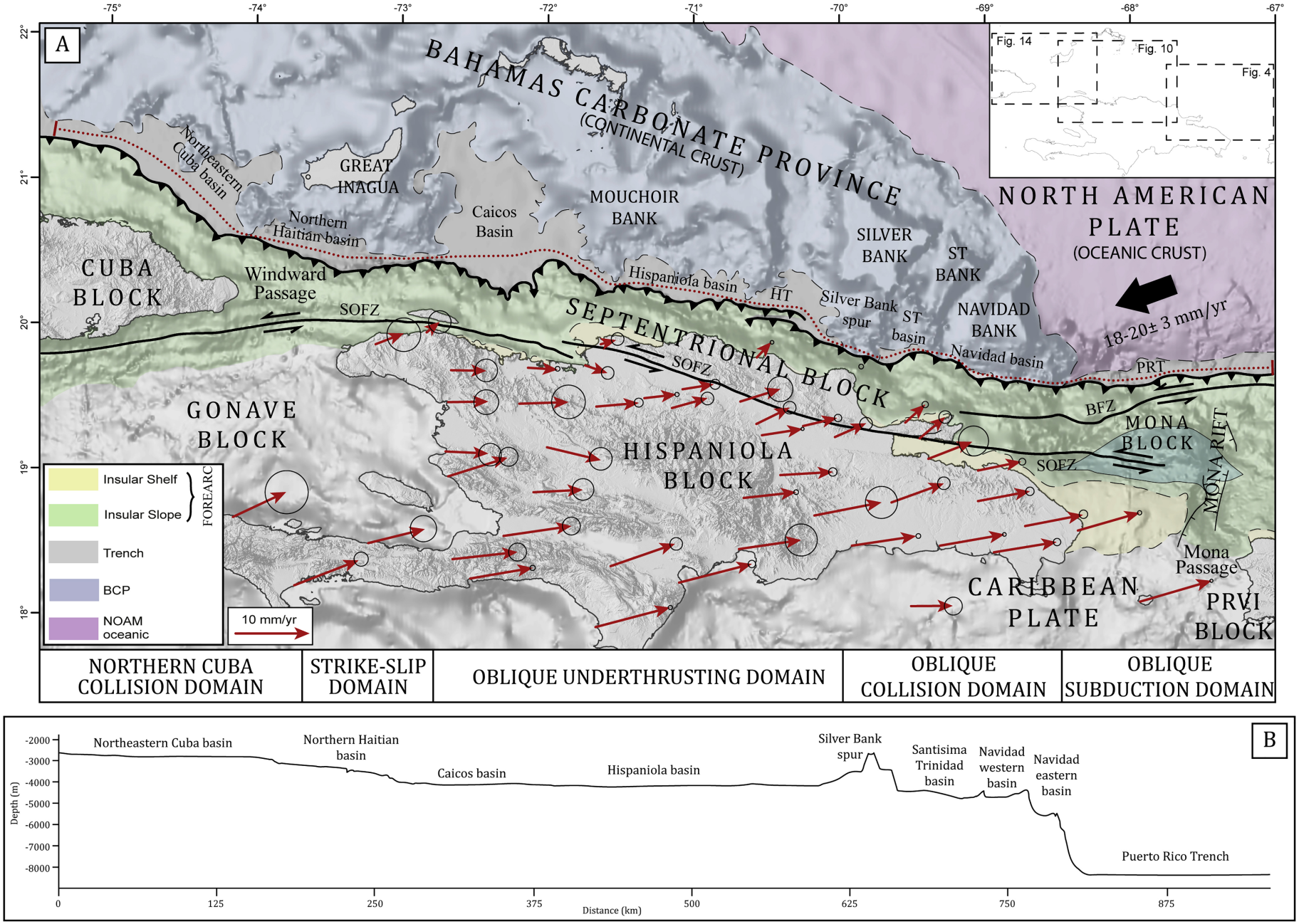
A
BAHAMAS CARBONATE PROVINCE
(CONTINENTAL CRUST)
NORTH AMERICAN PLATE
(OCEANIC CRUST)
18-20± 3 mm/yr
Fig. 14
Fig. 10
Fig. 4
Northeastern Cuba basin
Northern Haitian basin
GREAT INAGUA
Caicos Basin
MOUCHOIR BANK
SILVER BANK
ST BANK
NAVIDAD BANK
Hispaniola basin
HT
Silver Bank spur
ST basin
Navidad basin
PRT
CUBA BLOCK
Windward Passage
SOFZ
SEPTENTRIONAL BLOCK
GONAVE BLOCK
HISPANIOLA BLOCK
BFZ
MONA BLOCK
SOEZ
MONA RIFT
Mona Passage
CARIBBEAN PLATE
PRVI BLOCK
Insular Shelf
Insular Slope
FOREARC
Trench
BCP
NOAM oceanic
10 mm/yr
NORTHERN CUBA COLLISION DOMAIN
STRIKE-SLIP DOMAIN
OBLIQUE UNDERTHRUSTING DOMAIN
OBLIQUE COLLISION DOMAIN
OBLIQUE SUBDUCTION DOMAIN
B
Depth (m)
Distance (km)
Northeastern Cuba basin
Northern Haitian basin
Caicos basin
Hispaniola basin
Silver Bank spur
Santisima Trinidad basin
Navidad western basin
Navidad eastern basin
Puerto Rico Trench

Figure 3

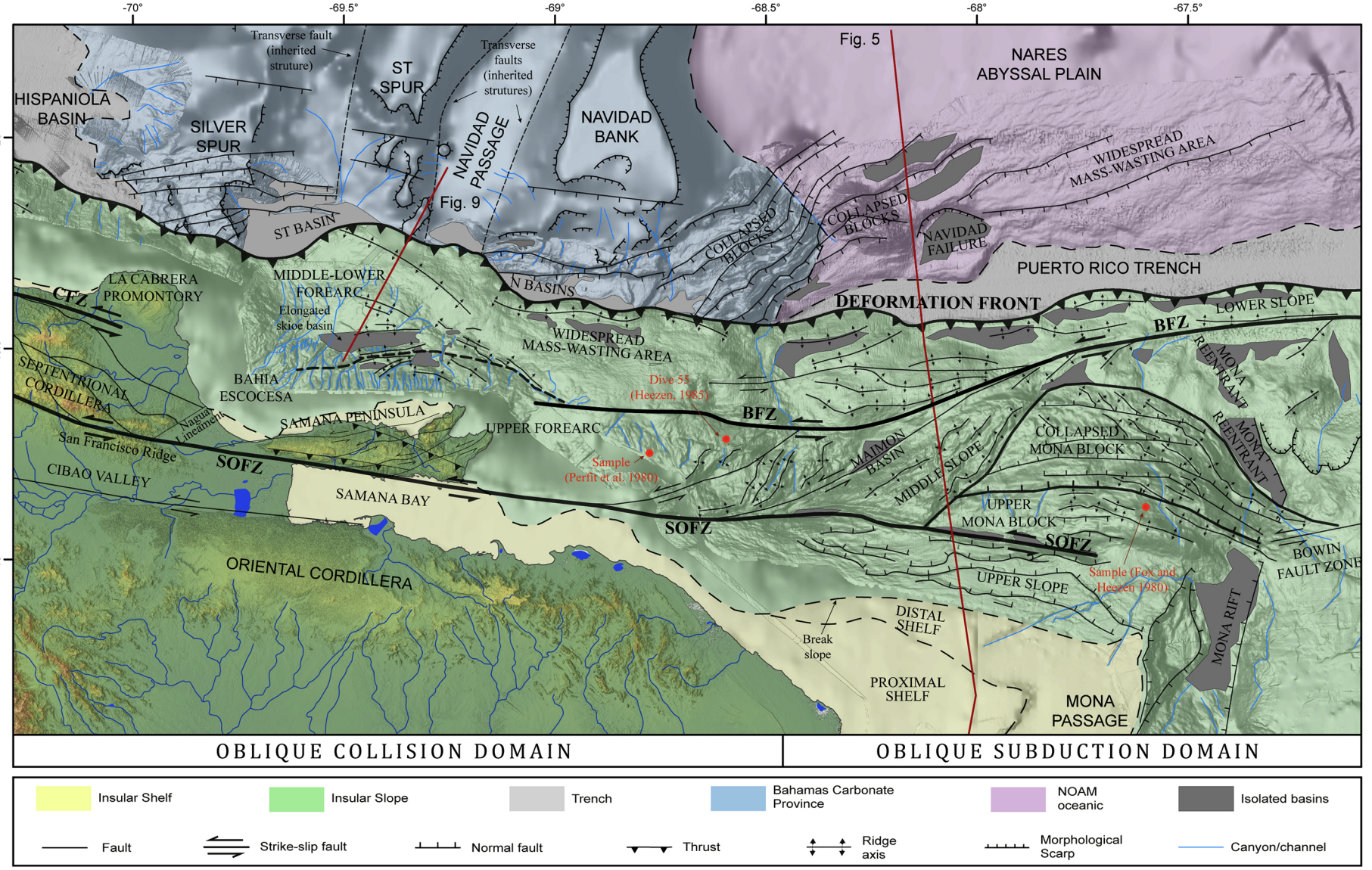
-70°
-69.5°
-69°
-68.5°
-68°
-67.5°
20°
19.5°
19°
Transverse fault (inherited struture)
Transverse faults (inherited strutures)
HISPANIOLA BASIN
SILVER SPUR
ST SPUR
NAVIDAD PASSAGE
NAVIDAD BANK
Fig. 5
Fig. 9
NARES ABYSSAL PLAIN
WIDESPREAD MASS-WASTING AREA
ST BASIN
COLLAPSED BLOCKS
COLLAPSED BLOCKS
NAVIDAD FAILURE
PUERTO RICO TRENCH
LA CABRERA PROMONTORY
CFZ
MIDDLE-LOWER FOREARC
Elongated skioe basin
N BASINS
DEFORMATION FRONT
LOWER SLOPE
BFZ
MONA REENTRANT
WIDESPREAD MASS-WASTING AREA
SEPTENTRIONAL CORDILLERA
BAHIA ESCOCESA
Dive 55 (Heezen, 1985)
BFZ
SAMANA PENINSULA
Nagua Lineament
UPPER FOREARC
MAIMON BASIN
MIDDLE SLOPE
COLLAPSED MONA BLOCK
MONA REENTRANT
San Francisco Ridge
SOFZ
Sample (Perfit et al. 1980)
CIBAO VALLEY
SAMANA BAY
SOFZ
UPPER MONA BLOCK
SOFZ
BOWIN FAULT ZONE
ORIENTAL CORDILLERA
UPPER SLOPE
Sample (Fox and Heezen 1980)
DISTAL SHELF
Break slope
MONA RIFT
PROXIMAL SHELF
MONA PASSAGE
OBLIQUE COLLISION DOMAIN
OBLIQUE SUBDUCTION DOMAIN
Insular Shelf
Insular Slope
Trench
Bahamas Carbonate Province
NOAM oceanic
Isolated basins
Fault
Strike-slip fault
Normal fault
Thrust
Ridge axis
Morphological Scarp
Canyon/channel

Figure 4

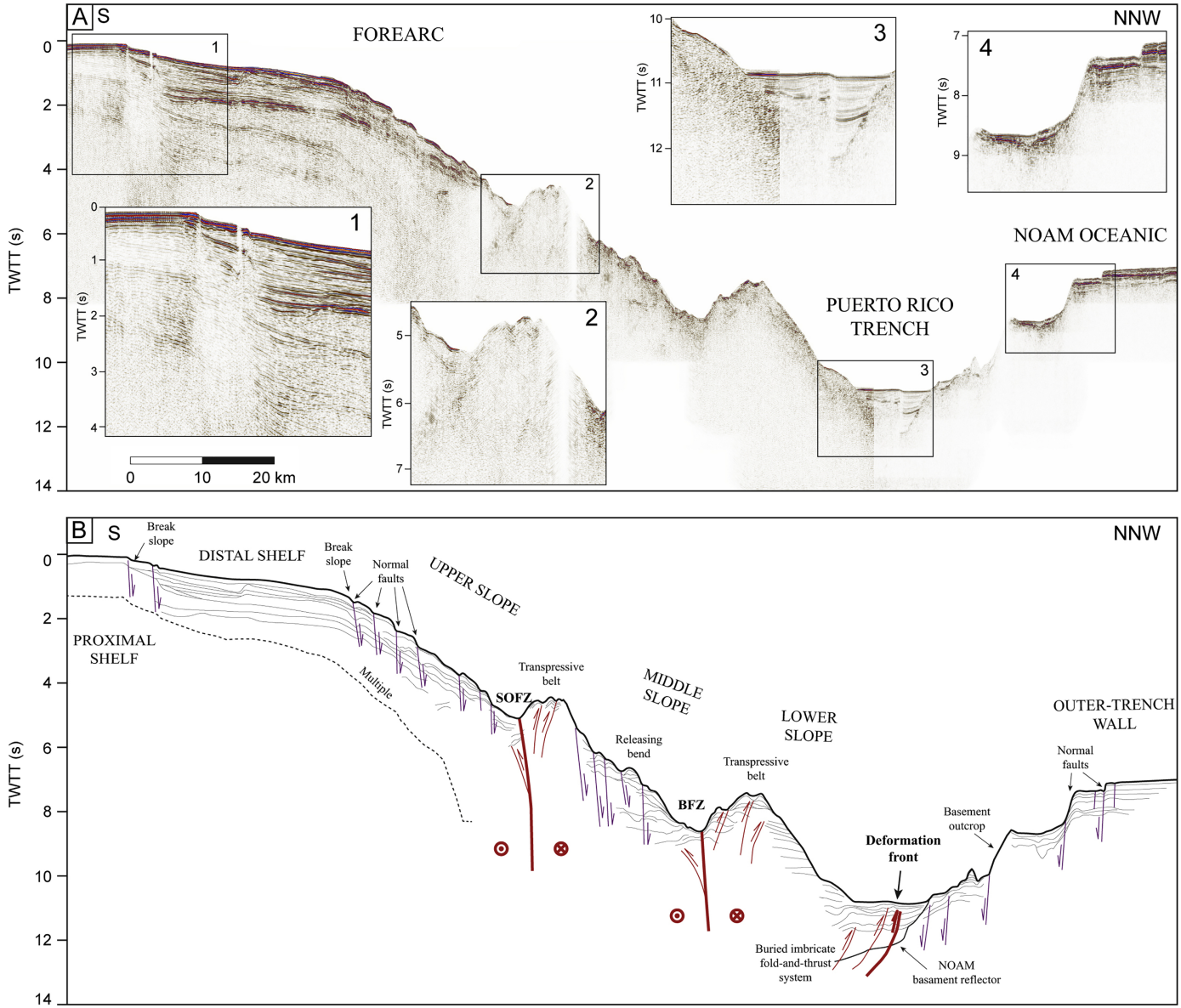
A
S
NNW
FOREARC
PUERTO RICO TRENCH
NOAM OCEANIC
TWTT (s)
0 10 20 km
B
S
NNW
Break slope
DISTAL SHELF
Break slope
Normal faults
UPPER SLOPE
PROXIMAL SHELF
Multiple
Transpressive belt
SOFZ
MIDDLE SLOPE
Releasing bend
LOWER SLOPE
Transpressive belt
BFZ
OUTER-TRENCH WALL
Normal faults
Basement outcrop
Deformation front
Buried imbricate fold-and-thrust system
NOAM basement reflector
TWTT (s)

Figure 5

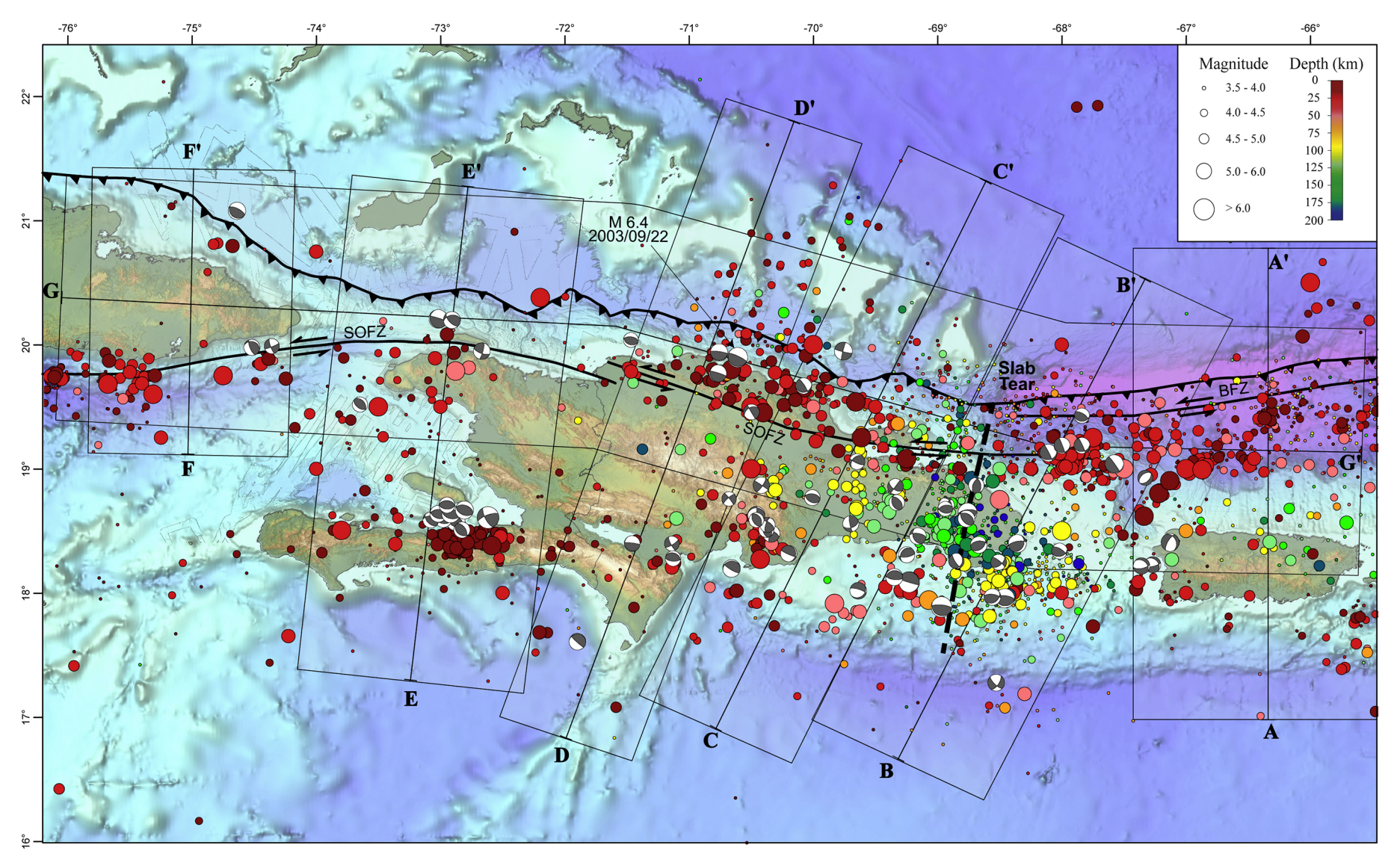
-76°
-75°
-74°
-73°
-72°
-71°
-70°
-69°
-68°
-67°
-66°
22°
21°
20°
19°
18°
17°
16°
Magnitude
3.5 - 4.0
4.0 - 4.5
4.5 - 5.0
5.0 - 6.0
> 6.0
Depth (km)
0
25
50
75
100
125
150
175
200
M 6.4
2003/09/22
SOFZ
SOFZ
BFZ
Slab
Tear
A
A'
B
B'
C
C'
D
D'
E
E'
F
F'
G
G'

Figure 6

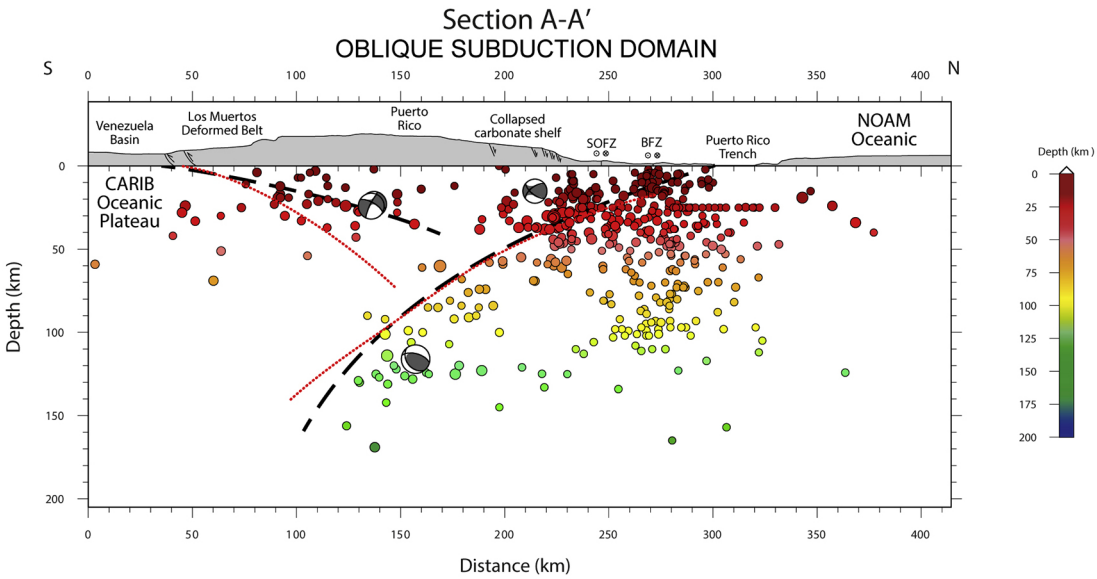
Section A-A′
OBLIQUE SUBDUCTION DOMAIN
S
N
Venezuela Basin
Los Muertos Deformed Belt
Puerto Rico
Collapsed carbonate shelf
SOFZ
BFZ
Puerto Rico Trench
NOAM Oceanic
CARIB Oceanic Plateau
Depth (km)
Distance (km)
Depth (km)

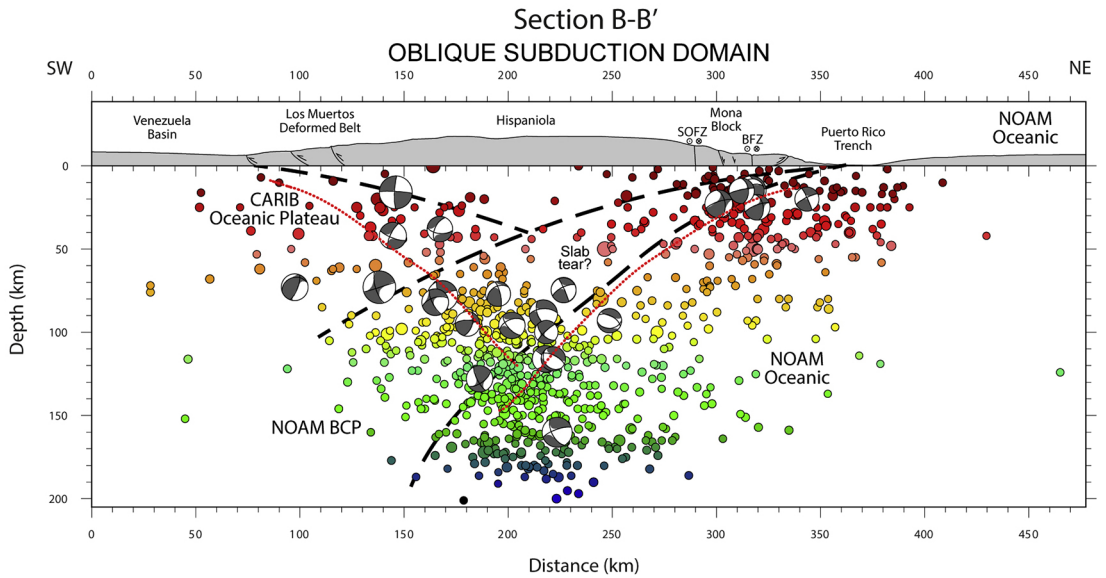
Section B-B′
OBLIQUE SUBDUCTION DOMAIN
SW
NE
Venezuela Basin
Los Muertos Deformed Belt
Hispaniola
Mona Block
SOFZ
BFZ
Puerto Rico Trench
NOAM Oceanic
CARIB Oceanic Plateau
Slab tear?
NOAM Oceanic
NOAM BCP
Depth (km)
Distance (km)

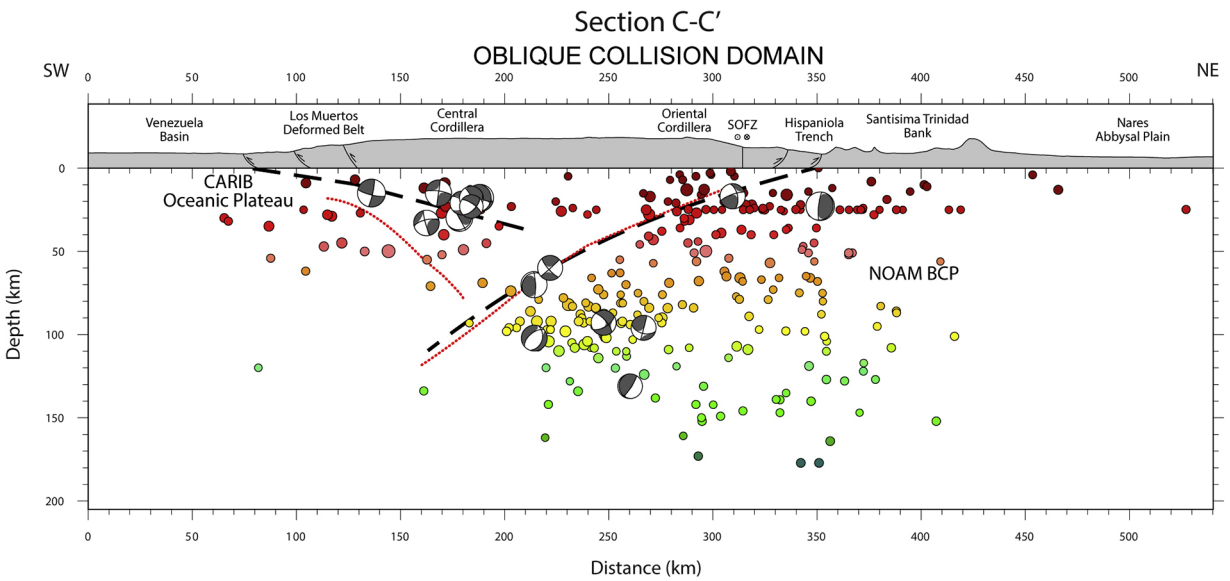
Section C-C′
OBLIQUE COLLISION DOMAIN
SW
NE
Venezuela Basin
Los Muertos Deformed Belt
Central Cordillera
Oriental Cordillera
SOFZ
Hispaniola Trench
Santisima Trinidad Bank
Nares Abbysal Plain
CARIB Oceanic Plateau
NOAM BCP
Depth (km)
Distance (km)

Figure 7

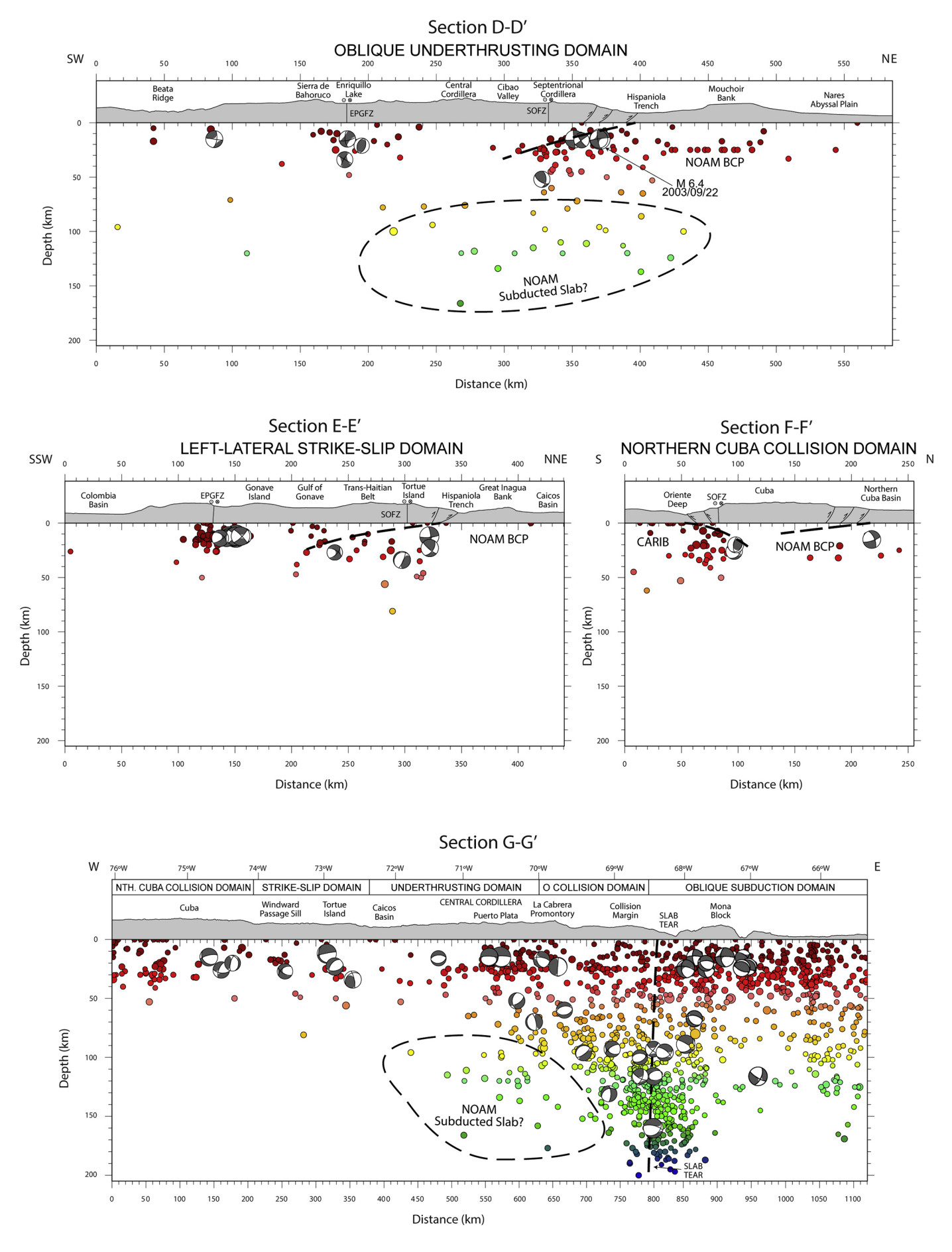
Section D-D′
OBLIQUE UNDERTHRUSTING DOMAIN
SW
NE
Beata Ridge
Sierra de Bahoruco
Enriquillo Lake
EPGFZ
Central Cordillera
Cibao Valley
Septentrional Cordillera
SOFZ
Hispaniola Trench
Mouchoir Bank
Nares Abyssal Plain
NOAM BCP
M 6.4
2003/09/22
NOAM
Subducted Slab?
Depth (km)
Distance (km)
Section E-E′
LEFT-LATERAL STRIKE-SLIP DOMAIN
SSW
NNE
Colombia Basin
EPGFZ
Gonave Island
Gulf of Gonave
Trans-Haitian Belt
Tortue Island
SOFZ
Hispaniola Trench
Great Inagua Bank
Caicos Basin
NOAM BCP
Depth (km)
Distance (km)
Section F-F′
NORTHERN CUBA COLLISION DOMAIN
S
N
Oriente Deep
SOFZ
Cuba
Northern Cuba Basin
CARIB
NOAM BCP
Depth (km)
Distance (km)
Section G-G′
W
E
NTH. CUBA COLLISION DOMAIN
STRIKE-SLIP DOMAIN
UNDERTHRUSTING DOMAIN
O COLLISION DOMAIN
OBLIQUE SUBDUCTION DOMAIN
Cuba
Windward Passage Sill
Tortue Island
Caicos Basin
CENTRAL CORDILLERA
Puerto Plata
La Cabrera Promontory
Collision Margin
SLAB TEAR
Mona Block
NOAM
Subducted Slab?
SLAB TEAR
Depth (km)
Distance (km)

Figure 8

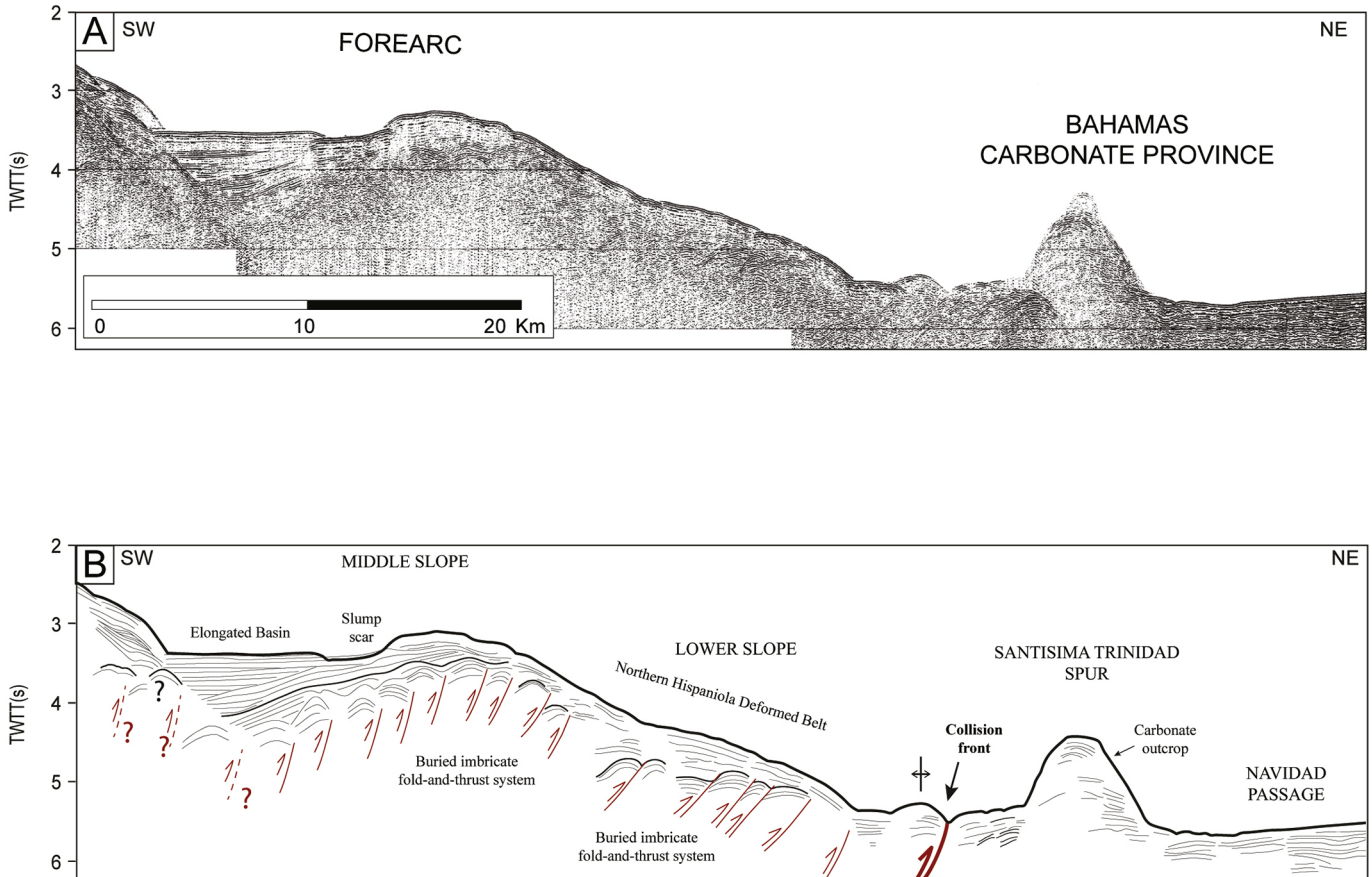
A
SW
NE
FOREARC
BAHAMAS
CARBONATE PROVINCE
TWTT(s)
2
3
4
5
6
0
10
20 Km
B
SW
NE
MIDDLE SLOPE
LOWER SLOPE
SANTISIMA TRINIDAD
SPUR
Elongated Basin
Slump
scar
Northern Hispaniola Deformed Belt
Collision
front
Carbonate
outcrop
NAVIDAD
PASSAGE
Buried imbricate
fold-and-thrust system
Buried imbricate
fold-and-thrust system
TWTT(s)
2
3
4
5
6

Figure 9

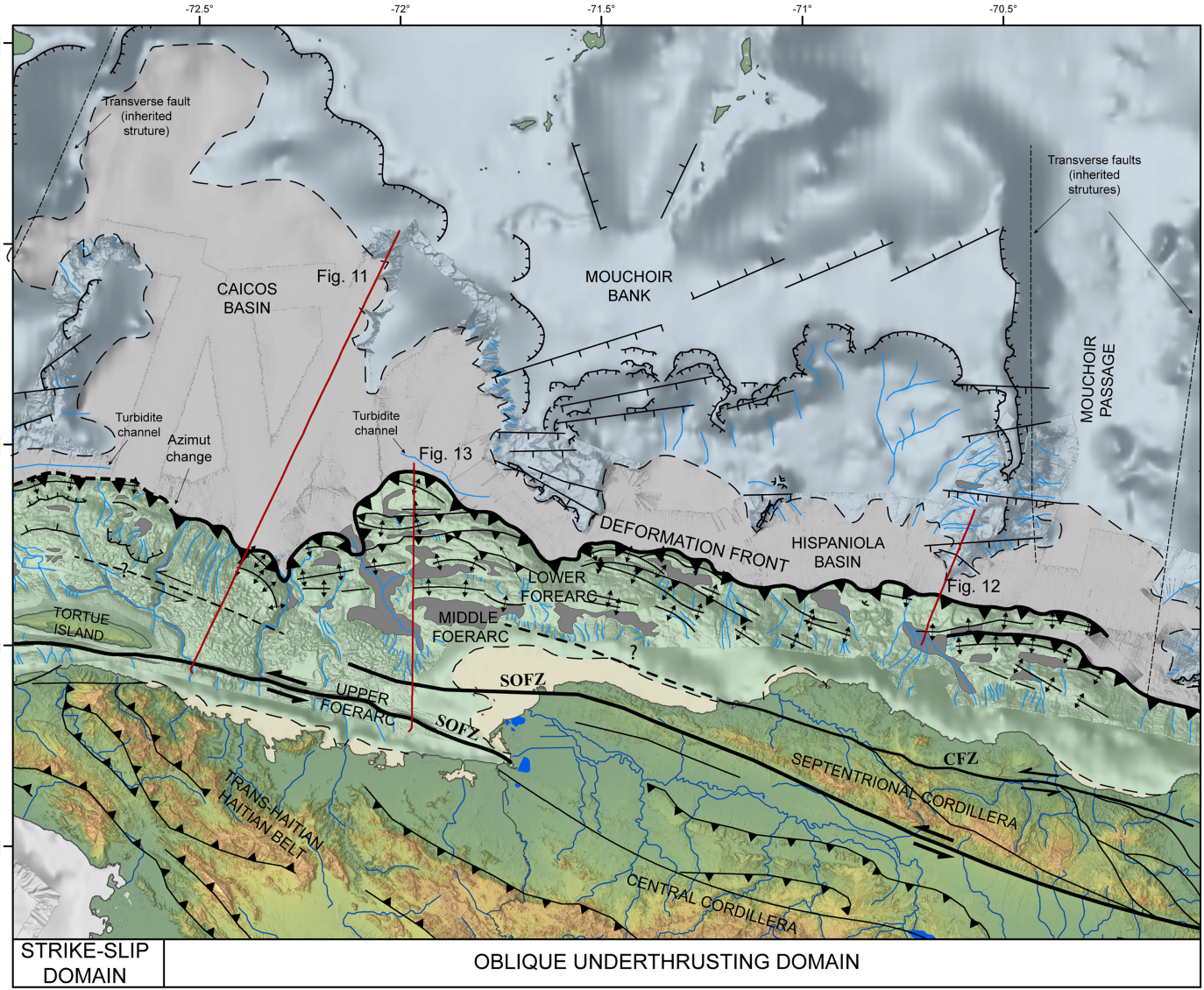
-72.5°
-72°
-71.5°
-71°
-70.5°
21.5°
21°
20.5°
20°
19.5°
Transverse fault (inherited struture)
CAICOS BASIN
Fig. 11
MOUCHOIR BANK
Transverse faults (inherited strutures)
MOUCHOIR PASSAGE
Turbidite channel
Azimut change
Turbidite channel
Fig. 13
DEFORMATION FRONT
HISPANIOLA BASIN
Fig. 12
LOWER FOREARC
MIDDLE FOERARC
TORTUE ISLAND
SOFZ
UPPER FOERARC
SOFZ
CFZ
SEPTENTRIONAL CORDILLERA
TRANS-HAITIAN HAITIAN BELT
CENTRAL CORDILLERA
STRIKE-SLIP DOMAIN
OBLIQUE UNDERTHRUSTING DOMAIN

Figure 10

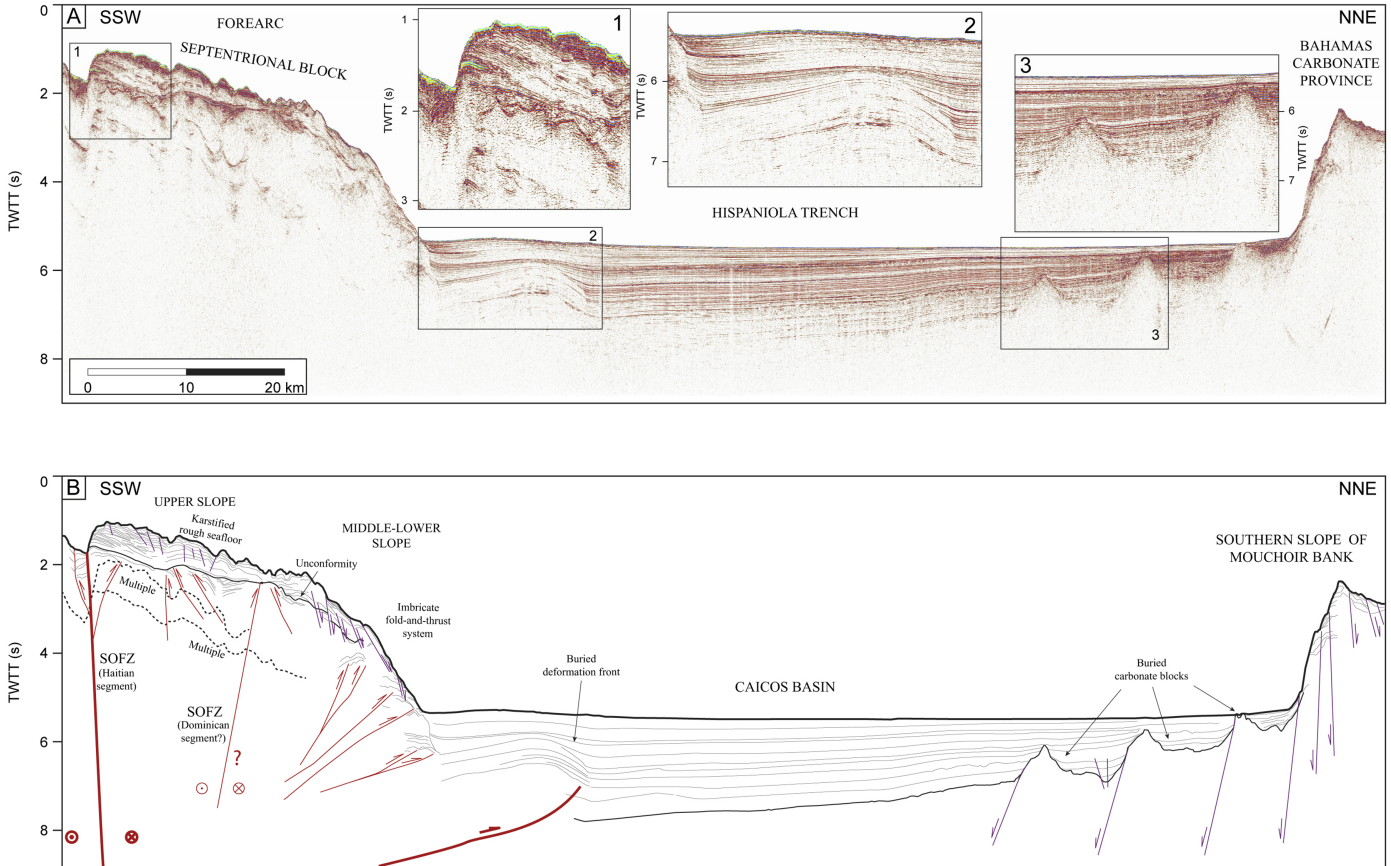
A
SSW
NNE
FOREARC
SEPTENTRIONAL BLOCK
HISPANIOLA TRENCH
BAHAMAS
CARBONATE
PROVINCE
TWTT (s)
0
10
20 km
B
SSW
NNE
UPPER SLOPE
Karstified
rough seafloor
MIDDLE-LOWER
SLOPE
Unconformity
Multiple
Multiple
Imbricate
fold-and-thrust
system
SOFZ
(Haitian
segment)
SOFZ
(Dominican
segment?)
?
Buried
deformation front
CAICOS BASIN
Buried
carbonate blocks
SOUTHERN SLOPE OF
MOUCHOIR BANK
TWTT (s)

Figure 11

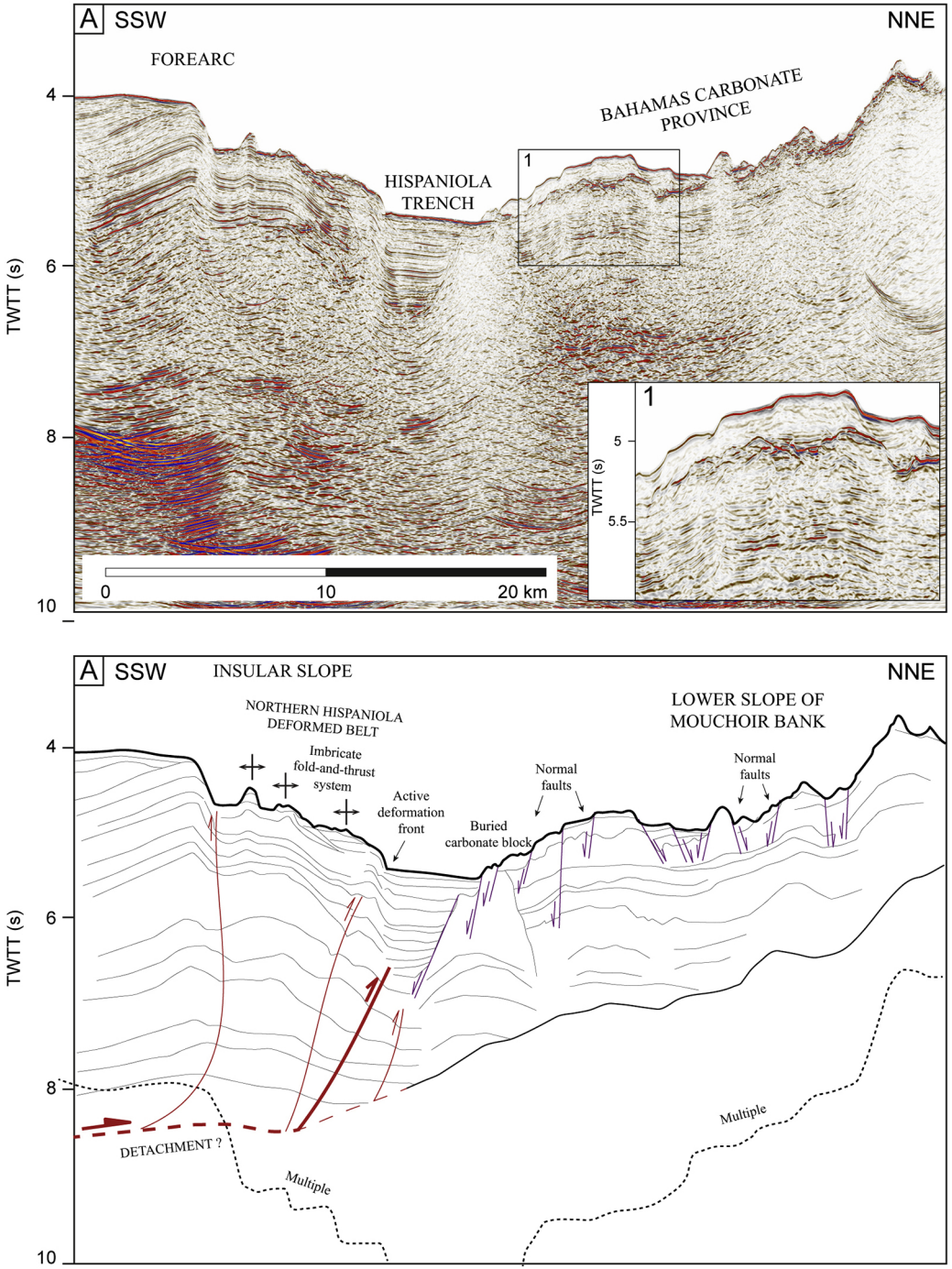
A
SSW
NNE
FOREARC
BAHAMAS CARBONATE PROVINCE
HISPANIOLA TRENCH
1
TWTT (s)
4
6
8
10
0
10
20 km
5
5.5
INSULAR SLOPE
NORTHERN HISPANIOLA DEFORMED BELT
LOWER SLOPE OF MOUCHOIR BANK
Imbricate fold-and-thrust system
Active deformation front
Buried carbonate block
Normal faults
DETACHMENT ?
Multiple

Figure 12

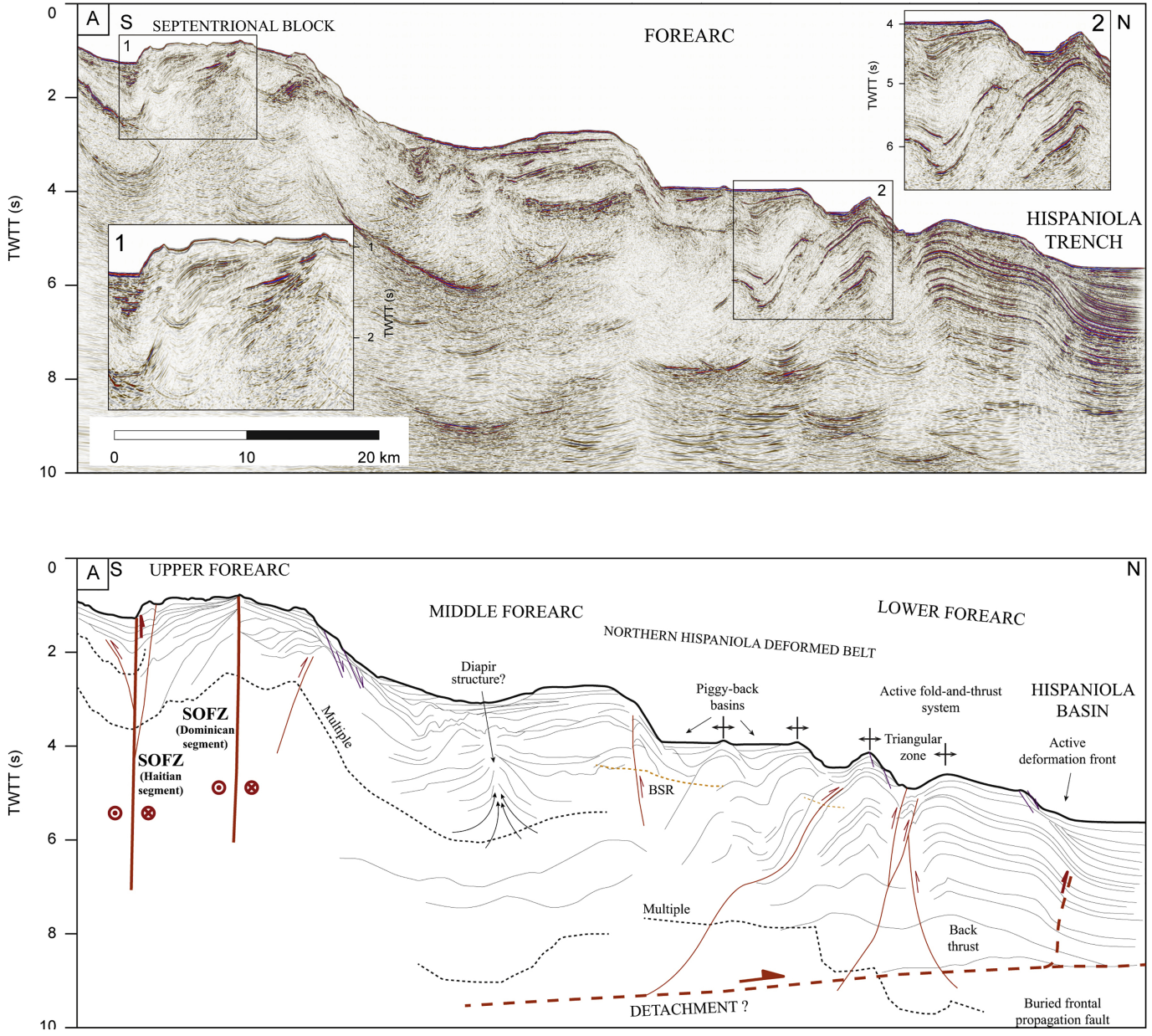
A
S
SEPTENTRIONAL BLOCK
FOREARC
N
HISPANIOLA TRENCH
TWTT (s)
0
2
4
6
8
10
1
2
0
10
20 km
UPPER FOREARC
MIDDLE FOREARC
LOWER FOREARC
NORTHERN HISPANIOLA DEFORMED BELT
HISPANIOLA BASIN
SOFZ (Dominican segment)
SOFZ (Haitian segment)
Multiple
Diapir structure?
Piggy-back basins
Active fold-and-thrust system
Triangular zone
Active deformation front
BSR
Multiple
Back thrust
DETACHMENT ?
Buried frontal propagation fault

Figure 13

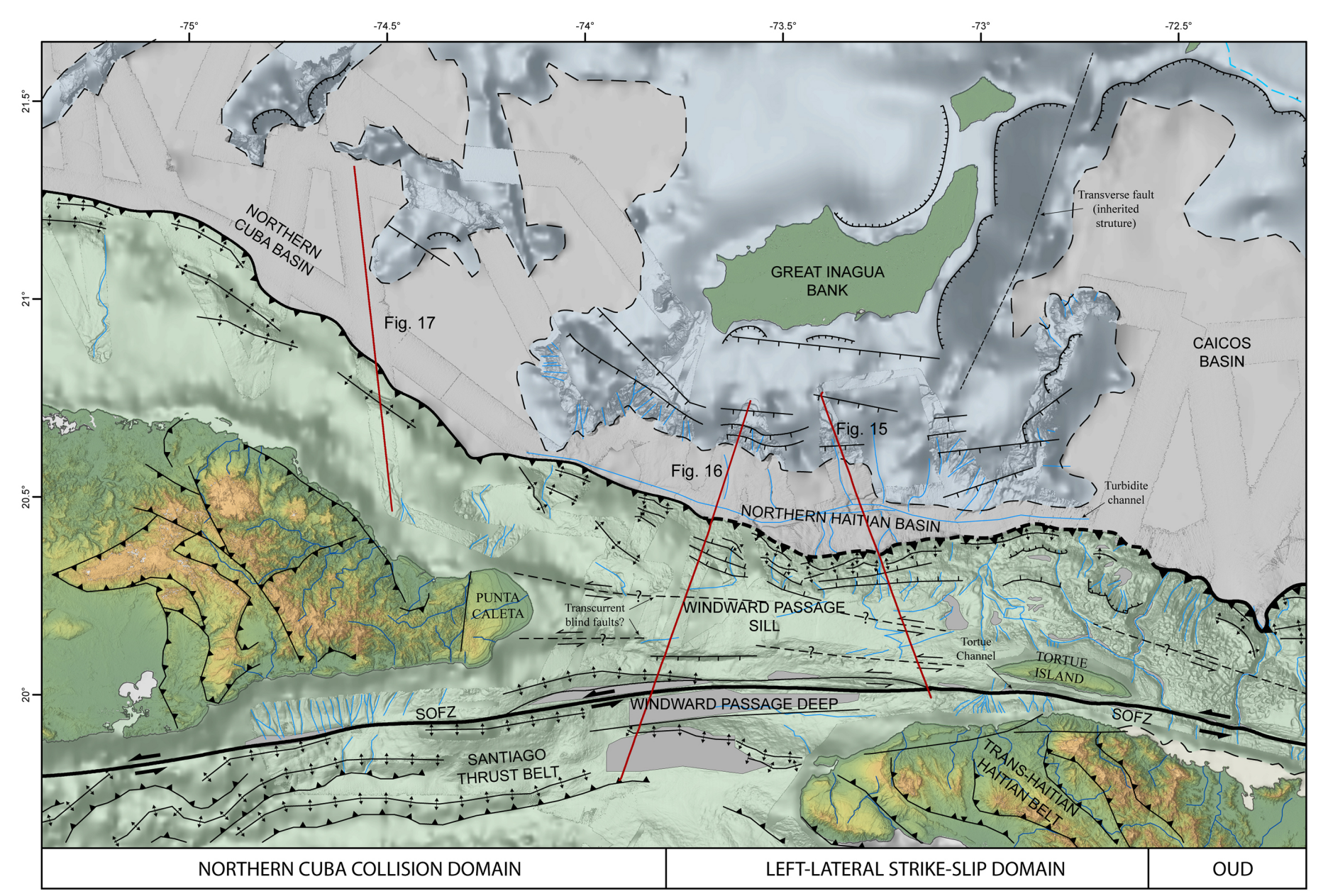
-75°
-74.5°
-74°
-73.5°
-73°
-72.5°
21.5°
21°
20.5°
20°
NORTHERN CUBA BASIN
Fig. 17
GREAT INAGUA BANK
Transverse fault (inherited struture)
CAICOS BASIN
Fig. 15
Fig. 16
Turbidite channel
NORTHERN HAITIAN BASIN
PUNTA CALETA
Transcurrent blind faults?
WINDWARD PASSAGE SILL
Tortue Channel
TORTUE ISLAND
SOFZ
WINDWARD PASSAGE DEEP
SOFZ
SANTIAGO THRUST BELT
TRANS-HAITIAN HAITIAN BELT
NORTHERN CUBA COLLISION DOMAIN
LEFT-LATERAL STRIKE-SLIP DOMAIN
OUD

Figure 14

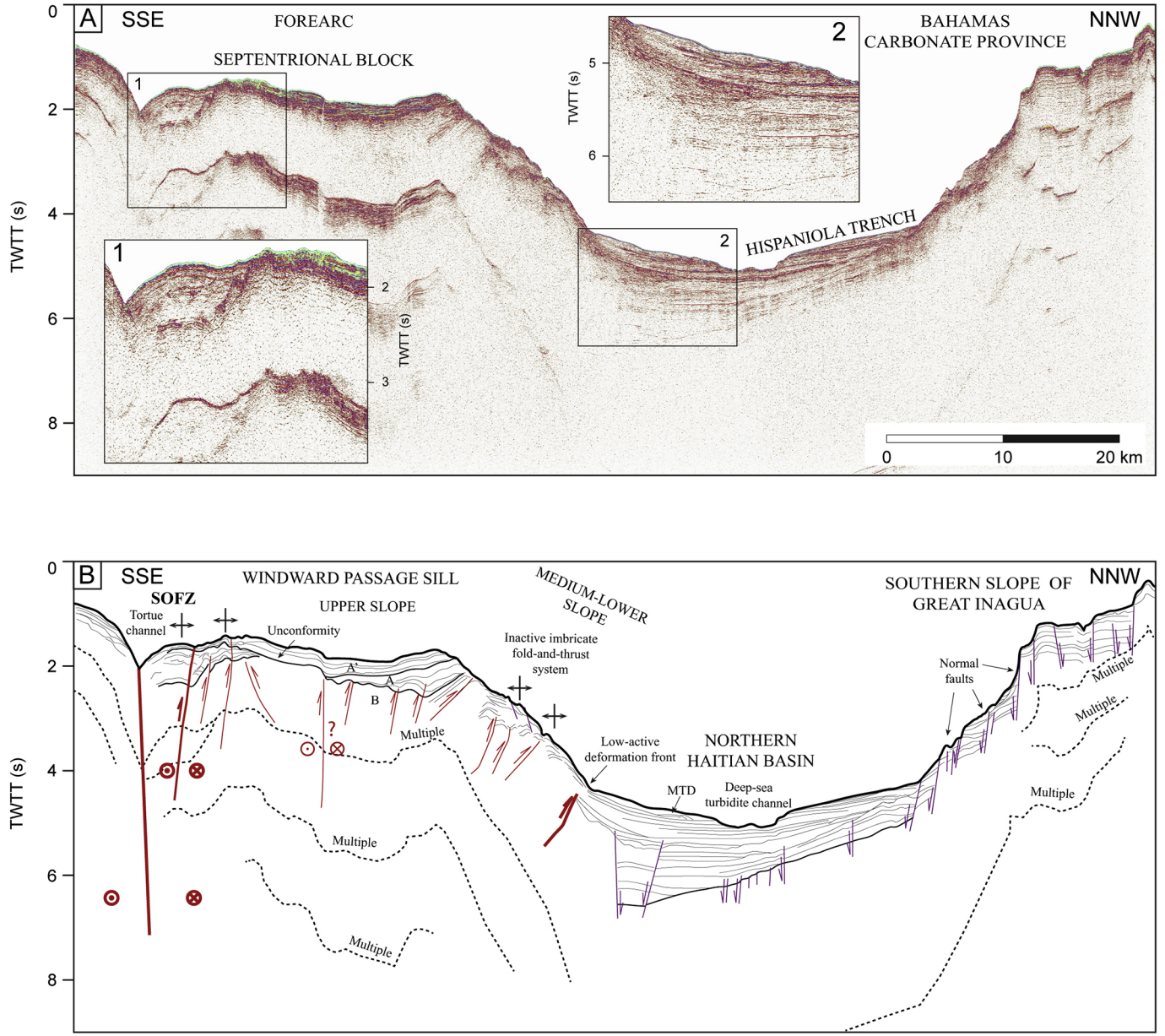
A
SSE
FOREARC
SEPTENTRIONAL BLOCK
BAHAMAS
CARBONATE PROVINCE
NNW
HISPANIOLA TRENCH
TWTT (s)
0 10 20 km
B
SSE
SOFZ
Tortue channel
WINDWARD PASSAGE SILL
UPPER SLOPE
Unconformity
MEDIUM-LOWER SLOPE
Inactive imbricate fold-and-thrust system
SOUTHERN SLOPE OF GREAT INAGUA
NNW
Normal faults
Low-active deformation front
NORTHERN HAITIAN BASIN
MTD
Deep-sea turbidite channel
Multiple
A'
A
B

Figure 15

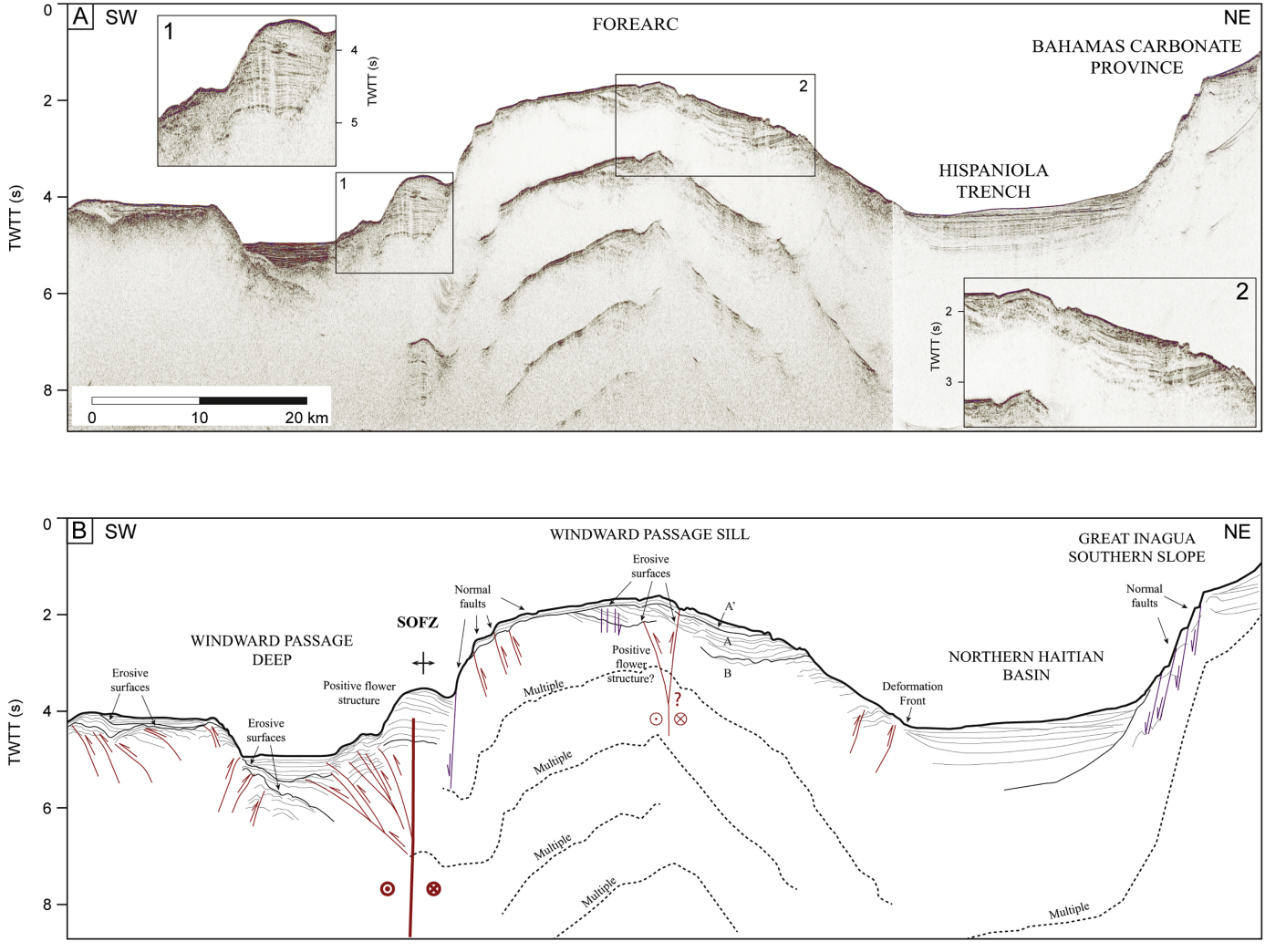
A
SW
NE
FOREARC
BAHAMAS CARBONATE PROVINCE
HISPANIOLA TRENCH
TWTT (s)
0
2
4
6
8
1
2
4
5
0
10
20 km
2
3
B
SW
NE
WINDWARD PASSAGE SILL
GREAT INAGUA SOUTHERN SLOPE
WINDWARD PASSAGE DEEP
SOFZ
NORTHERN HAITIAN BASIN
Erosive surfaces
Normal faults
Positive flower structure
Positive flower structure?
Deformation Front
Multiple
A
A'
B

Figure 16

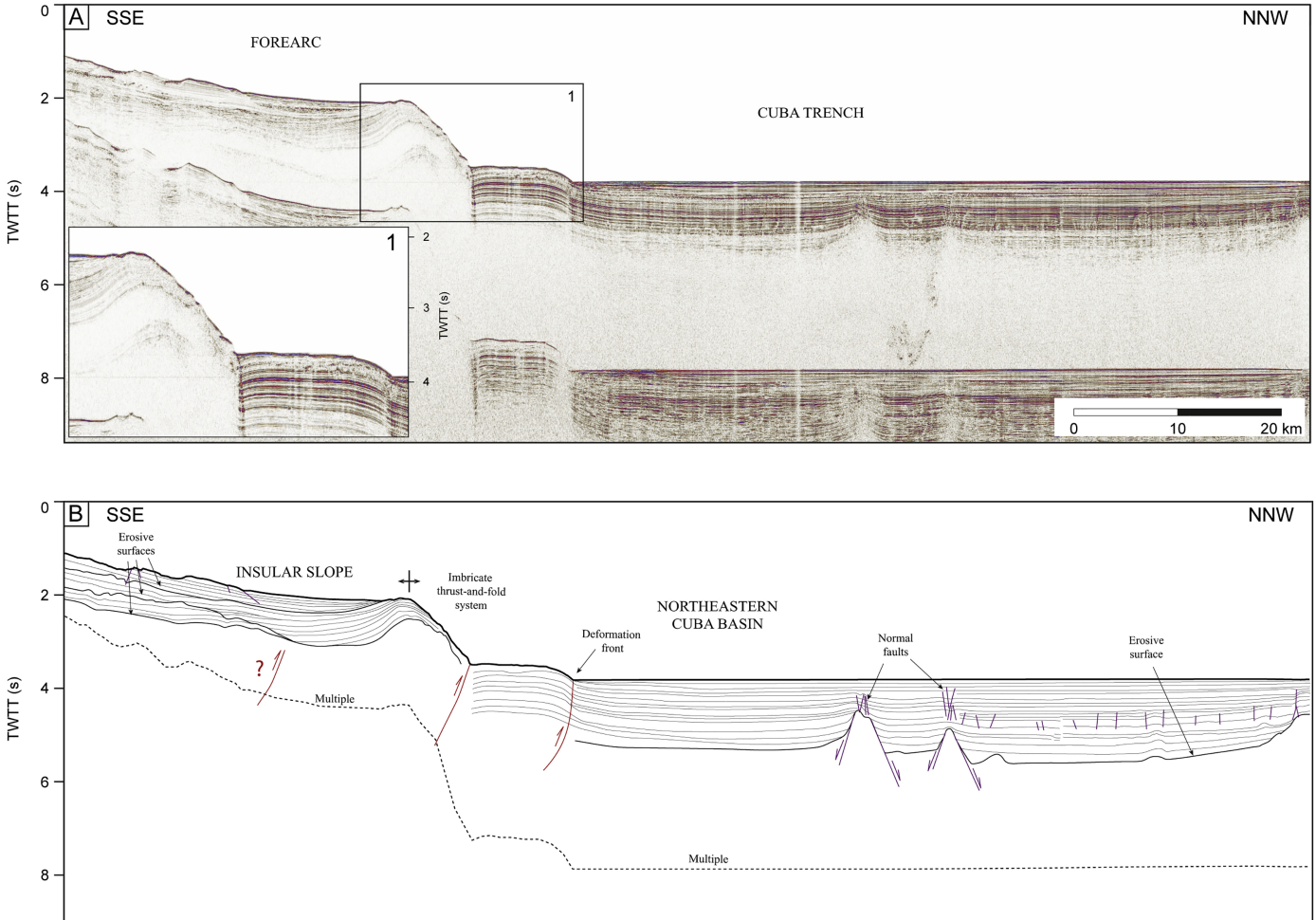
A
SSE
NNW
FOREARC
CUBA TRENCH
1
TWTT (s)
0
2
4
6
8
0
10
20 km
B
SSE
NNW
Erosive surfaces
INSULAR SLOPE
Imbricate thrust-and-fold system
NORTHEASTERN CUBA BASIN
Deformation front
Normal faults
Erosive surface
?
Multiple
Multiple

Figure 17

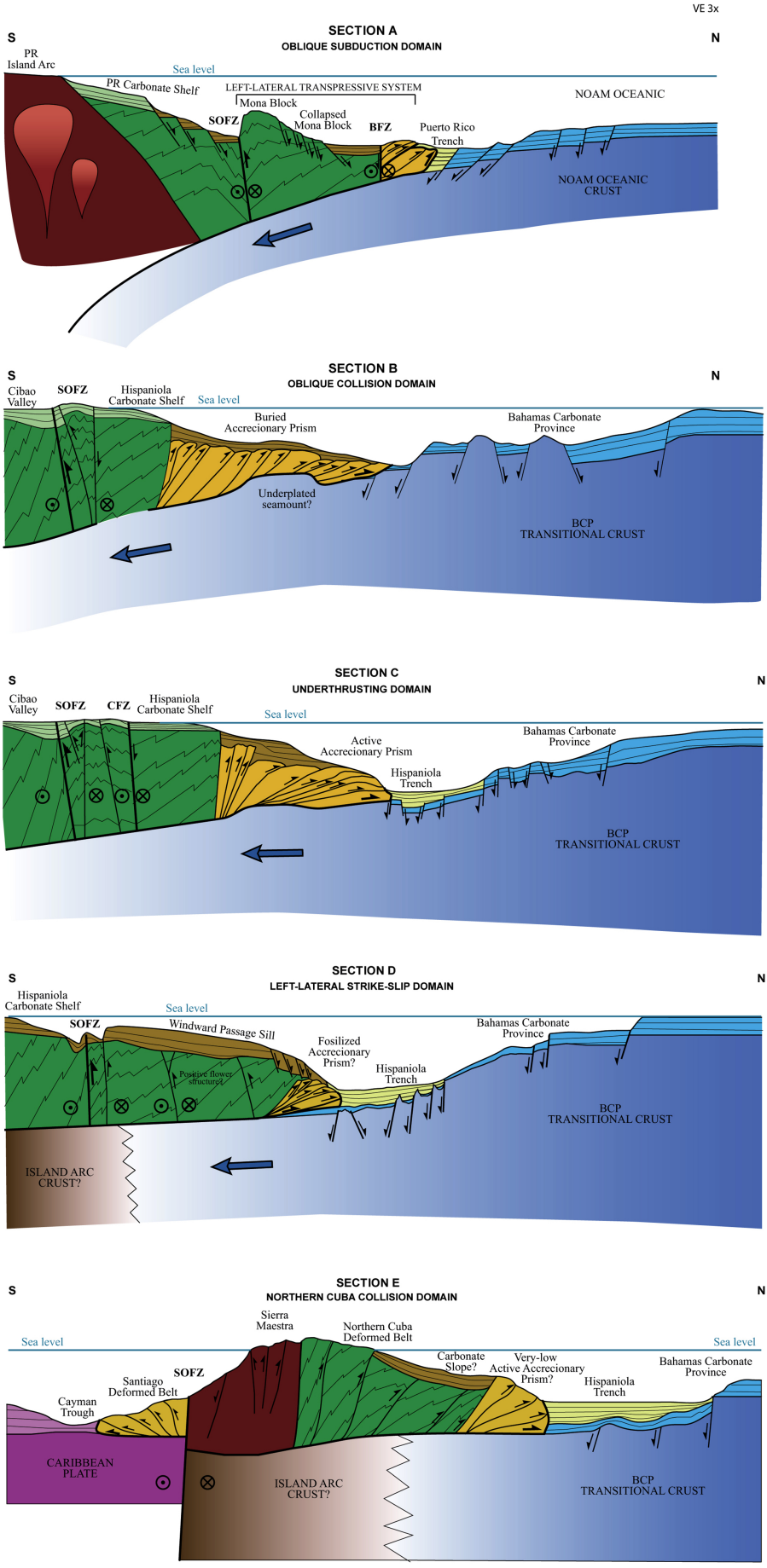
VE 3x
S
N
SECTION A
OBLIQUE SUBDUCTION DOMAIN
PR
Island Arc
Sea level
PR Carbonate Shelf
LEFT-LATERAL TRANSPRESSIVE SYSTEM
Mona Block
SOFZ
Collapsed
Mona Block
BFZ
Puerto Rico
Trench
NOAM OCEANIC
NOAM OCEANIC
CRUST
SECTION B
OBLIQUE COLLISION DOMAIN
Cibao
Valley
SOFZ
Hispaniola
Carbonate Shelf
Sea level
Buried
Accrecionary Prism
Bahamas Carbonate
Province
Underplated
seamount?
BCP
TRANSITIONAL CRUST
SECTION C
UNDERTHRUSTING DOMAIN
Cibao
Valley
SOFZ
CFZ
Hispaniola
Carbonate Shelf
Sea level
Active
Accrecionary Prism
Bahamas Carbonate
Province
Hispaniola
Trench
BCP
TRANSITIONAL CRUST
SECTION D
LEFT-LATERAL STRIKE-SLIP DOMAIN
Hispaniola
Carbonate Shelf
Sea level
SOFZ
Windward Passage Sill
Fosilized
Accrecionary
Prism?
Positive flower
structure?
Hispaniola
Trench
Bahamas Carbonate
Province
BCP
TRANSITIONAL CRUST
ISLAND ARC
CRUST?
SECTION E
NORTHERN CUBA COLLISION DOMAIN
Sierra
Maestra
Northern Cuba
Deformed Belt
Sea level
Sea level
Carbonate
Slope?
Very-low
Active Accrecionary
Prism?
Bahamas Carbonate
Province
SOFZ
Santiago
Deformed Belt
Hispaniola
Trench
Cayman
Trough
CARIBBEAN
PLATE
ISLAND ARC
CRUST?
BCP
TRANSITIONAL CRUST

Figure 18

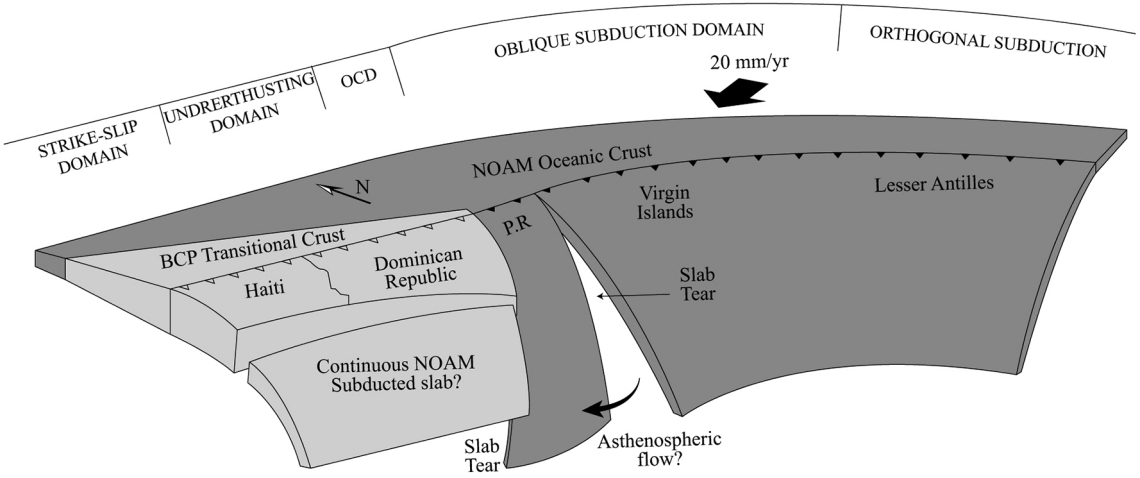
STRIKE-SLIP DOMAIN
UNDRERTHUSTING DOMAIN
OCD
OBLIQUE SUBDUCTION DOMAIN
ORTHOGONAL SUBDUCTION
20 mm/yr
N
NOAM Oceanic Crust
Virgin Islands
Lesser Antilles
P.R
BCP Transitional Crust
Haiti
Dominican Republic
Slab Tear
Continuous NOAM Subducted slab?
Slab Tear
Asthenospheric flow?

Figure 19